Università degli Studi di Napoli *Federico II*

DOTTORATO DI RICERCA IN

FISICA

Ciclo XXX

Coordinatore: prof. Salvatore Capozziello

Continuous Variable Entanglement and Optical Orbital Angular Momentum: a hybrid route to quantum communication

Settore Scientifico Disciplinare FIS/03

Dottorando
Adriana Pecoraro

Tutore
Prof. Lorenzo Marrucci
Dott. Alberto Porzio

Anni 2014/2017

Contents

Publications

[1] A. Pecoraro, D. Buono, G. Nocerino, A. Porzio, S. Olivares, and M. G. A. Paris, "Experimental pre-assessing of two-mode entanglement in Gaussian state mixing" J. Opt. Soc. Am. B 34, 404-411 (2017)

[2] A. Pecoraro, F. Cardano, L. Marrucci and A. Porzio, "Optical Bipartite Continuous Variable Entangled States carrying Orbital Angular Momentum" (*in preparation*)

List of abbreviations

AM Angular Momentum

BS Beam Splitter

CGH Computer Generated Hologram

CM Covariance Matrix

CV Continuous Variable

CW Continuous Wave

DFG Difference Frequency Generation

d.o.f. degree of freedom

EM Electro-Magnetic

EOM Electro Optic Modulator

FR Faraday Rotator

GS Gaussian State

HD Homodyne Detector

HG Hermite-Gauss

HWP Half Wave Plate

LC Liquid Crystal

LG Laguerre-Gauss

LO Local Oscillator

MC Mode Cleaner

OAM Orbital Angular Momentum

OPO Optical Parametric Oscillator

OR Optical Rectification

PBS Polarizing Beam Splitter

PD Photodiode

PDH Pound Drever Hall

PHS Peres–Horodecki-Simon

PPT Positivity under Partial Transposition

QP Q-Plate

QWP Quarter Wave Plate

SAM Spin Angular Momentum

SFG Sum Frequency Generation

SHG Second Harmonic Generation

SI International System of units

SLM Spatial Light Modulator

SPP Spiral Phase Plate

Abstract

The demand for improved measurements, communication and computation has led to search for new physical systems suitable to encode, manipulate and transmit information. Quantum systems have proven to be a major resource since they allow for information processing that could not be performed by classical ones, e.g. providing speedups over classical algorithms or improving channels capacity and security.

Basically, there exist two fundamental approches for encoding quantum information, the discrete- and the continuous-variable one, that can be endowed with a finite- or an infinite-dimensional Hilbert space. In the former approach, information is encoded into a quantum variable having a discrete spectrum so, when carrying out a measurement it is possible to obtain a discrete set of possible results (e.g. 0-1 for dichotomic variables). The latter provides information encoding into a system whose relevant degrees of freedom are represented by operators with continuous spectra.

The initial trend has been choosing the qubits (states of a quantum system with a two-dimensional Hilbert space) as the information unit. However two level systems are not the only possibility, since it turns out that it is possible to encode information in the continuous degrees of freedom of a quantum system. Although these approaches may seem to stand in opposition, recently they are converging into more powerful hybrid protocols [1].

In the context of quantum optics the system whose degrees of freedom are employed to store information is the electromagnetic field. The quantum information and computation approach that involves radiation modes has many advantages with respect to approaches that use matter degrees of freedom such as ion traps and nuclear magnetic resonance. Indeed

it reduces both the problems of decoherence and scalability at expense of requiring a greater effort to overcome the difficulties due to the absence of an interaction between photons as a consequence of the electromagnetism abelianity.

Radiation field offers the possibility to develop both discrete and continuous approches thanks to its particle- and wave-like behaviour. One common discrete approach stands in the use of photon polarization that lives in a two-dimensional Hilbert space. Another discrete degree of freedom is represented by the orbital angular momentum. This is a characteristic of light that occurs from single photon level up to intense classical beams and is independent from the polarization. Light carrying orbital angular momentum has a particular spatial distribution of the field and shows a peculiar shape of wavefronts that result to be helices.

The benefits of encoding information onto the orbital angular momentum, instead of exploiting polarization, reside in the amount of information storable into a single mode thanks to the fact that orbital angular momentum lives in a Hilbert space of a higher dimension [2] [3]. On the other hand, electromagnetic field possesses peculiarities allowing also a continuous variable approach [4]. Indeed electromagnetic field quadratures, a Hermitian combination of the bosonic mode operators, are observables with a continuous spectrum. It is possible to define a pair of "orthogonal" quadrature so that they represent the analogue, for the electromagnetic field, of the position and momentum of a quantum mechanical oscillator; they are the real and the imaginary amplitude of the field. They form a pair of Hermitian conjugate observables and then obey to an uncertainty principle that forbids measuring with an arbitrary precision both the quadratures. Among the continuous variable states of electromagnetic field a prominent role is played by Gaussian states. These states are of great practical relevance in applications to quantum information since they are experimentally easy to produce and manipulate and of simple theoretical description. Gaussian states description and characterization are carried out in phase space where they possess a Gaussian Wigner function. Despite being infinite dimensional states they can be described by few mathematical objects that are the first and the second moments of the field quadratures. These statistical objects form the covariance matrix of the state, a quantity actually measurable in experiments.

Non-classical correlations are another key element in quantum information and communication protocols. This pure quantum feature may occur in composite systems in which correlations, that cannot be explained classically, are estabilished among the quantum system subparts. These correlations can occur both among discrete and continuous degrees of freedom and give rise to a great variety of phenomena so being the basis for many applications in quantum science. Continuous variable (quadratures) and discrete variables (polarization and orbital angular momentum) are, together with entanglement the main building blocks constituing the scenario in which this thesis lies.

In the present dissertation we describe the generation of a Gaussian bipartite entangled state in which the two subsystems are multi-distinguishable thanks to the fact that they have different polarization and carry an opposite amount of orbital angular momentum along the propagation direction.

Polarization entangled states are produced by using an optical parametric oscillator as spontaneous parametric down conversion source. This is able to produce a bipartite state consisting of collinear thermal crossed polarized modes exhibiting entanglement. These two modes have the same frequency and constitute a continuous variable bipartite entangled system in which each of the modes can be labeled by the polarization degree of freedom. Once these two polarization entangled states are produced, the bipartite state is endowed with an additional degree of freedom constituted by orbital angular momentum, that makes possible to further distinguish between these two co-propagating modes. The two-dimensional Hilbert polarization space is mapped into the orbital angular momentum one by means of Gaussian operations i.e. physical trasformations that preserve Gaussianity. In order to achieve this task we used a liquid crystal optical device called q-plate, where q represents the plate topological charge. This device is able to couple polarization and orbital angular momentum degrees of freedom by making the passing through beam acquire orbital angular momentum that depends on the topological charge and the polarization of the incoming beam. Moreover, the setup enginereed to achieve this task is also capable of generating squeezed vortex beams i.e. single-mode states for which the quadrature noise is below the standard quantum limit.

After producing the bipartite entangled state it enters the characterizaton stage. Its

"quantumness" is investigated by witnessing both squeezing and non classical correlations via balanced optical homodyne, a phase sensitive detection method that permits, by measuring the electromagnetic field quadratures statistics to reconstruct the state of the system. In order to retrieve the quantum state with an high fidelity, homodyne detector needs to be optimized. This, besides imposing stringent conditions on the optical components involved in the setup, forces to improve the mode matching between the signal and the local oscillator that plays a central role in determining the overall detector efficiency. Although homodyne is a consolidated detection scheme, herein it is proposed an innovative extension of this technique to structured modes that opens the doors for homodyning directly in the orbital angulam momentum space. The very central role, in this detection method, is played by interference between the signal under investigation and a strong coherent reference beam called local oscillator. Besides behaving as an amplifier for the quadrature under scrutiny, local oscillator also acts as a spatial and frequency filter, selecting for the measure the part of the signal that shares with it the same spatio-temporal properties. Hence, in order to ensure interference, in case of a signal carrying orbital angular momentum a further effort is required. Indeed, also the local oscillator has to be in the same helical mode, in particular the two beams have to transport the same amount of orbital angular momentum along the propagation direction. So by suitably designing the overall experimental setup it is possible to homodyne the bipartite entangled state carrying orbital angular momentum directly in this degree of freedom Hilbert space. Once the covariance matrix of the bipartite Gaussian state has been reconstructed, thanks to Gaussianity, it is possible to assess entanglement between the vortex modes by means of entanglement criteria based on covariance matrix elements such as the Peres–Horodecki-Simon (PHS) and the Duan ones.

The present dissertation is organized as follows. The first chapter will deal with the theoretical concepts aiming at provide all the theoretical tools necessary for the comprehnsion of the experiment realization. In the second chapter the experimental realization of the entanglement source and the experimental scheme designed to add the further degree of freedom represented by the orbital angular momentum to the bipartite entangled state will be described. The third chapter will be devoted to the realization of a homodyne detection

scheme capable of fully characterize a bipartite entangled state constituted of vortex beams. Eventually in the last chapter results will be presented and commented.

Chapter 1

Theoretical Background

This chapter will briefly give all the theoretical tools and concepts necessary for the comprehension of the experiment we have performed. First of all, the key elements of the Electro-Magnetic (EM) field will be summarized, with particular attention to one of its main degrees of freedom: the Angular Momentum (AM). The problem of the analytical separation between its spin and orbital part will be faced both from a classical and a quantum point of view since these two independent degrees of freedom play a central role in the experiment. There will be also given examples of EM field modes carrying Orbital Angular Momentum (OAM) and will be presented some of the most diffuse techniques nowadays available to generate and manipulate the polarization and the spatial profile of laser beams. Later we will discuss some classes of quantum states of the EM field. In particular we will introduce squeezed states that are central to the nature of the experiment due to the intimate connection between squeezing and entanglement that are nothing but two faces of the same phenomenon.

Eventually, criteria to assess the presence of entanglement will be given with specific reference to the class of Gaussian States (GSs) that includes most of the EM states usually accessible in an optic laboratory.

1.1 Electromagnetic Field

1.1.1 Classical Electromagnetic Field

EM field can be regarded as the combination of electric and magnetic field and is responsible for the EM interaction, one of the four fundamental interactions of the nature. From a classical point of view, EM radiation propagates in form of waves and is generated both from electric currents and charged particles at rest. However, EM field is a real physical entity and can exist regardless the presence of sources since electric field can be generated by a time variation of the magnetic one and vice-versa, in a self-sustaining process.

A mathematical description of the EM field is provided by the Maxwell equations that, in the most general formulation using the SI, can be written as [5]:

$$\begin{aligned} \nabla \cdot \mathbf{D} &= \varrho & \nabla \cdot \mathbf{B} &= 0 \\ \nabla \times \mathbf{E} &= -\tfrac{\partial \mathbf{B}}{\partial t} & \nabla \times \mathbf{H} &= \mathbf{J} + \tfrac{\partial \mathbf{D}}{\partial t} \end{aligned} \tag{1.1}$$

where ϱ and $\mathbf{J}$ are respectively the charge and the current densities. This is a system of eight scalar partial differential equations in which $\mathbf{D}$ is the electric displacement field and $\mathbf{H}$ is the magnetic induction field, which, in a dielectric material, are respectively related to the electric field $\mathbf{E}$ and to the magnetic field $\mathbf{B}$ by:

$$\mathbf{D} = \varepsilon_0 \mathbf{E} + \mathbf{P} \tag{1.2}$$

$$\mathbf{H} = \frac{\mathbf{B}}{\mu_0} - \mathbf{M} \tag{1.3}$$

where $\varepsilon_\mathbf{0}$ and $\mu_\mathbf{0}$ are respectively the vacuum permittivity and the vacuum permeability, while $\mathbf{P}$ and $\mathbf{M}$ are respectively the polarization density and the magnetization of the material. In the free space, in absence of charges and currents, the system of equations (1.1) assumes the

following simpler form:

$$\begin{aligned} \nabla \cdot \mathbf{E} &= 0 & \nabla \cdot \mathbf{B} &= 0 \\ \nabla \times \mathbf{E} &= -\frac{\partial \mathbf{B}}{\partial t} & \nabla \times \mathbf{B} &= \frac{1}{c^2}\frac{\partial \mathbf{E}}{\partial t} \end{aligned} \tag{1.4}$$

where $c = (\varepsilon_{\mathbf{0}}\mu_{\mathbf{0}})^{-\frac{1}{2}}$ is the speed of light in vacuum.

As it is clear from the equation concerning the divergence of the electric field, despite the case with sources, in vacuum the electric field is transverse so it is forced to oscillate whitin a plane orthogonal to the propagation direction. The direction in which this field vibrates describes an important EM waves property: the polarization. Polarization is also known as Spin Angular Momentum (SAM) for reasons that will be more clear when we will move to the quantum description and we will treat it more in detail.

By suitably manipulating these equations it is possible to obtain the D'Alembert equations for both the fields:

$$\Box \mathbf{E} = 0 \qquad \Box \mathbf{B} = 0 \tag{1.5}$$

Similar equations hold when the vector and the scalar potential $\mathbf{A}(x, y, z, t)$ and $\phi(x, y, z, t)$ are introduced. These fields are related to the electric and the magnetic fields by the expressions:

$$\mathbf{E} = -\frac{\partial \mathbf{A}}{\partial t} - \nabla\phi. \tag{1.6}$$

$$\mathbf{B} = \boldsymbol{\nabla} \times \mathbf{A} \tag{1.7}$$

However, one can always perform the following transformation, with a scalar field χ:

$$\mathbf{A}' = \mathbf{A} + \nabla\chi \tag{1.8}$$

$$\phi' = \phi - \frac{\partial \chi}{\partial t} \tag{1.9}$$

that leads to the same fields $\mathbf{E}$ and $\mathbf{B}$. It means that there is not a one-to-one correspondence between fields and potentials. In order to have a univocal relation one has to fix the gauge;

two of the most used gauges are the Lorenz and the Coulomb ones:

$$\nabla \cdot \mathbf{A} = -\frac{1}{c^2}\frac{\partial \phi}{\partial t} \quad \text{Lorenz gauge} \tag{1.10}$$

$$\nabla \cdot \mathbf{A} = 0 \quad \text{Coulomb gauge} \tag{1.11}$$

When searching for harmonic monochromatic solutions (which posses a sinusoidal time dependence):

$$\mathbf{E}(x, y, z, t) = \mathcal{R}e\left[\mathbf{E}(x, y, z)e^{i\omega t}\right] \tag{1.12}$$

of the D'Alembert equations, it is easy to see that the spatial part of the field has to satisfy the Helmholtz equation:

$$\nabla^2\mathbf{E} + k^2\mathbf{E} = 0 \tag{1.13}$$

with $|k| = \frac{\omega}{c}$. Depending on the specific problem this equation can have different solutions e.g. plane waves, spherical waves and Bessel solutions. There are essentially four relevant quantities associated to the EM field, one is the EM density of energy stored by the field per unit volume, that is given, in vacuum, by:

$$u = \frac{\varepsilon_0}{2}|\mathbf{E}|^2 + \frac{1}{2\mu_0}|\mathbf{B}|^2 \tag{1.14}$$

Another important quantity is the *Poynting vector* defined as:

$$\mathbf{S} = \frac{1}{\mu_0}(\mathbf{E} \times \mathbf{B}) \tag{1.15}$$

that represents the density of energy transported by an EM wave per unit area and time. Besides transporting energy, an EM wave can carry momentum in its linear and angular components. Linear momentum density of light is defined in terms of the fields as:

$$\mathbf{p} = \frac{\langle \mathbf{S} \rangle}{c} \tag{1.16}$$

where $\langle \mathbf{S} \rangle$ is the time-averaged Poynting vector. The dimensions of (1.16) are that of a

preassure so it is known as *radiation preassure*. Eventually, the *angular momentum density* is defined as:

$$\mathbf{j} = \varepsilon_0 \mathbf{r} \times (\mathbf{E} \times \mathbf{B}) \tag{1.17}$$

and as it is evident it cannot possess a component along the propagation direction.

1.1.2 The quantized field

Quantum theory of light is of paramount importance expecially when the number of photons is small and the fields are not continuous, making the classical description to fail. The traditional approach of quantization consists in identifying the coordinates and the conjugate momenta of a quantum system, promoting them to operators, and stating their commutation rules. Following this approach, it will be shown that the quantized field is nothing more than a system of decoupled harmonic oscillators.

In order to carry out the quantization, it is convenient to start from the Helmholtz equation (1.13) whose solutions depend on the specific problem and geometry. In particular, when looking for solutions of the Maxwell equations in a cubic region of space, plane waves are good solutions satisfying the boundary conditions and represent a basis for each EM field with the same demands at the boundary. This implies that in free space it is possible to expand the EM field in the plane wave basis [6]:

$$\mathbf{E}(\mathbf{x}, t) = \sum_k \mathcal{E}_k \left(a_k(t) e^{-i\mathbf{kx}} + a_k^\dagger(t) e^{i\mathbf{kx}} \right) \tag{1.18}$$

where the coefficients of the expansion are $a_k(t) = a_k e^{i\omega t}$ and $\mathcal{E}_k$ is a normalization factor containing the information on the polarization. Quantization essentially consists in promoting the coefficients of this expansion to operators $\hat{a}_k$ and $\hat{a}_k^\dagger$, that are the creation and the annihilation operators of the standard harmonic oscillator, satisfying the following bosonic commutation rules:

$$\left[\hat{a}_k, \hat{a}_{k'}^\dagger \right] = \delta_{kk'} \tag{1.19}$$

Since an expression similar to (1.18) holds for the magnetic field, it is straightforward, by

using expression (1.14), to show that the Hamiltonian of the EM field is:

$$\hat{H} = \sum_k \hbar\omega_k \left(\hat{a}_k^\dagger \hat{a}_k + \frac{1}{2} \right) \tag{1.20}$$

where $\hat{n} = \hat{a}_k^\dagger \hat{a}_k$ is called *number operator*. As previously predicted, the Hamiltonian (1.20) is nothing but that the sum of an infinite number of harmonic oscillators each corresponding to a mode of the field.

1.1.3 Electromagnetic field quadratures

Bosonic mode operators $\hat{a}$ and $\hat{a}^\dagger$ are not observables associated to the EM field since they are not represented by Hermitian operators and cannot be measured in a real physical experiment. In order to introduce quantities actually measurable let us consider, without any loss of generality, a single mode (fixed k):

$$\hat{\mathbf{E}}(\mathbf{x}, t) = \mathcal{E} \left(\hat{a} e^{-i(\mathbf{kx}-\omega t)} + \hat{a}^\dagger e^{i(\mathbf{kx}-\omega t)} \right) \tag{1.21}$$

By using the Eulero formula it is easy to rewrite (1.21) as:

$$\hat{\mathbf{E}}(\mathbf{x}, t) = \sqrt{2}\mathcal{E} \left[\hat{X} \cos(\mathbf{kx} - \omega t) + \hat{Y} \sin(\mathbf{kx} - \omega t) \right] \tag{1.22}$$

where $\hat{X}$ and $\hat{Y}$ are respectively the amplitude and the phase quadratures defined as the following combinations of the mode operators:

$$\hat{X} = \frac{\hat{a} + \hat{a}^\dagger}{\sqrt{2}} \tag{1.23}$$

$$\hat{Y} = \frac{\hat{a} - \hat{a}^\dagger}{\sqrt{2}i} \tag{1.24}$$

These dimensionless operators are Hermitian, and so observables, and are equivalent to the position and momentum operators for a harmonic oscillator. They are conjugate observables,

indeed by using expression (1.19) it is easy to show that:

$$\left[\hat{X}, \hat{Y}\right] = i \tag{1.25}$$

Moreover, they are Continuous Variables (CV) associated to the EM field since they are operators with a continuous spectrum defined in the Hilbert space.

1.1.4 Uncertainty principle

Heisenberg uncertainty principle is a pillar of quantum mechanics and can be enunciated in the following way:

Given two observables characterizing a quantum system, to whom are associated two non commuting and conjugate Hermitian operators $\hat{A}$ and $\hat{B}$, defined in the Hilbert space of the system so that:

$$\left[\hat{A}, \hat{B}\right] = i\hbar \tag{1.26}$$

then the product of their uncertainties cannot be smaller than $\frac{\hbar}{2}$

$$\triangle A \triangle B \geq \frac{\hbar}{2} \tag{1.27}$$

This inequality translates in an operational indetermination, i.e. the impossibility of carrying out measurements on one of the two observables without perturbing the other one. This principle has been then reformulated by Kennard for the standard deviations of conjugate Hermitian operators, instead of the uncertainties on a single measurement,

$$\sigma_A \sigma_B \geq \frac{\hbar}{2} \tag{1.28}$$

with $\sigma_A = \sqrt{\left\langle \hat{A}^2 \right\rangle - \left\langle \hat{A} \right\rangle^2}$ and $\sigma_B = \sqrt{\left\langle \hat{B}^2 \right\rangle - \left\langle \hat{B} \right\rangle^2}$ evaluated on a particular state of the system. In this case measurements are repeated on many identical copies of the quantum system. This means that the indetermination is intrinsic. The amplitude and the phase quadrature operators $\hat{X}$ and $\hat{Y}$, introduced before, are Hermitian and conjugate. Therefore,

by using the Kennard's term, it stands:

$$\sigma_X \sigma_Y \geq \frac{\hbar}{2} \tag{1.29}$$

As we will see in the following this inequality allows to make a classification of the EM field states. In particular, it permits to introduce a specific class of EM field states characterized by the fact that the fluctuations on the quadratures are distributed in an asymmetric manner.

1.1.5 Examples of states of the electromagnetic field

1.1.5.1 Vacuum and Fock states

Number states or Fock states are defined as the eigenstates of the number operator $\hat{n}$ and are suitable to describe the energy levels of the harmonic oscillator [6], so we have:

$$\hat{n} \left|n\right\rangle = n \left|n\right\rangle \tag{1.30}$$

where n is an integer number and corresponds to the number of the field excitations (photons) in the state. This number can be raised or lowered respectively through the bosonic mode operators $\hat{a}^\dagger$ and $\hat{a}$ that are therefore said the creation and the annihilation operators. It can be shown that,

$$\hat{a}^\dagger \left|n\right\rangle = \sqrt{n+1} \left|n+1\right\rangle \tag{1.31}$$

$$\hat{a} \left|n\right\rangle = \sqrt{n} \left|n-1\right\rangle \tag{1.32}$$

The state in which there are not photons is said to be the vacuum state $|0\rangle$ and is a Hamiltonian eigenstate with energy $E = \frac{\omega\hbar}{2}$. Starting from it, it is possible to obtain any Fock state by using:

$$\left|n\right\rangle = \frac{1}{\sqrt{n!}} \left(\hat{a}^\dagger\right)^n \left|0\right\rangle \tag{1.33}$$

These states are a basis for the Hilbert space being a complete and orthonormal system:

$$\sum_n |n\rangle \langle n| = \hat{I} \quad \text{Completeness relation} \tag{1.34}$$

$$\langle m|\, n\rangle = \delta_{nm} \quad \text{Orthonormality condition} \tag{1.35}$$

where $\hat{I}$ is the identity operator. For a Fock state we have:

$$\left\langle n \left| \hat{X} \right| n \right\rangle = \left\langle n \left| \hat{Y} \right| n \right\rangle = 0 \tag{1.36}$$

$$\left\langle n \left| \hat{X}^2 \right| n \right\rangle = \left\langle n \left| \hat{Y}^2 \right| n \right\rangle = \frac{2n+1}{2} \tag{1.37}$$

so being

$$\sigma_X \sigma_Y = \frac{2n+1}{2} \tag{1.38}$$

Only the vacuum state ($n = 0$) fullfills the Heisenberg inequality with the equal sign. A pictorial representation of the vacuum state in phase space is shown in fig. 1.1

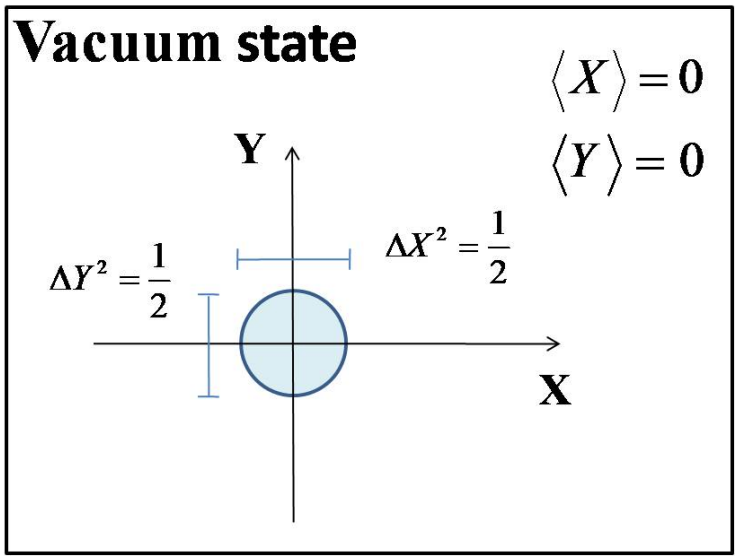

Figure 1.1: Pictorial representation of the vacuum state in phase space. The mean value of both the quadratures is zero and the relative fluctuations are equal to $\frac{1}{2}$.

Eventually, since these states are eigenstates of the number operator, we have

$$\sigma_n^2 = \left\langle n \left| \hat{n}^2 \right| n \right\rangle - \left\langle n \left| \hat{n} \right| n \right\rangle^2 = 0 \tag{1.39}$$

and the number of quanta in the state can be known exactly.

1.1.5.2 Coherent states

Coherent states are defined as being the eigenstates of the annihilation operator [6],

$$\hat{a} \left| \alpha \right\rangle = \alpha \left| \alpha \right\rangle \tag{1.40}$$

where $\alpha = \left| \alpha \right| e^{i\varphi}$ is a complex number and φ represents the phase of the quantum state. Coherent states can be obtained by applying to the vacuum state the *displacement operator* $\hat{D}(\alpha)$,

$$\left| \alpha \right\rangle = \hat{D}(\alpha) \left| 0 \right\rangle = \exp\left(\alpha \hat{a}^\dagger - \alpha^* \hat{a} \right) \left| 0 \right\rangle \tag{1.41}$$

that is a unitary operator such that:

$$\begin{cases} \hat{D}^{-1}(\alpha) = \hat{D}\left(-\alpha\right) \\ \hat{D}\left(\alpha\right) \hat{D}^\dagger\left(\alpha\right) = \hat{D}\left(\alpha\right) \hat{D}^{-1}\left(\alpha\right) = \hat{I} \end{cases} \tag{1.42}$$

Coherent states satisfy the following completeness relation:

$$\frac{1}{\pi} \int d^2\alpha \ \left| \alpha \right\rangle \left\langle \alpha \right| = \hat{I} \tag{1.43}$$

where $d^2\alpha = d(\mathrm{Re}[\alpha]) d(\mathrm{Im}[\alpha])$. However, they form an overcomplete system since they are not a set of mutually orthogonal vectors, indeed,

$$\left| \left\langle \alpha \right| \left. \beta \right\rangle \right|^2 = exp\left(- \left| \alpha - \beta \right|^2 \right) \tag{1.44}$$

Despite the case of Fock states for which the number of photons is known exactly, for a coherent state, whose expression in Fock basis is the following,

$$|\alpha\rangle = \sum_{n=0}^{\infty} e^{-\frac{1}{2}|\alpha|^2} \frac{\alpha^n}{\sqrt{n!}} |n\rangle \tag{1.45}$$

the probability to find n photons in the state $|\alpha\rangle$ is given by the Poisson distribution,

$$P_n(\alpha) = |\langle n|\ \alpha\rangle|^2 = \frac{|\alpha|^{2n}}{n!} e^{-|\alpha|^2} \tag{1.46}$$

and $(\triangle n_\alpha)^2 = \langle \hat{n} \rangle_\alpha = |\alpha|^2$. Beyond these features, coherent states have an important peculiarity for what concerns the uncertainty principle, indeed they are states with minimum uncertainity:

$$\sigma_X \sigma_Y = \frac{1}{2} \tag{1.47}$$

since $\sigma_X^2 = \sigma_Y^2 = \frac{1}{2}$. A pictorial representation of a coherent state is shown in fig 1.2

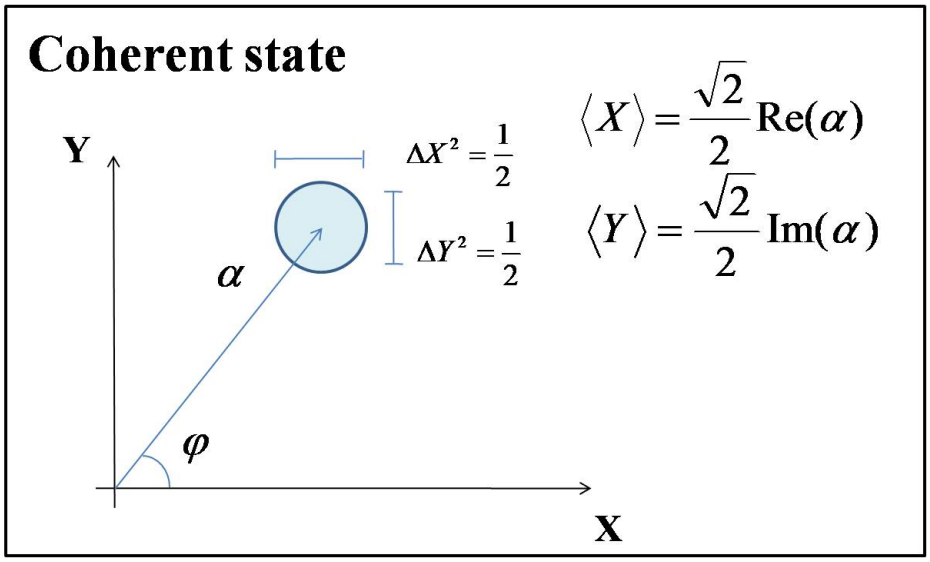

Figure 1.2: Pictorial representation of a coherent state in phase space. Uncertainities on both the quadratures are equal.

1.1.5.3 Thermal states

When the EM field is at thermal equilibrium with a heat bath at temperature T it is in a thermal state and its radiation is said to be black body radiation. The energy distribution of the state is described by the Boltzmann distribution [6],

$$\hat{\rho} = \frac{\exp\left\{-\hat{H}/k_B T\right\}}{\mathrm{Tr}\left[\exp\left\{-\hat{H}/k_B T\right\}\right]} \tag{1.48}$$

where k_B is the Boltzmann constant and $\hat{H} = \hbar\omega_k\left(\hat{n}_k + \frac{1}{2}\right)$ is the energy of the k-th mode of the field. By using expression (1.48) it is possible to calculate the density matrix of a thermal state,

$$\hat{\rho} = \sum_{n_k} P_{n_k} \left|n_k\right\rangle \left\langle n_k\right| \tag{1.49}$$

where

$$\begin{aligned} P_{n_k} &= \left\langle n_k\right| \hat{\rho} \left|n_k\right\rangle \\ &= e^{-n_k \hbar\omega_k / k_B T}\left(1 - e^{-\hbar\omega_k / k_B T}\right) \end{aligned} \tag{1.50}$$

and where the formula $\sum_{n=0}^{N} x^n = \frac{1}{1-x}$ has been employed. By setting $\beta_k = \frac{\hbar\omega_k}{k_B T}$, we get:

$$P_{n_k} = e^{-\beta_k n_k}\left(1 - e^{-\beta_k}\right) \tag{1.51}$$

so

$$\hat{\rho} = \sum_{n_k} e^{-\beta_k n_k}\left(1 - e^{-\beta_k}\right) \left|n_k\right\rangle \left\langle n_k\right| \tag{1.52}$$

Let us now calculate:

$$\begin{aligned} \langle \hat{n}_k \rangle &= \mathrm{Tr}\left(\hat{n}_k \hat{\rho}\right) \\ &= \sum_{n_k} n_k \; e^{-\beta_k n_k} \left(1 - e^{-\beta_k}\right) \end{aligned} \tag{1.53}$$

By using the relation $\sum_{n_k} n_k \; e^{-\beta_k n_k} = \frac{e^{\beta_k}}{\left(e^{\beta_k}-1\right)^2}$, expression (1.53) becomes:

$$\langle \hat{n}_k \rangle = \frac{e^{\beta_k}}{\left(e^{\beta_k}-1\right)^2} \left(1 - e^{-\beta_k}\right) = \frac{1}{e^{\beta_k}-1} \tag{1.54}$$

so from (1.54) we get:

$$e^{\beta_k} = \frac{\langle \hat{n}_k \rangle + 1}{\langle \hat{n}_k \rangle} \tag{1.55}$$

and eventually the expression of the density matrix becomes:

$$\hat{\rho} = \frac{1}{1 + \langle \hat{n}_k \rangle} \sum_{n_k} \left(\frac{\langle \hat{n}_k \rangle}{1 + \langle \hat{n}_k \rangle} \right)^{n_k} |n_k\rangle \langle n_k| \tag{1.56}$$

It is also possible to calculate:

$$\left\langle \hat{n}_k^2 \right\rangle = \frac{e^{\beta_k}+1}{e^{\beta_k}-1} = 2 \langle \hat{n}_k \rangle \left(\langle \hat{n}_k \rangle + \frac{1}{2} \right) \tag{1.57}$$

in order to obtain the following expression of the fluctuation on the photon number:

$$\triangle n_k^2 = \left\langle \hat{n}_k^2 \right\rangle - \langle \hat{n}_k \rangle^2 = \langle \hat{n}_k \rangle \left(1 + \langle \hat{n}_k \rangle\right) \tag{1.58}$$

1.1.5.4 Squeezed states

Squeezing is a pure quantum feature of light and has many applications in optical communications [7] and optical measurements [8]. As we have seen before, coherent states are those states for which the uncertainty region is circularly symmetric since both phase and amplitude have identical variances $\sigma_X^2 = \sigma_Y^2 = \frac{1}{2}$. However, the Heisenberg uncertainty principle only fixes a lower limit for the product of the variances so, in principle, it is possible to reduce

one of the two fluctuations under this limit at the expense of the fluctuation on the other conjugate variable. Light that shows such a behaviour is said to be (quadrature) squeezed; in other words a squeezed state of EM radiation, is a state for which [6]:

$$\triangle X^2 < \frac{1}{2} \quad \left(\triangle Y^2 < \frac{1}{2}\right) \tag{1.59}$$

In particular, if even stands

$$\triangle X \triangle Y = \frac{1}{2} \tag{1.60}$$

the state is also a minimum uncertainity state. A single mode squeezed state can be obtained through the action of the squeezing operator:

$$\hat{S}(\xi) = \exp\left[\frac{1}{2}\left(\xi^* \hat{a}^2 - \xi\left(\hat{a}^\dagger\right)^2\right)\right] \tag{1.61}$$

on a coherent state, where the complex number $\xi = re^{i\phi}$ is the squeezing parameter. This operator is a sort of "evolution operator" under the Hamiltonian,

$$\hat{H} = i\hbar\left(g\left(\hat{a}^\dagger\right)^2 - g^*\hat{a}^2\right) \tag{1.62}$$

representing a non-linear two-photon interaction process, with g coupling constant and ξ playing the role of time. By using the Heisenberg equations it is easy to show that:

$$\begin{cases} \hat{S}^\dagger(\xi)\,\hat{a}\hat{S}(\xi) = \hat{a}\cosh r - e^{i\phi}\hat{a}^\dagger \sinh r \\ \hat{S}^\dagger(\xi)\,\hat{a}^\dagger\hat{S}(\xi) = \hat{a}^\dagger\cosh r - e^{-i\phi}\hat{a}\sinh r \end{cases} \tag{1.63}$$

Since, as we will see, squeezing is a phase dependent property, it is convenient to generalize the expression for the field quadratures by introducing:

$$\hat{X}(\vartheta) = \frac{\hat{a}e^{-i\vartheta} + \hat{a}^\dagger e^{i\vartheta}}{\sqrt{2}} \tag{1.64}$$

It is clear from this expression that (1.23) and (1.24) are particular cases of (1.64) corresponding respectively to $\vartheta = 0$ and $\vartheta = \frac{\pi}{2}$. As previously said, a squeezed coherent state can be easily obtained by applying the squeezing operator to a coherent state, so without loss of generality let us consider the vacuum state

$$|\xi\rangle = \hat{S}(\xi)|0\rangle \tag{1.65}$$

so obtaining a squeezed vacuum. The variance of the generalized quadrature $\hat{X}(\vartheta)$ is:

$$\begin{aligned}(\triangle X(\vartheta))_{\xi}^{2} &= \left\langle \xi \left| \hat{X}^{2}(\vartheta) \right| \xi \right\rangle - \left\langle \xi \left| \hat{X}(\vartheta) \right| \xi \right\rangle^{2} \\ &= \left\langle \xi \left| \hat{X}^{2}(\vartheta) \right| \xi \right\rangle \\ &= \frac{1}{2}\left[e^{2r} \sin^{2}\left(\vartheta - \frac{\phi}{2}\right) + e^{-2r} \cos^{2}\left(\vartheta - \frac{\phi}{2}\right)\right]\end{aligned} \tag{1.66}$$

so the state $|\xi\rangle$ is squeezed if

$$\sin^{2}\left(\vartheta - \frac{\phi}{2}\right) < \left(e^{2r} + 1\right)^{-1} \tag{1.67}$$

In particular, when $\vartheta - \frac{\phi}{2} = n\pi$ the state is a minimum uncertainity squeezed state since:

$$(\triangle X(\vartheta))^{2} = \frac{1}{2}e^{-2r} \tag{1.68}$$

$$\left(\triangle X\left(\vartheta + \frac{\pi}{2}\right)\right)^{2} = \frac{1}{2}e^{2r} \tag{1.69}$$

and

$$(\triangle X(\vartheta))\left(\triangle X\left(\vartheta + \frac{\pi}{2}\right)\right) = \frac{1}{2} \tag{1.70}$$

It can be seen that a squeezed vacuum state can be written in Fock basis as [9]:

$$|\xi\rangle = \frac{1}{\sqrt{\cosh r}} \sum_{n=0}^{\infty} \left(\frac{e^{i\phi}\tanh r}{2}\right)^{n} \frac{\sqrt{(2n)!}}{n!} |2n\rangle \tag{1.71}$$

So the squeezed vacuum state is a superposition of states with an even number of photons. It is also easy to show that:

$$\langle \hat{n} \rangle = \langle \xi | \, \hat{n} \, | \xi \rangle = |\sinh r|^2 \tag{1.72}$$

while,

$$\left\langle \hat{n}^2 \right\rangle = \langle \xi | \, \hat{n}^2 \, | \xi \rangle = \langle \hat{n} \rangle \left(3 \langle \hat{n} \rangle + 2 \right) \tag{1.73}$$

so

$$\triangle n^2 = 2 \langle \hat{n} \rangle \left(\langle \hat{n} \rangle + 1 \right) \tag{1.74}$$

that is twice the variance of the photon number of a thermal state. In fig 1.3 and in fig 1.4 are shown the pictorial representations of a squeezed coherent state and the squeezed vacuum with respect both the quadratures.

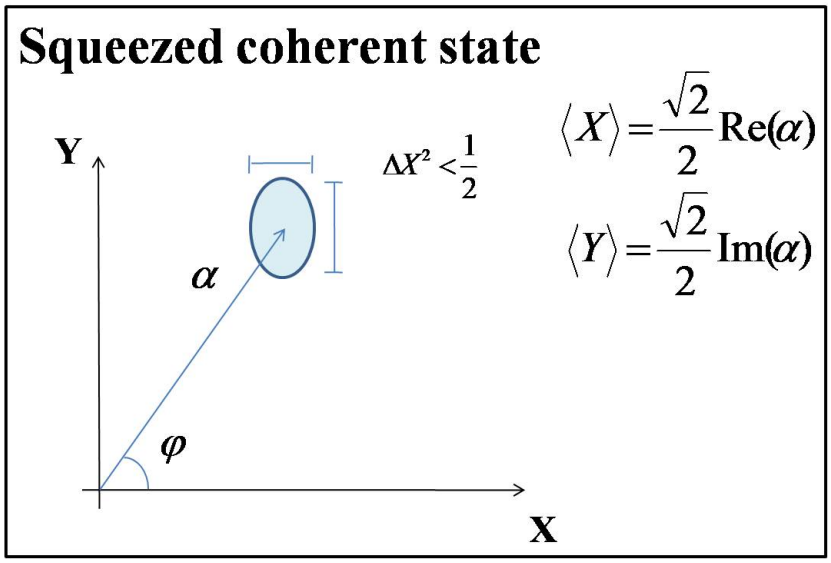

Figure 1.3: Pictorial representation of a squeezed coherent state in phase space. Uncertainities on the quadratures are distributed in an asymmetric way.

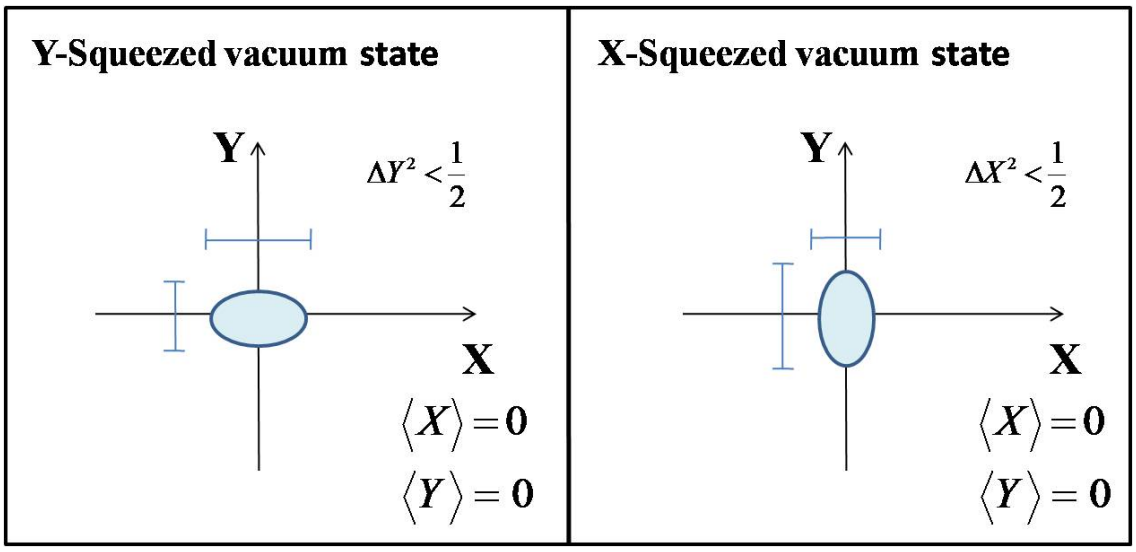

Figure 1.4: Pictorial representation of a X- and Y-squeezed state in phase space.

1.1.5.5 Two-mode squeezed states

The two-mode squeezing operator is given by the following expression:

$$\hat{S}_2(\xi) = \exp\left(\xi^* \hat{a}\hat{b} - \xi \hat{a}^\dagger \hat{b}^\dagger\right) \tag{1.75}$$

where $\hat{a} = \hat{a}_{\nu+\delta\nu}$ and $\hat{b} = \hat{a}_{\nu-\delta\nu}$ are the bosonic mode operators for modes symmetrically placed around a certain frequency ν. The form of this operator is due to the interaction Hamiltonian that in this case is:

$$\hat{H} = i\hbar\left(g\hat{a}^\dagger \hat{b}^\dagger - g^* \hat{a}\hat{b}\right) \tag{1.76}$$

with g coupling constant. A two-mode squeezed state can be obtained by applying this operator to the two-mode vacuum state:

$$|\xi_a \xi_b\rangle = \hat{S}_2(\xi)\,|0_a 0_b\rangle \tag{1.77}$$

As in the case of single-mode squeezed state, it is possible to expand this state in the number basis, obtaining [9]:

$$|\xi_a \xi_b\rangle = \frac{1}{\cosh r} \sum_{n=0}^{\infty} \left(e^{-i\phi} \tanh r\right)^n |n_a n_b\rangle \tag{1.78}$$

This state is an entangled state, as will be more clear in the following, in which the two modes $\hat{a}$ and $\hat{b}$ contain the same photon number. Moreover, each of the two modes is a single-mode thermal state of EM radiation. Indeed, when calculating the expectation value of an observable $\hat{A}$, only acting on the mode $\hat{a}$ subspace, we get:

$$\langle \xi_a \xi_b | \hat{A} | \xi_a \xi_b \rangle = \frac{1}{(\cosh r)^2} \sum_{n=0}^{\infty} (\tanh r)^{2n} \langle n_a | \hat{A} | n_a \rangle \tag{1.79}$$

that is the same expression that is possible to obtain from (1.49) and (1.56) by:

$$e^{-\beta \hbar \omega} \to \tanh^2 r \tag{1.80}$$

in order to have $\langle \hat{n} \rangle = \sinh^2 r$. Starting from the modes $\hat{a}$ and $\hat{b}$, it is possible to define two additional modes as:

$$\begin{cases} \hat{B} = \frac{1}{\sqrt{2}} \left[\hat{a} + e^{-i\delta} \hat{b}\right] \\ \hat{B}^\dagger = \frac{1}{\sqrt{2}} \left[\hat{a}^\dagger + e^{i\delta} \hat{b}^\dagger\right] \end{cases} \tag{1.81}$$

and their respective amplitude and phase quadrature operators:

$$\hat{X}_B = \frac{\hat{B} + \hat{B}^\dagger}{\sqrt{2}} \tag{1.82}$$

$$\hat{Y}_B = \frac{\hat{B} - \hat{B}^\dagger}{\sqrt{2} i} \tag{1.83}$$

By using the commmutation rules for $\hat{a}$ and $\hat{b}$:

$$\left[\hat{a}, \hat{a}^\dagger\right] = \left[\hat{b}, \hat{b}^\dagger\right] = 1 \qquad \left[\hat{a}, \hat{b}\right] = 0 \tag{1.84}$$

it is easy to show that $\hat{X}_B$ and $\hat{Y}_B^\dagger$ are conjugate operators,

$$\left[\hat{X}_B, \hat{Y}_B\right] = i \implies \triangle X_B \triangle Y_B \geq \frac{1}{2} \tag{1.85}$$

By defining the generalized quadrature:

$$\hat{X_B}(\vartheta) = \frac{\hat{B}e^{-i\vartheta} + \hat{B}^\dagger e^{i\vartheta}}{\sqrt{2}} \tag{1.86}$$

it is possible to show that [6]:

$$\triangle X_B(\vartheta) = \frac{1}{2}\left[e^{2r}\text{sin}^2\left(\frac{\delta}{2} - \vartheta\right) + e^{-2r}\text{cos}^2\left(\frac{\delta}{2} - \vartheta\right)\right] \tag{1.87}$$

So, similary to the single-mode case there is squeezing in correspondence of $\vartheta = \frac{\delta}{2} + n\pi$ (and antisqueezing for $\vartheta + \frac{\pi}{2}$).

In addition to the modes $\hat{a}$ and $\hat{b}$, we can make some additional cases:

1. **Mode c**: $\delta = 0,\ \hat{B} \to \hat{c} = \frac{\hat{a}+\hat{b}^\dagger}{\sqrt{2}}$

$$\triangle X_c(\vartheta) = \frac{1}{2}\left[e^{2r}\sin^2(\vartheta) + e^{-2r}\cos^2(\vartheta)\right] \tag{1.88}$$

   and the mode $\hat{c}$ is coherent squeezed for $\vartheta = 0$;

2. **Mode d**: $\delta = \pi,\ \hat{B} \to \hat{d} = \frac{\hat{a}-\hat{b}^\dagger}{\sqrt{2}}$

$$\triangle X_d(\vartheta) = \frac{1}{2}\left[e^{2r}\cos^2(\vartheta) + e^{-2r}\sin^2(\vartheta)\right] \tag{1.89}$$

   so the mode $\hat{d}$ is coherent squeezed for $\vartheta = \frac{\pi}{2}$;

3. **Mode e**: $\delta = \frac{\pi}{2},\ \hat{B} \to \hat{e} = \frac{\hat{a}-i\hat{b}^\dagger}{\sqrt{2}}$

$$\triangle X_e(\vartheta) = \frac{1}{2}\left[e^{2r}\sin^2\left(\frac{\pi}{4} - \vartheta\right) + e^{-2r}\cos^2\left(\frac{\pi}{4} - \vartheta\right)\right] \tag{1.90}$$

so the mode $\hat{e}$ is coherent squeezed for $\vartheta = \frac{\pi}{4}$;

4. **Mode f**: $\delta = -\frac{\pi}{2},\ \hat{B} \to \hat{f} = \frac{\hat{a}+i\hat{b}^\dagger}{\sqrt{2}}$

$$\triangle X_f(\vartheta) = \frac{1}{2}\left[e^{2r}\sin^2\left(-\frac{\pi}{4}-\vartheta\right) + e^{-2r}\cos^2\left(-\frac{\pi}{4}-\vartheta\right)\right] \tag{1.91}$$

so the mode $\hat{f}$ is coherent squeezed for $\vartheta = -\frac{\pi}{4}$.

In conclusion, a squeezing source possessing a Hamiltonian of interaction corresponding to the two-mode squeezing operator (1.75) generates a two-mode entangled state in which the single modes are thermal states of radiation. When considering particular combinations of two-modes, it is possibile to find single-mode squeezing in correspondence of particular angles, like those introduced just before for the modes c, d, e and f that will be usefull in the following of this dissertation.

1.2 Angular Momentum of light: fundations and manipulation

1.2.1 SAM and OAM of the classical radiation field

As well known, when dealing with a system of pointlike masses there are two independent components contributing to the total AM. One is linked to rotations of the center of mass of the system with respect to some origin and it is strictly dependent on the choice of the reference frame (external degree of freedom (d.o.f.)). The other component is related to rotations with respect to the center of mass itself and cannot be canceled by a change of reference (internal d.o.f). This clear distinction is not so trivial when dealing with light, which is constituted by photons that are massless particles. Despite the total AM of light is a well defined quantity descending from the invariance of the free EM field action under the Poincaré group of transformations, the analytical separation between the spin and the angular part is impossible [10, 11].

SAM is related to an intrinsic property of the EM field carrier; the photon. This elementary particle is a massless gauge boson impossible to be observed in its rest frame, so instead of speaking about spin it is more correct to refer to its helicity that is the component of the spin along the propagation direction. Photon helicity can only assume the values $\pm\hbar$ depending on whether the projection of spin onto the momentum and the momentum itself are parallel or antiparallel. These two values correspond, pictorially, to right- ($-\hbar$) and left-handed ($+\hbar$) rotations of the particle around itself that macroscopically coincide with two possible states of photon polarization: the right and the left circular ones.

OAM [12, 13], whose existence has been experimentally proven [14], is a light degree of freedom unrelated to polarization that arises at single photon level and is related to the field spatial distribution. It consists of two components, one that is "internal" since it is different from zero for any possible choice of the origin of coordinates and is associated to beams with helical wavefronts, and one that is "external" since it depends on the choice of the reference.

A starting point to attempt the analytical separation between these two d.o.f. could be the angular momentum density in the expression (1.17). It is worth noting that this formula implies that for a plane wave the AM component along the propagation direction is always null. However this feature is in contrast with the fact that a left- or right-handed circularly polarized plane wave carries an AM in the direction of propagation, as proven by Beth in 1936 [15]. Even if this seeming paradox can be solved by asserting that plane waves are only a pure abstraction, other drawbacks arise in attempting the separation.

When computing the conserved charges due to rotational invariance of the free EM field, one come across the following expression for the total AM in which the requested separation shows up,

$$\mathbf{J} = \sum_{i=x,y,z} \varepsilon_0 \int d^3r \; E_i(\mathbf{r} \times \nabla) A_i + \varepsilon_0 \int d^3r \; \mathbf{E} \times \mathbf{A} \tag{1.92}$$

This is the expression of the canonical angular momentum and is obtained by choosing the Coulomb gauge. It can be shown that expressions (1.92) and (1.17) (once integrated over all to space) coincide in the case of fields that vanish fast enough outside a finite region of space. However, even though the total AM $\mathbf{J}$ is gauge invariant, its two components are ill defined

since they depend on the gauge. Indeed expression (1.92) holds in the Coulomb gauge. A way to circumvent this problem consists in rewriting the total AM from the density in (1.17) and using the expression $\mathbf{B} = \nabla \otimes \mathbf{A}_\perp$ in which only the radiative (gauge invariant) part of the vector potential is involved. In this way we obtain:

$$\mathbf{J}_{long} = \int d^3r \ \varrho(\mathbf{r} \times \mathbf{A}_\perp) \tag{1.93}$$

$$\begin{aligned} \mathbf{J}_{rad} &= \varepsilon_0 \sum_{i=x,y,z} \int d^3r \ E_i^\perp (\mathbf{r} \times \nabla) A_i^\perp + \varepsilon_0 \int d^3r \ \mathbf{E}_\perp \times \mathbf{A}_\perp \\ &= \mathbf{L}_{rad} + \mathbf{S}_{rad} \end{aligned} \tag{1.94}$$

Since we are dealing with free EM fields (there are no charges or electric currents) the longitudinal part can be neglected, and it seems that we have finally obtained the desired separation and the gauge independence of both the components. Unfortunately this expression leads to other problems when moving to a quantum treatment. In particular these problems concern the fact that the respective quantum operators do not satisfy the algebra of angular momenta. In this way they do not generate rotations nor in physical space neither in the polarization one.

Among the various efforts to solve this problem it has been suggested that for a correct separation to hold, one has to take into account the angular momentum flux density rather than the angular momentum density [16]. However, fortunately most of the case we will deal with can be treated in the so called "paraxial approximation" for which this separation works finely.

1.2.2 Angular Momentum separation in Paraxial Wave Approximation

Dealing with solutions that are "paraxial", the problem of the separation between the internal and the external component of the AM can be easily carried out. A paraxial wave is

essentially a wave for which energy travels in a defined direction. Solutions of the Helmholtz equation (1.13) such as plane waves and spherical waves are not suited to describe light beams commonly used in laboratories since the former have an infinite extension while the latter do not possess a privileged direction for the propagation.

In order to solve this issue, the so called paraxial wave approximation is used. This consists in searching for solutions of (1.13) of the form:

$$E(x,y,z) = A(x,y,z)e^{-ikz} \tag{1.95}$$

where we have supposed the wave to propagate along the z direction. The complex envelope $A(x,y,z)$ is a slowly varying function of z within distances of the order of wavelenght λ:

$$\frac{d^2A}{dz^2} \ll k\frac{dA}{dz} \tag{1.96}$$

so that this wave locally behaves as a plane wave with the normals to the wave fronts that are paraxial rays, i.e. they form small angles with the propagation direction. Taking into account (1.96), by substituting (1.95) into the Helmholtz equation, we obtain the following paraxial Helmholtz equation:

$$\nabla_T^2 A + 2ik\frac{dA}{dz} = 0 \tag{1.97}$$

where ∇_T is the transverse Laplace operator,

$$\nabla_T^2 = \frac{\partial^2}{\partial r^2} + \frac{1}{r}\frac{\partial}{\partial r} + \frac{1}{r^2}\frac{\partial^2}{\partial \varphi^2} \tag{1.98}$$

As previously said in section 1.2.1, the general expression for the total AM emerging from Noether theorem is:

$$\mathbf{J} = \sum_{i=x,y,z} \varepsilon_0 \int d^3r\ E_i(\mathbf{r}\times\nabla)A_i + \varepsilon_0 \int d^3r\ \mathbf{E}\times\mathbf{A} \tag{1.99}$$

Expression (1.99) for a plane wave given by:

$$\mathbf{E} = \mathbf{E_0} e^{-i\omega t} + \mathbf{E_0}^* e^{i\omega t} \tag{1.100}$$

can be written as:

$$\mathbf{J} \;=\; \tfrac{\varepsilon_0}{2i\omega} \sum_{i=x,y,z} \int d^3r \; E_i^* (\mathbf{r} \times \nabla) E_i + \varepsilon_0 \int d^3r \; \mathbf{E}^* \times \mathbf{E} \tag{1.101}$$

It can be demonstrated that in paraxial approximation, when considering the z component of the total AM J_z, its two components [11]:

$$S_z \simeq \frac{\varepsilon_0}{2i\omega} \iint r dr d\varphi (E_x^* E_y - E_y^* E_x) \tag{1.102}$$

$$L_z \simeq \frac{\varepsilon_0}{2i\omega} \iint r dr d\varphi (E_x^* \frac{\partial}{\partial \varphi} E_x + E_y^* \frac{\partial}{\partial \varphi} E_y) \tag{1.103}$$

behave as real angular momenta even in the quantum regime.

1.2.3 Hermite-Gauss and Laguerre-Gauss modes

There are many solutions of pratical interest of the equation (1.97) depending on the specific problem and on the particular choice of the coordinate system. In cartesian coordinates this equation leads to the so called Hermite-Gauss (HG) beams that are a family of spatial modes whose field distribution has the following expression:

$$E_{lm}(x,y,z) = E_{lm} \frac{w_0}{w(z)} H_l \left(\frac{\sqrt{2}x}{w(z)} \right) H_m \left(\frac{\sqrt{2}y}{w(z)} \right) e^{-\frac{x^2+y^2}{w^2(z)}} e^{-i\left(\frac{kr^2}{2R(z)} + kz + (m+l+1)\xi\right)} \tag{1.104}$$

where $H_l(x)$ are the Hermite polynomials of order l. These modes have an intensity distribution in a transverse plane, with respect to the propagation direction, shown in fig. 1.5 and propagate with paraboloidal wavefronts.

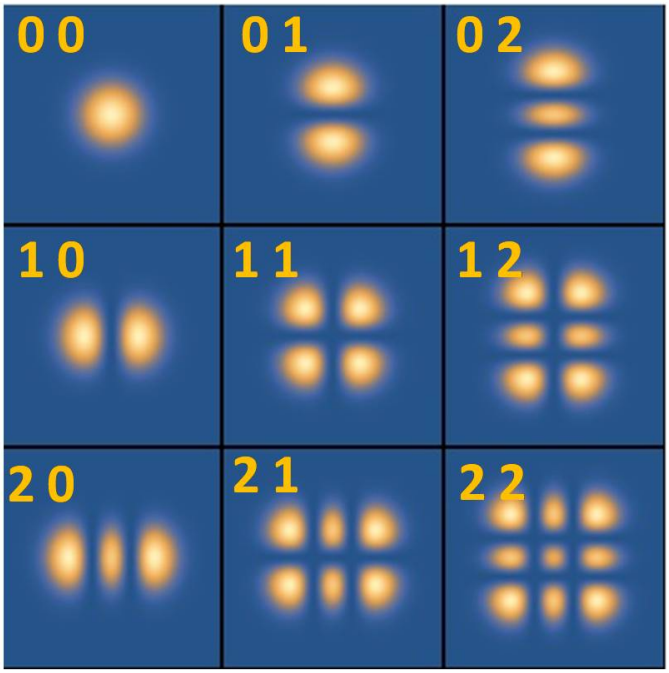

Figure 1.5: Hermite-Gauss modes intensity profiles. The numbers in the picture correspond respectively to the couple l, m.

The lowest order corresponding to the choice $l = m = 0$ represents the so called "*Gaussian beams*" suitable to describe the radiation field produced by a common laser source, whose expression is:

$$E(x, y, z) = E_{00} \frac{w_0}{w(z)} e^{-\frac{x^2+y^2}{w^2(z)}} e^{-i\left(\frac{kr^2}{2R(z)} + kz + \xi\right)} \tag{1.105}$$

The attribute "Gaussian" is referred to the fact that its intensity distribution, in a plane orthogonal to the propagation direction, is a Gaussian with a width given by $w(z)$, called *spot size*. The latest depends on z in the following way:

$$w(z) = w_0 \sqrt{1 + \left(\frac{z}{z_0}\right)^2} \tag{1.106}$$

and assumes the smallest value w_0, called *beam waist*, in $z = 0$, given by:

$$w_0 = \sqrt{\frac{\lambda z_0}{\pi}} \tag{1.107}$$

with z_0 being the *Raileigh distance* where $w(z_0) = \sqrt{2}w_0$. In expression (1.105) $R(z)$ is the *curvature radius*,

$$R(z) = z\left[1 + \left(\frac{z}{z_0}\right)^2\right] \tag{1.108}$$

that is null in correspondence of the waist, determining an infinite value for the curvature (plane wavefront). Eventually $\xi = \tan^{-1}(\frac{z}{z_0})$ is the *Gouy phase* and denotes the retardation with respect to a plane wave. A different choice of the coordinate system, more convenient for problems exhibiting a cylindrical simmetry, leads to the so called Laguerre-Gauss (LG) beams:

$$E(r,\theta,z) = E_{mp}\frac{w_0}{w(z)}\left(\frac{\sqrt{2}r}{w(z)}\right)^{|m|} L_p^{|m|}\left(\frac{2r^2}{w^2(z)}\right) e^{-\frac{r^2}{w^2(z)}} e^{-i\left(k\frac{r^2}{2R(z)}+kz+m\theta-(2p+1+|m|)\xi\right)} \tag{1.109}$$

that are a family of solutions of the paraxial Helmholtz equation in cylindrical coordinates. $L_p^{|m|}$ are the generalized Laguerre polynomials, whose expression is given by:

$$L_p^{|m|} = \sum_{k=0}^{p}(-1)^k\binom{p+m}{p-k}\frac{x^k}{k!} \tag{1.110}$$

where $x = \frac{2r^2}{w^2(z)}$ and p and m are two parameters. The intensity distribution of this familiy of spatial modes, shown in fig. 1.6, is deeply different from the one of (1.104). LG modes have an intensity distribution, in a transverse plane, characterized by the presence of alternating dark and bright concentric rings whose number is given by $p+1$, where p is the radial index and corresponds to the number of radial nodes.

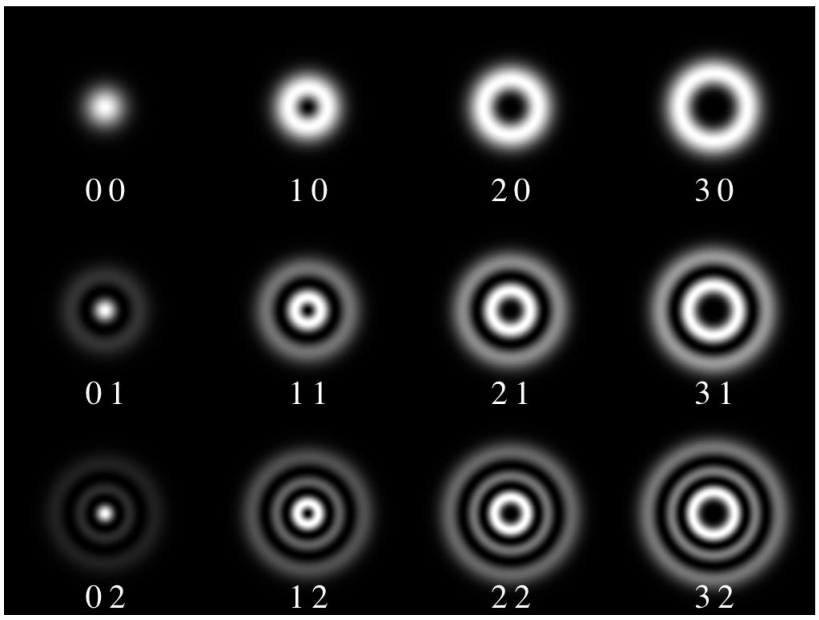

Figure 1.6: Laguerre-Gauss modes intensity profile. Image taken from Wikipedia.

This behaviour is due to the presence in (1.109) of the azimuthal phase term $e^{im\theta}$. The central point ($r = 0$) in which the field vanishes is a phase singularity (where both the real and the imaginary amplitude of the field vanish making the phase undefined) referred to as *optical vortex*. Besides having a different intensity distribution, (1.104) and (1.109) possess different physical properties. Indeed another consequence of the presence of an azimuthal phase dependence is the fact that LG modes carry OAM whose amount is determined by the value of $|m|$. This value is the *topological charge* of the vortex and is defined as:

$$m = \oint_C \nabla\chi d\mathbf{s} \tag{1.111}$$

that is the closed path integral of the gradient of the phase $\chi = k\frac{r^2}{2R(z)} + kz + m\theta - (2p+1+|m|)\xi$ around the singularity. This translates into helical wavefronts, see fig. 1.7, consituted by $|m|$ winding helices.

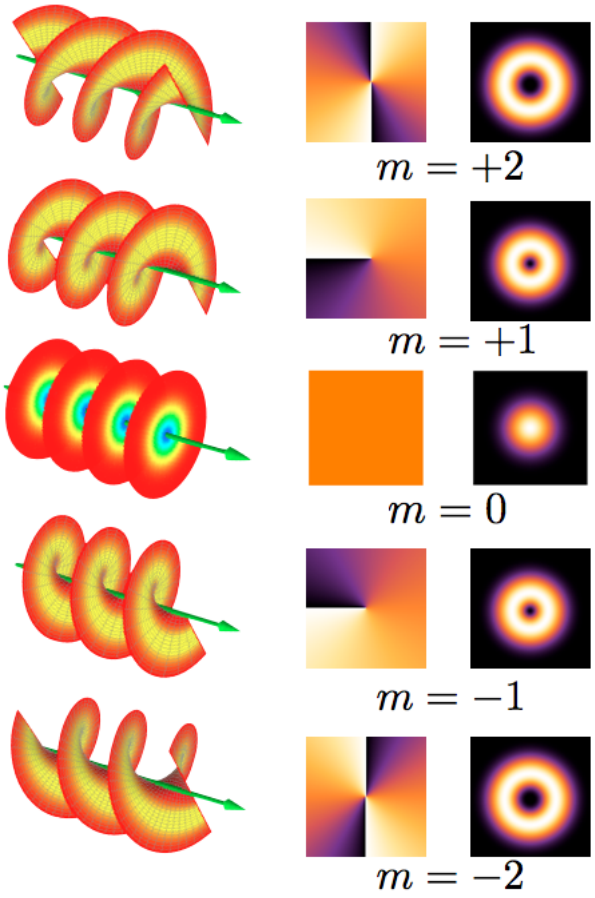

Figure 1.7: Different helical wavefronts are shown in the left column. In the central column the phase fronts, and in the right one the corresponding intensity distributions. Image taken from Wikipedia.

LG beams are not the only ones carrying OAM, indeed Ince-Gaussian modes [17], Bessel-Gaussian modes [18], Hypergeometric modes [19], Hypergeometric-Gaussian modes [20] are all eigenstates of OAM.

1.2.4 How to generate and manipulate SAM

The polarization of the EM field can be manipulated through optical devices that take advantage of the anisotropies of matter. These devices are capable to modify the state of polarization of a single photon or a light beam. The polarization state of a light beam can be manipulated via wave plates and polarizers. When a light beam crosses a polarizer,

the emerging field is linearly polarized and its electric field oscillates along a well defined direction.

A convenient way to treat analitically the problem is to introduce the Jones matrix formalism. In this formalism the polarization state of the field is represented by a two-dimensional vector. By using the Dirac notation, if we choose the two-dimentional basis constituted by the vectors $|H\rangle$ and $|V\rangle$ given by:

$$|H\rangle = \begin{pmatrix} 1 \\ 0 \end{pmatrix} \tag{1.112}$$

$$|V\rangle = \begin{pmatrix} 0 \\ 1 \end{pmatrix} \tag{1.113}$$

where $|H\rangle$ and $|V\rangle$ stand for horizontal and vertical linear polarization, then a polarizer that transmits radiation only along the horizontal direction is represented in a such space by a 2×2 matrix:

$$P_H = \begin{pmatrix} 1 & 0 \\ 0 & 0 \end{pmatrix} \tag{1.114}$$

The general expression for a polarizer that transmits only the component of the field along a certain direction $\hat{n}$ is given by the following matrix:

$$P_\phi = \begin{pmatrix} \mathrm{cos}^2\phi & \frac{1}{2}\mathrm{sin}2\phi \\ \frac{1}{2}\mathrm{sin}2\phi & \mathrm{sin}^2\phi \end{pmatrix} \tag{1.115}$$

where ϕ is the angle that the direction of the electric field forms with the horizontal direction.

There are other equivalent basis suitable to describe the state of polarization of light, one is the circular basis constituted by the vectors $|R\rangle$ and $|L\rangle$ respectively indicating right circular polarization and the left circular one. A way to circularly polarize a previously linearly polarized beam is through wave plates. These optical devices are constituted by a slab of material exhibiting birefringence. In the Jones formalism a wave plate is represented

by the matrix:

$$WP(\delta,\phi) = \begin{pmatrix} \cos\frac{\delta}{2} + i\sin\frac{\delta}{2}\cos 2\phi & i\sin\frac{\delta}{2}\sin 2\phi \\ i\sin\frac{\delta}{2}\sin 2\phi & \cos\frac{\delta}{2} - i\sin\frac{\delta}{2}\cos 2\phi \end{pmatrix} \tag{1.116}$$

where δ represents the retardation introduced by the device while ϕ is the direction in which the fast axis is oriented with respect to the horizontal. The value of δ individuates different kinds of wave plate carrying out different transformations:

$$\delta = \frac{\pi}{2} \quad \text{quarter wave plate} \tag{1.117}$$

$$\delta = \pi \quad \text{half wave plate} \tag{1.118}$$

$$\delta = 2\pi \quad \text{full wave plate} \tag{1.119}$$

A full wave plate acts as an identical transformation leaving unchanged the state of polarization. A Half Wave Plate (HWP),

$$HWP = WP(\pi,\phi) = \begin{pmatrix} i\cos 2\phi & i\sin 2\phi \\ i\sin 2\phi & -i\cos 2\phi \end{pmatrix} \tag{1.120}$$

when crossed by a linearly polarized wave, rotates of 2ϕ its direction of polarization. Eventually a Quarter Wave Plate (QWP) can transform the polarization of a beam from linear to circular if the direction of polarization forms a $\pm\frac{\pi}{4}$ angle with the fast axis.

$$QWP = WP(\frac{\pi}{2},\pm\frac{\pi}{4}) = \frac{1}{\sqrt{2}}\begin{pmatrix} 1 & \pm i \\ \pm i & 1 \end{pmatrix} \tag{1.121}$$

1.2.5 How to generate and manipulate OAM carrying beams

Vortex beams find many applications in fundamental investigation but also in many pratical uses. In this context the generation and the manipulation of both single photons and beams carrying an intented amount of OAM is a crucial issue. In other words there is the need to

have a device capable of converting a Gaussian mode outing from a common laser source into a helical beam with the desired $e^{im\varphi}$ phase dependence.

Nowadays there are many ways to generate OAM such as Spiral Phase Plates (SPP), Spatial Light Modulators (SLM), Computer-Generated Holograms (CGH), or Q-Plates (QP). Only one of these methods, involving QP, will be treated more in detail in the following since this is the device we employ in this thesis to generate vortex beams.

1.2.5.1 Q-Plate

The optical devices we have mentioned up to now act only on the spatial distribution of the field that can be modulated through the non-uniformity of isotropic media (such as holograms). On the other hand, as we have seen before, polarization can be controlled by taking advantage of the anisotropy.

Combining these two properties of materials gives rise to a spin-orbit coupling device, the QP. More in detail QP is constituted by a thin Liquid Crystal (LC) film sandwiched between two glasses whose optic axis form a non-uniform pattern in the transverse plane characterized by the topological charge q that is an integer or half-integer number. This device is able to couple polarization and OAM degrees of freedom by making the crossing beam acquire OAM with an amount depending on the topological charge ($l = 2q\hbar$), and a sign, along the propagation direction, depending on the polarization of the incoming beam.

Due to the intrinsic birefringence of liquid crystals q-plate acts as an ordinary waveplate by introducing a retardation δ between the components of the field in the directions of the slow and the fast axis. This retardation depends on the thickness of the plate (that is homogenous), the wavelength of the radiation, the ordinary and extraordinary refractive indices of LCs and the orientation of the optic axes of the molecules with respect to the propagation direction. As will be more clear in the following, in optimal "working conditions" this retardation has to be π, so that the device acts as a half wave plate on the polarizarization:

$$HWP = \begin{pmatrix} \cos 2\alpha & \sin 2\alpha \\ \sin 2\alpha & -\cos 2\alpha \end{pmatrix} \tag{1.122}$$

where $\alpha = \tan^{-1}\left(\frac{n_y}{n_x}\right)$, and $\hat{n} = (n_x, n_y)$ the direction of the LCs molecular director. For example for a circularly polarized input beam:

$$HWP\,|R\rangle \propto |L\rangle\, e^{-2i\alpha} \tag{1.123}$$

$$HWP\,|L\rangle \propto |R\rangle\, e^{2i\alpha} \tag{1.124}$$

In a q-plate α is patterned:

$$\alpha = q\varphi + \alpha_0 \tag{1.125}$$

so, by substituting (1.125) into (1.123) and (1.124) we have:

$$QP_\pi\,|L,0\rangle \propto |R\rangle\, e^{2iq\varphi} e^{2i\alpha_0} = |R,2q\rangle\, e^{2i\alpha_0} \tag{1.126}$$

$$QP_\pi\,|R,0\rangle \propto |L\rangle\, e^{-2iq\varphi} e^{-2i\alpha_0} = |R,-2q\rangle\, e^{-2i\alpha_0} \tag{1.127}$$

Eventually in the most general case in which δ can assume all values in the range $[0, 2\pi]$

$$QP_\delta\,|L,m\rangle = \cos\left(\frac{\delta}{2}\right)|L,m\rangle + i\sin\left(\frac{\delta}{2}\right) e^{2i\alpha_0}\,|R,m+2q\rangle \tag{1.128}$$

$$QP_\delta\,|R,m\rangle = \cos\left(\frac{\delta}{2}\right)|R,m\rangle + i\sin\left(\frac{\delta}{2}\right) e^{-2i\alpha_0}\,|L,m-2q\rangle \tag{1.129}$$

So in this case a part of the incoming signal remains unconverted while the other part inverts its circular polarization and acquires $\pm 2q$ unit of OAM, in the direction of propagation, depending on whether the intial polarization is left or right respectively. If the ingoing beam is linearly polarized, the action of the q-plate can be derived by rewriting it in the circular basis:

$$|H\rangle = \frac{1}{\sqrt{2}}\left(|R\rangle + |L\rangle\right) \tag{1.130}$$

$$|V\rangle = \frac{1}{\sqrt{2}}\left(|R\rangle - |L\rangle\right) \tag{1.131}$$

and using (1.128) and (1.129) for each component. The retardation can be controlled by

applying to the plates an alternate voltage [21] and depends on the temperature [22]. In fig 1.8 an example of the action of a QP.

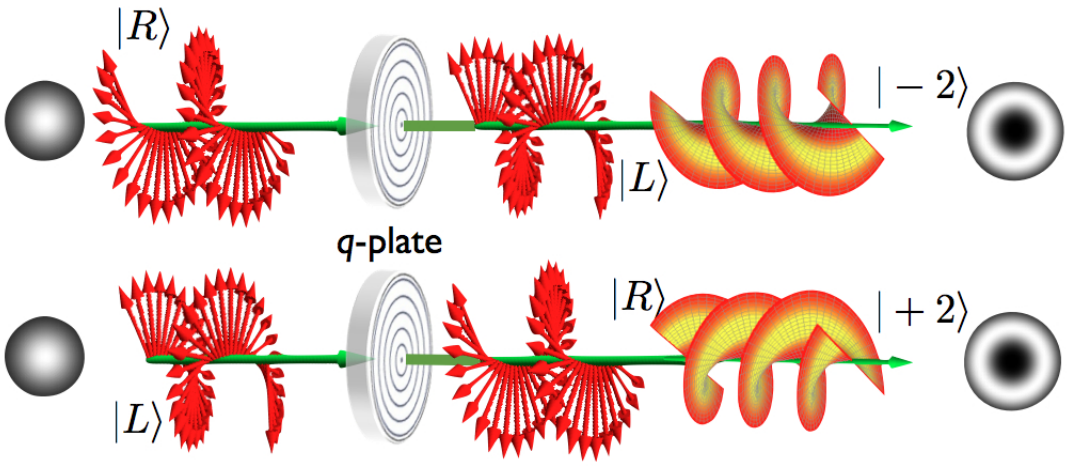

Figure 1.8: Example of a QP with topological charge 1 acting on a right- and a left- circular polarized Gaussian input. Image taken from Wikipedia.

1.3 Entanglement

1.3.1 Entanglement for pure states

Entanglement is a genuine quantum property that arises when two subparts of a compound system share correlations stronger than any classical interaction. These quantum correlations are so intense that it is impossible to describe each single part of the system independently of the other one, whatever their reciprocal distance is.

Entanglement finds a lot of applications in many quantum communication protocols, hence it is important to build a formal apparatus to achieve both characterization and quantification of this property. Bipartite pure states are the simplest scenario to define entanglement, although many efforts are oriented to achieve a conclusive characterization even in the cases of mixedness and multipartite systems; not the least the case of systems with an infinite Hilbert space where entanglement can occur among degrees of freedom with continuous spectra.

Let us now recall the concept of pure states. A quantum system is in a pure quantum

state when it can be described by a vector $|\psi\rangle$ in its Hilbert space. Pureness corresponds to the maximum information encodable in a state, that is the ability of predicting the outcome of a measurement performed on it. Indeed in pure states the uncertainity is restricted only to the quantum one. A bipartite state is constituted by two subsystems A and B and its Hilbert space turns to be the vector product of the two Hilbert subspaces $\mathcal{H}_A$ and $\mathcal{H}_B$:

$$\mathcal{H} = \mathcal{H}_A \otimes \mathcal{H}_B \tag{1.132}$$

We can finally define an *entangled* or *not separable* state as a state that cannot be written as a product:

$$|\psi\rangle_{AB} \text{ is entangled } \iff |\psi\rangle_{AB} \neq |\varphi\rangle_A \otimes |\eta\rangle_B \tag{1.133}$$

where $|\varphi\rangle_A \epsilon\, \mathcal{H}_A$ and $|\eta\rangle_B \epsilon\, \mathcal{H}_B$. Although being intuitive, this definition is not suitable to pratical uses and an operational criterion to state whether a system is entangled or not is needed. It can be seen that for a bipartite pure state it is always possible to find the following decomposition:

$$|\psi\rangle_{AB} = \sum_{i=1}^{d} \lambda_i |\varphi_i\rangle_A |\chi_i\rangle_B \qquad \lambda_i \geq 0, \qquad \sum_{i=1}^{d} \lambda_i = 1 \tag{1.134}$$

where $d = \min\{\dim\mathcal{H}_A, \dim\mathcal{H}_B\}$ and $|\varphi_i\rangle$ and $|\chi_i\rangle$ are orthonormal vectors belonging respectively to $\mathcal{H}_A$ and $\mathcal{H}_B$. This decomposition is known as *Schmidt decomposition* and is unique, while the number d (number of the $\lambda_i \neq 0$) is the *Schmidt number*. Relation (1.134) provides the following criterion to witness the presence of entanglement:

$$|\psi\rangle_{AB} \text{ is entangled } \iff d > 1 \tag{1.135}$$

1.3.2 Entanglement for mixed states

Opposed to pure states there are mixed states that are statistical ensambles in which the state of the system is described by a sum of vectors belonging to the Hilbert space, each with a certain probability (e.g. the state of unpolarized light). The case of mixedness is more plausible in the practice since in most of the cases the state of the system is not known and

the previous description fades making way for the density matrix formalism. The density matrix is analog to phase-space probability in classical statistical mechanics. It is defined as:

$$\hat{\rho} = \sum_n p_n \left|\psi_n\right\rangle \left\langle\psi_n\right| \tag{1.136}$$

where the coefficients p_n are non-negative and add up to 1 and $|\psi_n\rangle$ are vectors of the Hilbert space not necessary mutually orthogonal. These are classical probabilities making this state different from a quantum supersposition. Indeed while a quantum superposition, descending from the linearity of the Schrödinger equation, is characterized by a quantum uncertainty on the measure of an observable, the indetermination on a mixed state is both classical and quantum. The density matrix operator is semi-positive definite, Hermitian and $\mathrm{Tr}\,(\hat{\rho}) = 1$. In case of pure states, it assumes the following form of a projector:

$$\hat{\rho} = \left|\psi\right\rangle \left\langle\psi\right| \tag{1.137}$$

and, besides the property listed above, the operator is also idempotent $\rho^2 = \rho$. Due to this property characterizing pure states, it is natural to introduce a measurement of the pureness of a quantum state as to be

$$\mu = \mathrm{Tr}\left(\hat{\rho}^2\right) = 1 \tag{1.138}$$

that can take values in the range $[1/N, 1]$ for a system endowing a $n-$dimensional Hilbert space. The minimum of the range corresponds to a maximally mixed state that coincides with the maximum blindness on the knowledge of the state. It is worth noting that the density matrix does not identify univocally the state of the system since different ensambles of states can possess the same density operator. In particular it is possible to define a class of states sharing the same density matrix as those states that are equal up to a unitary transformation. Up to now we have dealt with systems defined on a single Hilbert space. Let us consider a bipartite state constituted by two susbsystems A and B endowing the Hilbert space $\mathcal{H} = \mathcal{H}_A \otimes \mathcal{H}_B$. If $\hat{\rho}_{AB}$ is the density matrix of the whole system, it is possible to define

the reduced density matrix relative to one of the two subsystems as:

$$\hat{\rho}_A = \mathrm{Tr}_B(\hat{\rho}_{AB}) \quad (\hat{\rho}_B = \mathrm{Tr}_A(\hat{\rho}_{AB})) \tag{1.139}$$

that is itself a density matrix. Once the partial density matrix is defined, it is worth noting that the Schmidt decomposition, previously introduced, corresponds to the pure states:

$$\hat{\rho}_A = |\varphi\rangle \langle\varphi| \tag{1.140}$$

$$\hat{\rho}_B = |\chi\rangle \langle\chi| \tag{1.141}$$

when the Schmidt number is 1. Conversely if $d > 1$

$$\hat{\rho}_A = \sum_{i=1}^{d} \lambda_i^2 |\varphi_i\rangle \langle\varphi_i| \tag{1.142}$$

$$\hat{\rho}_B = \sum_{i=1}^{d} \lambda_i^2 |\chi_i\rangle \langle\chi_i| \tag{1.143}$$

this means that entanglement has something to do with local mixedness. In analogy with pure states, we can now define a mixed bipartite state to be separable if and only if:

$$\hat{\rho}_{AB} = \sum_i \lambda_i (\phi_A \otimes \phi_B) \tag{1.144}$$

with $\lambda_i > 0$,$\sum_i \lambda_i = 1$, and ϕ_A and ϕ_B states respectively belonging to the two Hilbert subspaces.

An operative way to witness entanglement in such a case is represented by the *Peres–Horodecki condition* [23, 24]. This criterion is also known as "*Positivity under Partial Trasposition*" (PPT) since it is based on the simple idea that if a quantum system is separable, a local trasformation (e.g. partial transposition) carried out on one of its subparts has not to have consequences on the other subsystems.

More in detail, this criterion states that by taking the partial transpose of the density

matrix belonging to only to one of the subsystems A or B of a state that is separable, i.e. for which relation (1.144) stands, none of the eigenvalues of $\varrho_k^{T(A)}$ has to be negative. Hence if $(\varrho^i)^T \ngeq 0,\ (i = A, B)$ then the bipartite state is entangled. This criterion represents a necessary and sufficient condition for separability for 2×2 and 2×3 Hilbert spaces as proven by Horodecki.

Up to now we have considered systems with a discrete Hilbert space. In the next section the characterization of entanglement will be discussed for CV systems with particular attention to GSs of continuos variable for which, as will be more clear in the following, this problem considerably simplifes.

1.4 Gaussian states

A particular class of CV states is that of Gaussian states. The paramount importance of this class of quantum states in CV systems stems from the feasibility to both generate and manipulate them with a high degree of control, thanks to the techniques and devices commonly present in optics labs. Beyond their formal definition, that will be given in the following, GSs have privileges both from a theoretical and an experimental point of view.

GSs include ground and thermal states of all physical systems in the harmonic approximation in particular for what concerns the EM field are Gaussian states, thermal states, squeezed and squeezed thermal states but also coherent states that are the ones currently produced by a common laser source. As we are going to see more in detail the formalism required to completely characterize a GS consists of few elements making this class of states equally powerful and essential. Moreover the Gaussianity of the state survives to most of the transformations carried out in a laboratory with linear optical devices since they are represented, in the Hilbert space of the system, by transformations that map GSs into GSs.

Moreover the understanding and the quantification of entanglement properties are easily handling for this class of states. In particular for bipartite Gaussian states there are some necessary and sufficient criteria to witness the presence of quantum correlations. In this section we are going to hint, without claiming to be complete, the phase space description of

a quantum system since GSs live in such space. Then we will formally define GSs and their basic properties. After introducing single-mode GSs a particular attention will be devoted to bipartite GSs since they have a leading role in this dissertation and are the simplest scenario to investigate CV Gaussian states entanglement. Eventually there will be given the tools to establish whether a state is entangled and the topic of Gaussian states transmission over a noisy channel, essential for communications, will be faced.

1.4.1 Phase space description of quantum systems

When considering a quantum system there are different ways to construct a formal apparatus convenient for its description. The most common one is the operator formalism in which a quantum system is characterized by observables (that are the quantities actually accessible via experiments) represented by Hermitian operators defined in the Hilbert space of the system itself. Also the quantum state of the system is described by an operator, the density matrix, whose knowledge gives the full information about its current state and its evolution. An alternative approach consists in the phase space formulation in which a $2n$-dimensional phase space, instead of a n-dimensional Hilbert space, is involved. This approach is similar to the classical Hamiltonian formalism so making easier the understanding of the "transition" between the classical and the quantum regime.

More in detail, from a classical perspective, the Hamiltonian formalism takes place on the phase space that is a manifold on which the Poisson parenthesis are introduced. Observables are represented by functions of the canonical position and momentum $f(q(t), p(t), t)$ defined in phase space and their evolution, under a certain Hamiltonian H, is determined by the Poisson parenthesis:

$$\{f, g\} = \sum_{i=1}^{n} \frac{\partial f}{\partial q_i}\frac{\partial g}{\partial p_i} - \frac{\partial f}{\partial p_i}\frac{\partial g}{\partial q_i} \tag{1.145}$$

as:

$$\frac{df(q(t), p(t), t)}{dt} = \{f, H\} + \frac{\partial f}{\partial t} \tag{1.146}$$

In the usual operatorial approach, when "switching to quantum", positions and momenta

become non-commuting operators defined on a Hilbert space and the state of the system is no more a point of phase space but it becomes a vector of the Hilbert space or in the more general case, in which the description of mixed states is encompassed, a density matrix ϱ. The canonical quantization is made by adopting the so called *correspondence principle* that associates to each classical function g of the phase space an operator $\hat{g}$ in Hilbert space and replaces Poisson parenthesis with commutators. Although being quite easy in the case of position and momentum operators, for more complex operators this quantization method is affected by the operators ordering problem that becomes crucial. This problem has been solved by Weyl who introduced a map stating a one-to-one correspondence between functions and normal ordered operators. Moreover Wigner introduced a quasi-probability distribution (it can assume negative values) that is exactly the function associated in the phase space by the Weyl map to the density matrix.

The Wigner distribution is not the only possible one, there exist other distributions such as Husimi quasi-probability distribution and the Glauber-Sudarshan one, depending respectively on whether observables are expressed by using normal or symmetric ordering.

When dealing with electromagnetic field it is more correct to talk about *optical phase space* that is the space of EM field quadratures X and Y (position- and momentum-like operators) whose definition and commutation rules have been given in previous sections and will be recalled later.

1.4.2 Gaussian states definition

The best way to deal with GSs is to use the theoretical phase-space approach [9, 25]. Let us start by introducing the basic notation and concepts essential to provide a formal definition of a GS. As discussed before, the quantized EM field, or more in general a system made of n bosons, can be treated by considering each mode k ($k = 1, ..., n$) of the field as an independent harmonic oscillator described by the annihilation and the creation operators $\hat{a}_k$ and $\hat{a}_k^\dagger$ that respectively destroy and create a photon with frequency ω_k. We recall that these

two operators satisfy the following commutation rule:

$$\left[\hat{a}_k, \hat{a}_l^\dagger\right] = \delta_{kl} \tag{1.147}$$

from wich descends the non-commutativity of the position- and momentum-like operators for the $k-th$ mode that we defined as to be the amplitude and the phase quadratures of the EM field. The commutation rule between the quadratures can be written in the following more convenient way that is more suitable to the symplectic structure of the phase space and enables us to use a more compact notation,

$$\left[\hat{R}_k, \hat{R}_l\right] = i\Omega_{kl} \tag{1.148}$$

where $\hat{R}$ is the column vector $\hat{R} = \left(\hat{X}_1, \hat{Y}_1, ...\hat{X}_n, \hat{Y}_n\right)^T$ and Ω is the symplectic matrix, given by:

$$\Omega = \bigoplus_{k=1}^{n} \omega \qquad \omega = \begin{pmatrix} 0 & 1 \\ -1 & 0 \end{pmatrix} \tag{1.149}$$

satisfying $\Omega^T = -\Omega = \Omega^{-1}$. So we have abandoned the tensor product structure of the $n-$dimensional Hilbert space to switch to a $2n-$dimensional phase space $\wp = (\mathbb{R}^{2n}, \Omega)$ having a direct sum structure.

While the system is described by a density matrix $\hat{\varrho}$ in the Hilbert space, it is possible to associate to it the following *characteristic function* in phase space:

$$\chi\left[\hat{\varrho}\right](\Lambda) = \mathrm{Tr}\left[\hat{\varrho}\,\exp\left\{-i\Lambda^T\Omega\hat{R}\right\}\right] \tag{1.150}$$

where $\Lambda = (a_1, b_1, ...a_n, b_n)^T \epsilon\, \mathbb{R}^{2N}$, $\hat{D}(\Lambda) = \exp\left\{-i\Lambda^T\Omega\hat{R}\right\} = \bigotimes_{k=1}^{n} \hat{D}_k(\lambda_k)$, with $\hat{D}_k(\lambda_k) = \exp\left\{\lambda_k\hat{a}_k^\dagger - \lambda_k^*\hat{a}_k\right\}$ being the single-mode displacement operator defined in subsection 1.1.5.2 and $\lambda_k = \frac{1}{\sqrt{2}}(a_k + ib_k)$. We are now ready to define a GS state as a continuous variable state with a Gaussian characteristic function, in other words a state is Gaussian if and only if its

characteristic function can be written as:

$$\chi\left[\hat{\varrho}\right](\Lambda) = \exp\left\{-\frac{1}{2}\Lambda^T\Omega\sigma\Omega^T\Lambda - i\Lambda^T\Omega\left\langle\hat{R}\right\rangle\right\} \tag{1.151}$$

where σ is the Covariance Matrix (CM) (second moments) whose elements are:

$$\sigma_{kl} = \frac{1}{2}\left\langle\left\{\hat{R}_{k,},\hat{R}_l\right\}\right\rangle - \left\langle\hat{R}_k\right\rangle\left\langle\hat{R}_l\right\rangle \tag{1.152}$$

with $\left\{\hat{R}_{k,},\hat{R}_l\right\} = \hat{R}_k\hat{R}_l + \hat{R}_l\hat{R}_k$ being the anticommutator and $\left\langle\hat{R}\right\rangle = \mathrm{Tr}\left[\hat{\varrho}\hat{R}\right]$ the *first-moment vector*. Since the commutation rule (1.147) holds, it can be proven that this matrix has to fulfill the following constraint,

$$\sigma + \frac{i}{2}\Omega \geq 0 \quad \text{(bona fide condition)} \tag{1.153}$$

also implying $\sigma \geq 0$; in order to have a corresponding positive-semidefinite matrix $\hat{\varrho}$ and consequently a "physical" GS. The CM can be re-organized in a block form that will prove to be usefull in the following when we will deal with entanglement of GSs:

$$\sigma = \begin{pmatrix} \sigma_1 & \upsilon_{12} & \cdots & \upsilon_{1n} \\ \upsilon_{12}^T & \sigma_2 & \cdots & \upsilon_{2n} \\ \vdots & \vdots & \ddots & \vdots \\ \upsilon_{1n}^T & \upsilon_{2n}^T & \cdots & \sigma_n \end{pmatrix} \tag{1.154}$$

σ_k are 2×2 matrices corresponding to the single-mode k while υ_{ij} are 2×2 matrices too, but they relate a mode to each other indicating potential correlations both quantum and classical. In particular for a product state the off-diagonal matrices vanish and the covariance matrix simply reduces to $\sigma = \bigoplus_{k=1}^{n}\sigma_k$. By taking the Fourier transform of the characteristic function we get the *Wigner function*:

$$W\left[\hat{\varrho}\right](X) = \frac{1}{(2\pi^2)^n}\int_{\mathbb{R}^{2n}} d^{2n}\Lambda\,\exp\left\{i\Lambda^T\Omega X\right\}\chi\left[\hat{\varrho}\right](\Lambda) \tag{1.155}$$

where $X = (x_1, y_1, ...x_n, y_n)^T \epsilon \mathbb{R}^{2n}$. It is possible to show that for a GS the Wigner function is still Gaussian and assumes the form:

$$W\left[\hat{\varrho}\right](X) = \frac{\exp\left\{-\frac{1}{2}\left(X - \left\langle \hat{R} \right\rangle\right)^T \sigma^{-1}\left(X - \left\langle \hat{R} \right\rangle\right)\right\}}{\pi^n \sqrt{\det\left[\sigma\right]}} \tag{1.156}$$

hence it is possible to indifferently refer to GSs as states with a Gaussian characteristic function or a Gaussian Wigner function in phase space. This function, as previously predicted, is real (if $\hat{\varrho}$ is Hermitian) and it is a quasi-probability distribution since it can assume negative values. A GS is completely specified by the first and the second statistical moments of the quadrature field operators.

Since it is possible to make the first moments to vanish by using local unitary operations, (e.g. displacements in phase space) while leaving unchanged any informationally relevant property, such as entanglement, from now on we will set them to 0 without any loss of generality. With this in mind, it is possible to rewrite the Wigner distribution as:

$$W\left[\hat{\varrho}\right](X) = \frac{\exp\left\{-\frac{1}{2}X^T\sigma^{-1}X\right\}}{\pi^n \sqrt{\det\left[\sigma\right]}} \tag{1.157}$$

So despite the infinite dimension of the Hilbert space, GSs have turned to be easy to characterize thanks to the fact that they can be simply encoded into the $2n \times 2n$ covariance matrix σ that contains all the information about the state. For instance the purity of a Gaussian state in phase space description is:

$$\mu\left(\hat{\varrho}\right) = \frac{1}{2^n \sqrt{\det\left[\sigma\right]}} \tag{1.158}$$

As predicted before, among the benefits of GSs, there is the Gaussianity robustness. GSs indeed, preserve their character, under all the unitary transformations generated by Hamiltonians that are at most bilinear in the bosonic mode operators. Indeed, this transformation carried out in the Hilbert space, corresponds to a symplectic transformation in phase space i.e. a transformation that does not alter the symplectic structure of the space. In other

words if we consider a classical system described by coordinates $\{q_1, ..., q_n\}$ and momenta $\{p_1, ..., p_n\}$, whose evolution is governed by the Hamiltonian H, then, equations of motion (Hamilton equations) are written as:

$$\dot{R}_m = \Omega_{mn} \frac{\partial H}{\partial R_n} \tag{1.159}$$

where the point stands for the time derivative and Ω is the symplectic matrix (1.149) introduced before. A transformation of coordinates represented by a $2n \times 2n$ matrix S, such that $R' = SR$, is canonical,

$$\dot{R}'_l = S_{lm} \Omega_{mn} S_{ni} \frac{\partial H}{\partial R'_i} \tag{1.160}$$

if and only if $S\Omega S^T = \Omega$ (*symplectic condition*), with $\det S = 1$. Such a transformation leaves unchanged the equations of motion and preserves the Poisson parenthesis. This, after quantization, translates in leaving unaffected the canonical commutation relations (1.148). It can be seen that all transformations fulfilling the symplectic condition form a group called the *symplectic group* $Sp(2n, \mathbb{R})$.

Among the symplectic transformations an extremely important role is played by the one that diagonalizes the CM. The diagonalizability of the CM is ensured by an important theorem due to Williamson [26] that states that the covariance matrix σ can always be written as:

$$\sigma = SWS^T \tag{1.161}$$

through a symplectic transformation $S \, \epsilon \, Sp(2n, \mathbb{R})$, where $W = \bigoplus_{k=1}^{n} d_k I_2$ is the covariance matrix of a n-mode thermal state with $N_k = d_k - \frac{1}{2}$ (average number of photons in the $k-th$ mode) and $\{d_k\}_{k=1}^n$ are the moduli of the symplectic eigenvalues $\{\pm d_k\}_{k=1}^n$ of $i\Omega\sigma$. In the Hilbert space formalism this translates in the statement that every Gaussian state $\hat{\varrho}$ can be obtained by starting from a thermal state $\hat{\nu}$ through a unitary transformation U_S associated to the symplectic matrix S that in turn has been generated by a Hamiltonian at most bilinear

in the field mode operators:

$$\hat{\varrho} = U_S \hat{\nu} U_S^\dagger \tag{1.162}$$

Eventually it can be shown that the uncertainty relation (1.153) imposes the following constraint:

$$d_k \geq \frac{1}{2} \; \forall k \tag{1.163}$$

on the covariance matrix symplectic eigenvalues. The above constraint represents nothing but that the symplectic representation of the uncertainty principle. Moreover from equation (1.158) it is easy to understand that for a pure GS, equation (1.163) is fulfilled with the equal sign.

It can be shown that the most general Hamiltonian that preserves Gaussianity can be written as:

$$\hat{H} = \sum_{k=1}^{n} g_k^{(1)} \hat{a}_k^\dagger + \sum_{k \geq l=1}^{n} g_{kl}^{(2)} \hat{a}_k^\dagger \hat{a}_l + \sum_{k,l=1}^{n} g_{kl}^{(3)} \hat{a}_k^\dagger \hat{a}_l^\dagger + h.c. \tag{1.164}$$

This Hamiltonian consists of three building blocks, each leading to a unitary evolution. The first term corresponds to the displacement operator, the second one instead encompasses two different processes. On one hand, when $k = l$ the process is that of free evolution and corresponds to nothing but that adding an overall phase term that although being meaningless in the case of a single-mode evolution, plays a crucial role in interference phenomena; in the context of optics this transformation is carried out by linear optical devices called *phase shifters*. On the other hand, the process that involves different mode operators corresponds to a linear mixing of the two modes; this is the typical transformation made by a *Beam Splitter* (BS).

Eventually the last addend describes the non-linear interaction in which starting from a photon of a certain energy and momentum, two photons are generated in the full respect of the energy and momentum conservation laws. This corresponds to the squeezing operator previously seen and, depending on the so called phase matching conditions, it is possible to generate the two photons in the same mode (single-mode squeezing) or in two different modes (two-mode squeezing). In order to carry out such a tansformation, due to the non

self-interacting character of EM, non-linear processes involving matter (non-linear crystals) are strictly necessary. So in conclusion a GS can be efficiently displaced, squeezed and rotated with current optical technologies without loosing its properties.

1.4.3 Single-mode Gaussian states

Let us now consider a single-mode GS starting from expression (1.162). It can be shown [9] that for a single-mode GS equation (1.162) can be rewritten as:

$$\hat{\varrho} = \hat{D}(\alpha)\,\hat{S}(\xi)\hat{\nu}_{th}(N)\,\hat{S}^{\dagger}(\xi)\hat{D}^{\dagger}(\alpha) \tag{1.165}$$

where $\hat{D}(\alpha)$ and $\hat{S}(\xi)$ are respectively the single-mode displacement and squeezing operators with $\xi = re^{i\psi}$, whose associated CM in phase space is given by:

$$\sigma = \frac{1+2N}{2}\begin{pmatrix} \cosh(2r)+\sinh(2r)\cos\psi & \sinh(2r)\sin\psi \\ \sinh(2r)\sin\psi & \cosh(2r)-\sinh(2r)\cos\psi \end{pmatrix} \tag{1.166}$$

while the first moments are $\left\langle \hat{R} \right\rangle = \sqrt{2}\left(\mathrm{Re}\left[\alpha\right], \mathrm{Im}\left[\alpha\right]\right)^{T}$. The purity of the state is given by:

$$\mu = \frac{1}{1+2N} \tag{1.167}$$

and depends only on the average number of thermal photons.

1.4.4 Two-mode Gaussian states

Two-mode GSs play an important role both in this dissertation and in the CV states scenario since they are the archetype of bipartite entanglement encoded into CV. According to what we said before, the 4×4 covariance matrix of a bipartite GS can be written in the following block form:

$$\sigma = \begin{pmatrix} A & C \\ C^{T} & B \end{pmatrix} \tag{1.168}$$

where A, B, C are two-dimentional matrices. It is possible to define four local symplectic invariats, i.e. quantities that are unaltered by a symplectic transformation,

$$I_1 = \det[A] \qquad I_2 = \det[B] \qquad I_3 = \det[C] \qquad I_4 = \det[\sigma] \tag{1.169}$$

It can be shown that the CM can be reduced to the following *standard* or *normal form*:

$$\sigma = \begin{pmatrix} a & 0 & c_1 & 0 \\ 0 & a & 0 & c_2 \\ c_1 & 0 & b & 0 \\ 0 & c_2 & 0 & b \end{pmatrix} \tag{1.170}$$

where:

$$a^2 = I_1 \qquad b^2 = I_2 \qquad c_1 c_2 = I_3 \qquad (ab - c_1^2)(ab - c_2^2) = I_4 \tag{1.171}$$

Also the two symplectic eigenvalues can be written in terms of these invariants as:

$$d_{\pm} = \sqrt{\frac{\triangle(\sigma) \pm \sqrt{\triangle(\sigma)^2 - 4I_4}}{2}} \tag{1.172}$$

with $\triangle(\sigma) = I_1 + I_2 + 2I_3$ and the uncertainty relation turns to be :

$$d_- \geq \frac{1}{2} \tag{1.173}$$

Among the two-mode GSs the two-mode squeezed thermal states are of huge relevance. These states are obtained by applying to a two-mode thermal state, the two-mode squeezing operator i.e.:

$$\varrho = S_2(\xi)\, \nu_{th}(N_1) \otimes \nu_{th}(N_2)\, S_2^{\dagger}(\xi) \tag{1.174}$$

The covariance matrix of such a state is proven to be:

$$\sigma = \frac{1}{2}\begin{pmatrix} A1_2 & CR_\xi \\ CR_\xi & B1_2 \end{pmatrix} \tag{1.175}$$

where $\xi = r$ is real and,

$$\begin{aligned} A &= (1 + N_1 + N_2)\cosh(2r) + (N_1 - N_2) \\ B &= (1 + N_1 + N_2)\cosh(2r) - (N_1 - N_2) \\ C &= (1 + N_1 + N_2)\sinh(2r) \end{aligned}$$

$$R_\xi = \text{sinh}r\begin{pmatrix} \cos\psi & \sin\psi \\ \sin\psi & -\cos\psi \end{pmatrix} \tag{1.176}$$

In particular if $N_1 = N_2 = 0$ the state is said to be a two-mode squeezed vacuum or a *Twin-Beam State* (TBS) since there is a perfect correlation in the number of photons of the two modes. A state of this kind can be generated by using single-mode squeezer and a linear mixer such as a BS.

1.4.5 Entanglement Criteria for Gaussian States

As stated before, entangled states are those states that are not separable; among them the simplest scenario is constituted by bipartite states.

In section (1.3.2) we introduced the PPT criterion as an operational way to assert whether a state is entangled or not. Although, the difficulties associated to perform both partial transposition and diagonalization, increase with the dimension of the space. In most of the cases, these operations are expected to became very difficult. These problems have been circumvented by Simon [27] who observed that the partial transposition on the density matrix corresponds to a mirror reflection for the Wigner distribution in phase space $\Lambda_A = diag(1, -1, 1, 1)$

$$\begin{array}{cc} \text{Hilbert Space} & \text{Phase Space} \\ \downarrow & \downarrow \\ \hat{\varrho} \longrightarrow \hat{\varrho}^T \quad \Leftrightarrow & W(X_A, Y_A, X_B, Y_B) \longrightarrow W_{\Lambda_A}(X_A, -Y_A, X_B, Y_B) \end{array} \tag{1.177}$$

So, in view of the above, a state ϱ is said to be separable if its Wigner distribution, under a partial transposition, goes into a mirror reflected and equally well defined Wigner distribution. This fact has consequences also on the covariance matrix of the state. Indeed also the transformed matrix $\tilde{\sigma} = \Lambda_A \sigma \Lambda_A$ has to fulfill the constraint imposed by the uncertainty relation,

$$\tilde{\sigma} + \frac{i}{2}\Omega \geq 0 \tag{1.178}$$

and the symplectic invariants become:

$$\tilde{I}_1 = I_1 \qquad \tilde{I}_2 = I_2 \qquad \tilde{I}_3 = -I_3 \qquad \tilde{I}_4 = I_4 \tag{1.179}$$

this leads to the following PPT condition:

$$\tilde{d}_- \geq \frac{1}{2} \tag{1.180}$$

where $\tilde{d}_-$ is the lower of the symplectic eignenvalues of $\tilde{\sigma}$,

$$\tilde{d}_\pm = \sqrt{\frac{\tilde{\triangle}(\sigma) \pm \sqrt{\tilde{\triangle}(\sigma)^2 - 4I_4}}{2}} \tag{1.181}$$

with $\tilde{\triangle}(\sigma) = I_1 + I_2 - 2I_3$. The state is entangled if and only if condition (1.180) is violated. Equivalently by referring to the standard form of the covariance matrix the PPT criterion

reads:

$$4\left(ab-c_1^2\right)\left(ab-c_2^2\right) \geq a^2+b^2+2\left|c_1c_2\right|-\frac{1}{4} \tag{1.182}$$

and the violation of this condition witnesses the presence of quantum correlation between the two subsystems.

Another entanglement witness is provided by the *Duan criterion* [28] that is based on the calculation of the total variance of a pair of Einstein-Poldolsky-Rosen (EPR) type operators. This quantity has a lower bound for a separable state due to the uncertainty principle. However this bound can be exceeded for an entangled state and this provides a sufficient condition for inseparability that turns to be also necessary for GSs. It can be demonstrated that for a bipartite Gaussian state with the covariance matrix in the standard form (1.170) this criterion reads as:

$$a\gamma^2+\frac{b}{\gamma^2}-\left|c_1\right|-2\left|c_2\right|<\gamma^2+\frac{1}{\gamma^2} \tag{1.183}$$

with $\gamma^2=\sqrt{\left(b-\frac{1}{2}\right)\left(a-\frac{1}{2}\right)}$. If for a state it stands this inequality the state is entangled.

1.4.6 Fidelity Criterion

Among the various crititeria to witness entanglement the *fidelity criterion* [29], we are going to introduce, involves the fidelity of the states and is able to predict if a state, obtained by mixing two squeezed not correlated states, will be entangled starting from the properties of the two input states. More in detail this criterion states that the interaction between two uncorrelated GSs through a bilinear exchange Hamiltonian, gives rise to entanglement if and only if the fidelity between the two input states is less than a threshold condition depending on their purities, first moments and on the strength of the coupling. In practice when two single mode Gaussian states interact through a bilinear Hamiltonian, their evolution is described, in the covariance matrix formalism, by the following block-matrix:

$$\Sigma=\begin{pmatrix}\Sigma_1 & \Sigma_{12}\\ \Sigma_{12} & \Sigma_2\end{pmatrix} \tag{1.184}$$

whose elements are

$$\Sigma_{1,2} = \tau\sigma_{1,2} + (1-\tau)\sigma_{2,1} \tag{1.185}$$

$$\Sigma_{12} = \tau(1-\tau)(\sigma_2 - \sigma_1) \tag{1.186}$$

with τ coupling parameter and $\sigma_{1,2}$ the covariance matrices of the two input single-mode states. The presence of the off-diagonal terms suggests the existence of a correlation between the two modes that depends on the "similarity" of the inputs. This similarity is quantified by the *fidelity* of the the states defined as to be:

$$\begin{aligned} F(\sigma_1,\sigma_2) &= \left(\sqrt{\det[\sigma_1+\sigma_2] + 4\left(\det[\sigma_1]-\frac{1}{4}\right)\left(\det[\sigma_2]-\frac{1}{4}\right)}\right. \\ &\left. -\sqrt{4\left(\det[\sigma_1]-\frac{1}{4}\right)\left(\det[\sigma_2]-\frac{1}{4}\right)}\right)^{-1} \end{aligned} \tag{1.187}$$

If and only if this quantity falls under the following threshold:

$$\begin{aligned} F_{th}(\sigma_1,\sigma_2) &= \left(4\mu_1\mu_2\sqrt{\tau(1-\tau)}\right)^{-1} \\ &\left(\sqrt{(1-\mu_1^2)(1-\mu_2^2) - 4\tau(1-\tau)(1+\mu_1^2)(1+\mu_2^2)}\right. \\ &\left. -\sqrt{4\tau(1-\tau)(1-\mu_1^2)(1-\mu_2^2)}\right)^{-1} \end{aligned} \tag{1.188}$$

that depends on the purities and the trasmission of the BS, entanglement is sat and the bipartite system emerging from the mixing is an unseparable state.

1.4.7 Propagation over a lossy channel

Pure states are far from being produced in a laboratory indeed, due to the unevoidable interaction with classical environment, pure states decohere, evolving into statistical mixtures.

Pure quantum features, such as entanglement, can be strongly compromised by this mechanism so it is of fundamental interest to know how the interaction alters the parameters determining the "quantumness" of a state. In optics due to absorption and diffraction, one of

the main cause producing decoherence is represented by the loss of photons. Another factor of noise arises from the interaction between the quantum system and a thermal environment. In the contest of open systems approach [30] by modeling the enviroment on a thermal bath, under the hypotesis of markovianity, secularity and validity of the Born approximation, the evolution of a quantum system experiencing a Gaussian noisy trasmission channel is well described, in the density matrix formalism, by the *Kossakowski-Lindblad* equation [9] that translates, for bipartite Gaussian states, into the *Fokker-Planck* Master equation written in terms of the Wigner quasi-probability distribution:

$$\partial_t W(\boldsymbol{K},t) = \frac{1}{2}\left(\partial_{\boldsymbol{K}}^T \Gamma \boldsymbol{K} + \partial_{\boldsymbol{K}}^T \Gamma \sigma_\infty \partial_{\boldsymbol{K}}\right) W(\boldsymbol{K}) \tag{1.189}$$

where $\boldsymbol{K}$ runs on the two modes quadratures, $\Gamma = \bigoplus_{h=1}^{2} \Gamma_h 1_2$, and $\sigma_\infty = \bigoplus_{h=1}^{2} \sigma_{h,\infty}$, with,

$$\sigma_{h,\infty} = \frac{1}{2}\begin{pmatrix} (\frac{1}{2}+N_h) + \mathrm{Re[M_h]} & \mathrm{Im[M_h]} \\ \mathrm{Im[M_h]} & (\frac{1}{2}+N_h) - \mathrm{Re[M_h]} \end{pmatrix} \tag{1.190}$$

This is the diffusion matrix and represents the asymptotic covariance matrix of the system with N_h and M_h respectively the effective photon number and the squeezing parameter of the bath. This, in terms of the covariance matrix, becomes:

$$\sigma(t) = \mathbb{G}_{\mathrm{t}}^{1/2}\sigma(0)\mathbb{G}_t^{1/2} + (1-\mathbb{G}_{\mathrm{t}})\sigma_\infty \tag{1.191}$$

with $\mathbb{G}_{\mathrm{t}} = \bigoplus_{h=1}^{2} e^{-\Gamma_h t} 1_2$. As one can see, expression (1.191) suggests that the action of the lossy channel on the covariance matrix characterizing the system is in all equivalent to the action of a fictitious BS that couples the system to the environment through its trasmission coefficient $T = e^{-\Gamma t}$.

Chapter 2

OAM-carrying entangled states generation

In this chapter we will illustrate the generation stage of our setup and we will report how the bipartite entangled state is produced. First of all, our source of polarization entangled states will be described. It is made of a triply resonant Optical Parametric Oscillator (OPO) working below threshold that provides two collinear entangled beams having the same frequency but cross polarized. The heart of this device is a second order non-linear process: the parametric down conversion. After a brief introduction, just to recall the main second-order non-linear phenomena, we will focus on parametric down conversion since this phenomenon generates both squeezing and entanglement.

We will illustrate this process both from a classical and a quantum point of view by further specializing to the case in which the presence of an optical cavity is encompassed. As it will be discussed later indeed, due to the small cross section of this phenomenon, for practical uses it is more convenient to enhance this process, placing the crystal into an optical resonator, obtaining in this way an OPO.

Once introduced the main features of the OPO source, the procedure for imprinting on the state OAM as a further d.o.f. will be reported in detail. Eventually it will be shown that the architecture of the setup, besides the generation of bipartite entangled vortex beams,

encompasses the possibility to generate single-mode squeezed vortex beams.

2.1 Non-linear optical phenomena

By observing the structure of the squeezing Hamiltonian (1.62), it is easy to understand that it describes a two-photon process. This translates, in practice, in the need of non-linear optical phenomena in order to produce squeeezing.

When talking about non-linear optical phenomena, it refers to the behaviour of some materials, usually crystals, that respond in a non-linear way when they are illuminated by strong EM radiations. The non-linearity in the response concerns the relation that stands between the polarization vector $P(t)$ and the electric field $E(t)$. In the linear optical regime they are proportional [31]:

$$P(t) = \chi^{(1)} E(t) \tag{2.1}$$

where $\chi^{(1)}$ is the linear susceptibility. This quantity is in general represented by a rank-2 tensor but for linear, homogeneous and isotropic dielectric media, it is simply a constant. To write (2.1) the material is also assumed to be lossless and not dispersive. In such a way it is possible to assume that the value taken by the polarization depends instantaneously on the value taken by the electric field. Out of the linear regime, equation (2.1) generalizes as follows:

$$P(t) = \chi^{(1)} E(t) + \chi^{(2)} E^2(t) + \chi^{(3)} E^3(t) + ... \tag{2.2}$$

where $\chi^{(1,2,3,..p)}$ are the susceptibilities at higher orders and are rank-$(p+1)$ tensors if the vectorial nature of both polarization and electric field is taken into account. Depending on the considered order, different processes take place; we will focus in particular on the second-order processes that occur exclusively in non-centrosymmetric crystals (not displaying inversion symmetry).

It is possible to show that in case of non-linearity the wave equation, in Gaussian units, assumes the following form:

$$\nabla^2 E - \frac{n^2}{c^2}\frac{\partial^2 E}{\partial t^2} = \frac{4\pi}{c^2}\frac{\partial^2 P}{\partial t^2} \tag{2.3}$$

being n the refractive index of the material. This is an inhomogeneous equation and expresses the fact that, when the right-hand side is different from zero, charges are accelerated so emitting EM radiation in agreement with the Larmor's theorem.

Let us suppose that the electric field impinging on a second order non-linear crystal has two-frequence components:

$$E = E_1 e^{-i\omega_1 t} + E_2 e^{-i\omega_2 t} + c.c. \tag{2.4}$$

By considering the second order term in (2.2) we get:

$$\begin{aligned} P^{(2)}(t) &= \chi^{(2)} E^2(t) \\ &= \chi^{(2)}[E_1^2 e^{-2i\omega_1 t} + E_2^2 e^{-2i\omega_2 t} + 2E_1 E_2 e^{-i(\omega_1+\omega_2)t} \\ &\quad +2E_1 E_2^* e^{-i(\omega_1-\omega_2)t} + c.c.] + 2\chi^{(2)}\left[E_1 E_1^* + E_2 E_2^*\right] \end{aligned} \tag{2.5}$$

By using the following notation:

$$P^{(2)}(t) = \sum_n P(\omega_n) e^{-i\omega_n t} \tag{2.6}$$

we have:

$$P(2\omega_1) = \chi^{(2)} E_1^2 \quad \text{(SHG)} \tag{2.7}$$

$$P(2\omega_2) = \chi^{(2)} E_2^2 \quad \text{(SHG)} \tag{2.8}$$

$$P(\omega_1 + \omega_2) = 2\chi^{(2)} E_1 E_2 \quad \text{(SFG)} \tag{2.9}$$

$$P(\omega_1 - \omega_2) = 2\chi^{(2)} E_1 E_2^* \quad \text{(DFG)} \tag{2.10}$$

$$P(0) = 2\chi^{(2)}\left(E_1 E_1^* + E_2 E_2^*\right) \quad \text{(OR)} \tag{2.11}$$

where the first to lines are referred as Second Harmonic Generation (SHG) while the terms involving the sum and the difference between the two frequencies are the Sum Frequency

Generation (SFG) and the Difference Frequency Generation (DFG). Eventually the last non-radiative term is the Optical Rectification (OR). Although there are four different frequency components, the related phenomena occur one at a time depending on the so called phase matching conditions that can be tailored by acting on the polarization of the beam illumunating the crystal and its relative orientation. We will focus now only on the DFG, essential for the generation of our entangled states.

2.2 Parametric down conversion and optical parametric oscillation

Expression (2.10) involves the phenomenon pictorially depicted in fig 2.1. A pump beam, with frequency ω_3 impinges on a second-order non-linear crystal together with a beam of energy $\hbar\omega_1$ that is used as a seed to stimulate the emission at its frequency. Consequently two beams at frequency ω_1 and $\omega_3 - \omega_1$ appear.

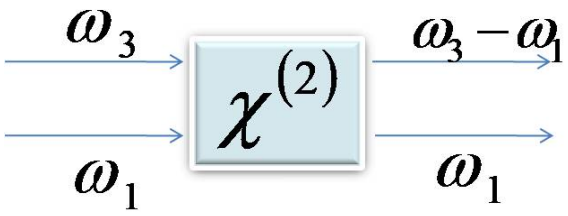

Figure 2.1: Pictorial representation of DFG. A pump beam at frequency ω_3 and a seed at frequency ω_1 impinge on a second-order non-linear crystal generating two beams in agreement with the energy conservation.

At single photon level, in view of the energy conservation, this phenomenon has to be seen as shown in fig 2.2.

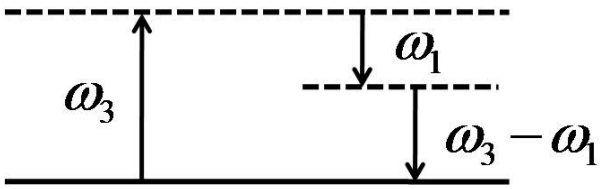

Figure 2.2: Pictorial representation of DFG at single photon level. A photon of energy $\hbar\omega_3$ is absorbed and due to the presence of a seed at frequency ω_1 a photon of energy $\hbar\omega_1$ is emitted with the consequent emission of another photon in agreement with the energy conservation.

Hence the process involves the absorption of a photon of energy $\hbar\omega_3$ with the consequent emission of a photon of frequency ω_1 and another one with the difference frequency [31]. This process acts as an amplifier with respect to the lower frequency. Indeed the presence of a seed with frequency ω_1 stimulates the emission of a photon at the frequency difference and another with frequency ω_1. This is the reason why this phenomenon is called *parametric amplification* or *parametric down conversion.* It occurs, with a reduced efficiency, even without the seed. In such a case the phenomenon is called *spontaneous parametric down conversion* or *parametric fluorescence.* In order to enhance the process efficiency without using a seed, the crystal can be placed into an optical resonator in this way realizing an OPO, whose schematic representation is shown in fig. 2.3.

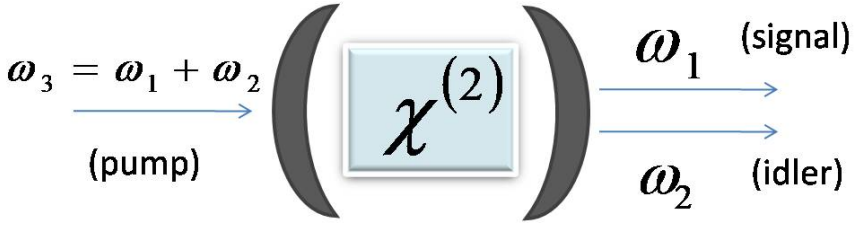

Figure 2.3: Pictorial representation of an OPO. A second order non-linear crystal is placed inside an optical resonator. A pump beam at frequency ω_3 determines the emission of two photons in agreement with the energy conservation.

The two mirrors have high reflectivity at ω_1 and/or $\omega_2 = \omega_3 - \omega_1$ so that this device is able to build up strong fields. The wanted photon at frequency ω_1 is said to be *signal* while the other unwanted one is called *idler*. Since does not exist a precise selection rule for the frequency of the signal (only the conservation of the total energy and momentum have to be

satisfied), its frequency can be controlled by adjusting the phase matching conditions.

2.3 Parametric down conversion: classical treatment

The starting point to treat non-linear optical phenomena is the wave equation for non-linear optical media (2.3). Let us recall that [31]:

$$\begin{aligned} \mathbf{P} &= \mathbf{P}^{(1)} + \mathbf{P}^{NL} \\ \mathbf{D} &= \mathbf{D}^{(\mathbf{1})} + 4\pi\mathbf{P}^{NL} \\ \mathbf{D}^{(1)} &= \mathbf{E} + 4\pi\mathbf{P}^{(1)} \end{aligned}$$

By substituting these relations into the wave equation (2.3) we obtain:

$$-\nabla^2\mathbf{E} + \frac{1}{c^2}\frac{\partial^2\mathbf{D}^{(1)}}{\partial t^2} = -\frac{4\pi}{c^2}\frac{\partial^2\mathbf{P}^{NL}}{\partial t^2} \tag{2.12}$$

If we assume the medium to be dispersive, each frequency component of $\mathbf{E}$, $\mathbf{D}$, and $\mathbf{P}$ must be considered. So, by only taking into account of positive frequencies, we get:

$$\mathbf{E}(\mathbf{r},t) = \sum_n \mathbf{E}_n(\mathbf{r},t) = \sum_n \mathbf{E}_n(\mathbf{r})\, e^{-i\omega_n t} + c.c. \tag{2.13}$$

$$\mathbf{D}^{(1)}(\mathbf{r},t) = \sum_n \mathbf{D}_n^{(1)}(\mathbf{r},t) = \sum_n \mathbf{D}_n^{(1)}(\mathbf{r})\, e^{-i\omega_n t} + c.c. \tag{2.14}$$

$$\mathbf{P}^{NL}(\mathbf{r},t) = \sum_n \mathbf{P}_n^{NL}(\mathbf{r},t) = \sum_n \mathbf{P}_n^{NL}(\mathbf{r})\, e^{-i\omega_n t} + c.c. \tag{2.15}$$

Moreover, $\mathbf{D}_n^{(1)}(\mathbf{r},t) = \epsilon^{(1)}(\omega_n)\,\mathbf{E_n}(\mathbf{r},t)$, where $\epsilon^{(1)}(\omega_n)$ is a frequency-dependent dielectric tensor. By taking all these relations into account equation (2.12) turns to be:

$$-\nabla^2\mathbf{E}_n(\mathbf{r},t) + \frac{\epsilon^{(1)}(\omega_n)}{c^2}\frac{\partial^2\mathbf{E}_n(\mathbf{r},t)}{\partial t^2} = -\frac{4\pi}{c^2}\frac{\partial^2\mathbf{P}_n^{NL}(\mathbf{r},t)}{\partial t^2} \tag{2.16}$$

valid for each frequency component. It can be seen that for the parametric down conversion for the signal ω_1 and the idler ω_2, in the case of strong non depleted pump one has:

$$\frac{dA_1}{dz} = \frac{8\pi i\omega_1^2 d}{k_1 c^2} A_3 A_2^* e^{i\triangle kz} \tag{2.17}$$

$$\frac{dA_2}{dz} = \frac{8\pi i\omega_2^2 d}{k_2 c^2} A_3 A_1^* e^{i\triangle kz} \tag{2.18}$$

being $\triangle k \equiv k_3 - k_1 - k_2$ and d a coupling constant between the fields and the polarization. $A_i(z)$ $(i = 1, 2, 3)$ are slowly varying amplitudes of the fields, respectively of the signal, the idler and the pump, considered as to be plane waves-like solutions,

$$E_i = A_i(z)\, e^{i(k_i z - \omega_i t)} \tag{2.19}$$

traveling along the $z-$axis inside the non-linear crystal. By introducing the quantities:

$$g = \sqrt{\kappa_1 \kappa_2^* - (\triangle k/2)^2} \quad \text{with} \quad \kappa_i = \frac{8\pi i d A_3}{k_j c^2}$$

the solutions of (2.17) and (2.18) are:

$$A_1(z) = \left[A_1(0)\left(\cosh gz - i\frac{\triangle k}{2g}\sinh gz\right) + \frac{\kappa_1}{g}A_2^*(0)\sinh gz\right] e^{i\triangle kz/2} \tag{2.20}$$

$$A_2(z) = \left[A_2(0)\left(\cosh gz - i\frac{\triangle k}{2g}\sinh gz\right) + \frac{\kappa_2}{g}A_1^*(0)\sinh gz\right] e^{i\triangle kz/2} \tag{2.21}$$

Under the hypothesis of perfect phase matching $\triangle k = 0$ and $A_2(0) = 0$, the solutions reduce to:

$$A_1(z) = A_1(0)\cosh gz \tag{2.22}$$

$$A_2(z) = i\left(\frac{n_1\omega_2}{n_2\omega_1}\right)\frac{A_3}{|A_3|}A_1^*(0)\sinh gz \tag{2.23}$$

for large z , the asymptotic behaviour of these two solutions, is given respectively by:

$$\text{for large } z \sim \frac{1}{2}A_1(0)\, e^{gz} \tag{2.24}$$

$$\text{for large } z \sim O(1) A_1^*(0) e^{gz} \tag{2.25}$$

where $O(1)$ means of the order of unity. So both solutions experience a growth with z.

When the presence of the cavity is encompassed, losses, due to the not perfect reflectivity of mirrors, have to be taken into account since they introduce a threshold for the parametric down conversion to occur. This threshold value can be obtained by imposing that in a single pass inside the cavity the fractional energy gain must equal the fractional energy loss. In perfect phase matching condition, by supposing reflectivities of the two mirrors to assume the same value R for the signal and the idler and $1 - R \ll 1$, the threshold condition becomes:

$$e^{2gL} - 1 = 2(1 - R) \tag{2.26}$$

where L is the crystal length. For $2gL \ll 1$,

$$gL = 1 - R \quad \text{Threshold condition} \tag{2.27}$$

This condition can be expressed as:

$$A_1(0) = \left[A_1(0) \cosh gL + \frac{\kappa_1}{g} A_2^*(0) \sinh gL \right] (1 - l_1) \tag{2.28}$$

$$A_2^*(0) = \left[A_2^*(0) \cosh gL + \frac{\kappa_2^*}{g} A_1(0) \sinh gL \right] (1 - l_2) \tag{2.29}$$

where $l_i = 1 - R_i e^{-\alpha_i L}$ is the fractional amplitude loss per pass and α_i the absorption coefficient of the crystal at frequency ω_i. The simultaneous validity of these two equations leads to:

$$\cosh gL = 1 + \frac{l_1 l_2}{2 - l_1 - l_2} \tag{2.30}$$

that is the trashold condition for both singly and doubly resonant OPO.

2.4 Parametric down conversion: quantum treatment

The parametric down conversion is one of the possible second-order non-linear phenomena in which a photon of the pump is annihilated to give a pair of photons (signal and idler) for which [31, 32]:

$$\omega_p = \omega_s + \omega_i \tag{2.31}$$

$$\mathbf{k}_p = \mathbf{k}_i + \mathbf{k}_s \tag{2.32}$$

energy (2.31) and momentum (2.32) conservations stand. The full Hamiltonian (free fields + interaction) under which the fields evolve is given by:

$$\hat{H} = \sum_i \hbar\omega_i \hat{a}_i^\dagger \hat{a}_i - i\hbar\chi^{(2)} \left(\hat{a}_p \hat{a}_i^\dagger \hat{a}_s^\dagger - \hat{a}_p^\dagger \hat{a}_i \hat{a}_s \right) \tag{2.33}$$

where i runs over $(s,\ i,\ p)$ and $\chi^{(2)}$ is the second order non-linear susceptibility of the crystal. For bosonic operators referring to the same EM field mode, the usual commutation relation (1.19) stands while operators referred to different modes commute with each other. The first term of the Hamiltonian is the sum of the three independent free field Hamiltonians of each mode involved in the process. The second term concerns the non-linear interaction occurring inside the crystal, i.e. the annihilation of a pump photon and the creation of the signal and the idler photons.

In most of cases, due to the weakness of the coupling constant $\chi^{(2)}$, the pump beam, that is tipically a strong coherent beam provided by a laser source, is not significantly depleted by the photon conversion. Hence, it is possible to make the following assumption of a classical pump field:

$$\hat{a}_p \longrightarrow A_p \quad \text{classicality of the pump} \tag{2.34}$$

in which the pump is no longer represented by an operator rather by a classical field amplitude.

We will face now the case in which the two fields (signal and idler) share the same frequency (that is half the value of the pump) but can be distinguished through their polar-

ization d.o.f since we suppose them to be cross polarized. By doing these assumptions the Hamiltonian (2.33) becomes:

$$\hat{H} = \frac{\hbar\omega_p}{2}\left(\hat{a}_s^\dagger\hat{a}_s + \hat{a}_i^\dagger\hat{a}_i\right) - i\hbar\frac{\chi^{(2)}}{2}A_p\left(\hat{a}_i^\dagger\hat{a}_s^\dagger - \hat{a}_i\hat{a}_s\right) \tag{2.35}$$

Looking to the interaction part it is easy to notice that it is equal to (1.76) as long as we make the substitution $g \to \frac{1}{2}\chi^{(2)}A_p$. Therefore, by recalling the results we obtained in the previous general treatment of subsection 1.1.6, we can assert that this Hamiltonian leads to a two-mode squeezed state in which the quadratures that show squeezing are the following combinations of the signal and the idler modes:

$$\hat{c} = \frac{\hat{a}_s + \hat{a}_i}{\sqrt{2}} \tag{2.36}$$

$$\hat{d} = \frac{\hat{a}_s - \hat{a}_i}{\sqrt{2}} \tag{2.37}$$

$$\hat{e} = \frac{\hat{a}_s - i\hat{a}_i}{\sqrt{2}} \tag{2.38}$$

$$\hat{f} = \frac{\hat{a}_s + i\hat{a}_i}{\sqrt{2}} \tag{2.39}$$

Since the signal and the idler are cross polarized, these combinations correspond respectively to the diagonal (2.36) and the anti-diagonal (2.37) modes, and the right-circular (2.38) and left-circular polarized(2.39) modes in the polarization basis of the signal and the idler pictorially represented in fig. 2.4.

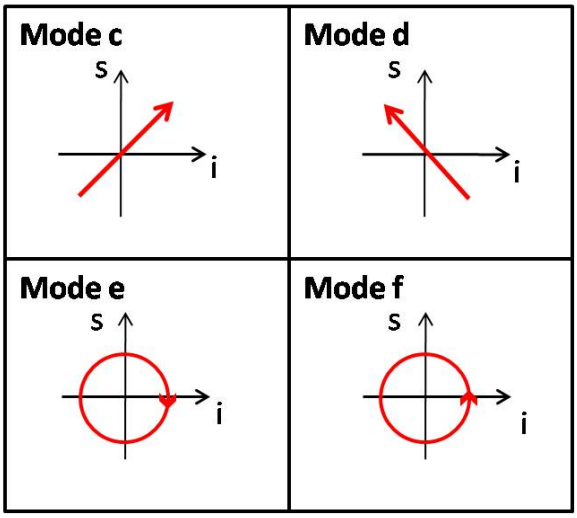

Figure 2.4: Pictorial representation of squeezed modes in the polarization basis of the signal and the idler.

Moreover since for each photon produced with frequency ω_s, also a photon with frequency $\omega_p - \omega_s$ is generated, the two modes at the OPO output show a strong correlation in the number of photons so being in an entangled state.

2.5 Optical parametric oscillator threshold

So far, the presence of an optical resonator has been neglected. When considering the case in which the crystal is placed inside an optical resonator, one can imagine the environment surrounding the cavity as a heat bath constituted by an infinite number of harmonic oscillators that, at room temperature, can be considered to be in their ground state. The interaction of the radiation confined inside the cavity with the external environment is caused by the not perfect reflectivity of the two mirrors that leads to unavoidable losses. The interaction Hamiltonian that couples a single mode of radiation $\hat{a}$ inside the cavity with a harmonic oscillator of the bath $\hat{b}$, has the following form [31, 32]:

$$\hat{H}_{in-out} = i\hbar \int_{-\infty}^{\infty} d\omega \; \kappa(\omega) \left(\hat{b}^{\dagger}(\omega) \hat{a} + \hat{b}(\omega) \hat{a}^{\dagger} \right) \tag{2.40}$$

where $\kappa(\omega)$ is the strength of the coupling. The evolution under the Hamiltonian (2.40) of the modes inside the cavity is governed by the following *Langevin equation:*

$$\frac{d\hat{a}}{dt} = -\frac{i}{\hbar}\left[\hat{a}(t), \hat{H}\right] - \gamma\hat{a}(t) + \sqrt{2\gamma}a^{in}(t) \tag{2.41}$$

where $\hat{H}$ is the Hamiltonian inside the cavity i.e., in our case, the non-linear Hamiltonian introduced in the previous section. The term $\gamma\hat{a}(t)$ is related to the losses due to absorption and diffractions of mirrors, while the driving term $\sqrt{2}\gamma a^{in}(t)$ is related to the interaction with the bath. In particular it describes the entrance, inside the cavity, of a vacuum mode coming from the external environment. When specifying equation (2.41) for the pump, the signal and the idler, we get:

$$\frac{d\hat{a}_s}{dt} = -\gamma\hat{a}_s + \chi^{(2)}\hat{a}_p\hat{a}_i^{\dagger} + \sqrt{2\gamma}\hat{a}_s^{in}(t) \tag{2.42}$$

$$\frac{d\hat{a}_i}{dt} = -\gamma\hat{a}_i + \chi^{(2)}\hat{a}_p\hat{a}_s^{\dagger} + \sqrt{2\gamma}\hat{a}_s^{in}(t) \tag{2.43}$$

$$\frac{d\hat{a}_p}{dt} = -\gamma_p\hat{a}_p - \left(\chi^{(2)}\right)^{*}\hat{a}_i\hat{a}_s^{\dagger} + A_p + \sqrt{2\gamma_p}\hat{a}_p^{in}(t) \tag{2.44}$$

being A_p the external coherent pump. These non-linear equations can be solved thanks to a linearization procedure according to which the operator,

$$\hat{a} \longrightarrow \alpha + \delta\hat{a} \tag{2.45}$$

is decomposed in a sum of a term involving a complex amplitude α and a term $\delta\hat{a}$ related to the operator fluctuations. By setting $\alpha = \alpha_s = \alpha_i$ the following equation is obtained:

$$\alpha^3 - \frac{\chi^{(2)}A_p - \gamma_p\gamma}{\left(\chi^{(2)}\right)^2}\alpha = 0 \tag{2.46}$$

Solutions of the equation (2.46) depend on the value of A_p. In particular there exsist a threshold $A_{th} = \frac{\gamma_p\gamma}{\chi^{(2)}}$, for the pump value, in order to parametric down conversion occurs even in presence of losses. In the above threshold case $A_p \geq A_{th}$ the system is proven to generate

the so called *twin beams* since they show a strong correlation between the fluctuations on the photon number. We will only focus on the case $A_p \leq A_{th}$ in which the system admits the stable solution $\alpha = 0$ and $\alpha_p = \frac{A_p}{\gamma_p}$ (*below threshold condition*). In this case the system has a non-classical behaviour with "non-classicality" increasing with getting closer to the threshold.

2.6 Fluctuations of the output fields

Let us consider the fields outing from the OPO cavity as a sum of a steady state and a quantum operator fluctuation $\alpha + \delta\hat{a}$. The Langevin equations turn out to be [32]:

$$\frac{d\left(\delta\hat{a}_i\right)}{dt} = -\gamma\delta\hat{a}_i + \chi^{(2)}\alpha_p\delta\hat{a}_s^\dagger + r\delta\hat{a}_p + \sqrt{2\gamma}a_i^{in}\left(t\right) \tag{2.47}$$

$$\frac{d\left(\delta\hat{a}_s\right)}{dt} = -\gamma\delta\hat{a}_s + \chi^{(2)}\alpha_p\delta\hat{a}_i^\dagger + r\delta\hat{a}_p + \sqrt{2\gamma}a_s^{in}\left(t\right) \tag{2.48}$$

$$\frac{d\left(\delta\hat{a}_p\right)}{dt} = -\gamma_p\delta\hat{a}_p - \chi^{(2)}\left[\delta\hat{a}_s + \delta\hat{a}_i\right] + \sqrt{2\gamma_p}a_p^{in}\left(t\right) \tag{2.49}$$

By introducing the modes $\hat{c}$ and $\hat{d}$, already defined in previous sections as combination of idler and signal modes, and their relative amplitude and phase quadtrature operators $\hat{X}_{c,d}$ and $\hat{Y}_{c,d}$ the fluctuations on these quantities satisfy the following uncoupled equations:

$$\frac{d\left(\delta\hat{X}_{c,d}\right)}{dt} = -\left(\gamma \mp \wp\right)\delta\hat{X}_{c,d} + \sqrt{2\gamma}\hat{X}_{c,d}^{in} \tag{2.50}$$

$$\frac{d\left(\delta\hat{Y}_{c,d}\right)}{dt} = -\left(\gamma \pm \wp\right)\delta\hat{Y}_{c,d} + \sqrt{2\gamma}\hat{Y}_{c,d}^{in} \tag{2.51}$$

where $\wp = \chi^{(2)}\alpha_p$. The squeezing spectrum for the fluctuations of outing fields results to be:

$$\left\langle \triangle\delta\hat{X}_c^{out}\left(\omega\right)\right\rangle^2 = S_c\left(\omega\right) = \left\langle \triangle\delta\hat{Y}_d^{out}\left(\omega\right)\right\rangle^2 \tag{2.52}$$

$$\left\langle \triangle\delta\hat{Y}_c^{out}\left(\omega\right)\right\rangle^2 = S_d\left(\omega\right) = \left\langle \triangle\delta\hat{X}_d^{out}\left(\omega\right)\right\rangle^2 \tag{2.53}$$

where,

$$S_{c,d}(\omega) = \frac{1}{2}\left(1 \pm 2\frac{\wp\gamma}{(\gamma \mp \wp)^2 + \omega^2}\right) \tag{2.54}$$

Hence the mode $\hat{c}$ ($\hat{d}$) exhibits antisqueezing (squeezing) on the amplitude quadrature and vice-versa for the phase quadrature.

2.7 Threshold in terms of the cavity parameters

If the OPO cavity is spherical, the inner fields have a Gaussian intensity profile. In such a case it is possible to show that the threshold value for the pump power can be written in terms of the cavity parameters as follows:

$$P_{th} = \frac{\pi^2}{4\mathcal{F}_s\mathcal{F}_i B_{up} E_{NL}} \tag{2.55}$$

where $\mathcal{F}_{s,i}$, are the *finesse* of the cavity at signal and idler frequency, B_{up} is the *build up* parameter for the pump and is given by the pump power inside the cavity over the one at the entrance, while E_{NL} is a non-linear coefficient depending on the second order susceptibility and on the phase matching $\triangle k = k_p - k_s - k_i$. Since it is better to work with a low pump power in order to avoid thermal effects on the crystal it is important to experimentally tailor its value. It is possible to show that $\mathcal{F}_i$ and B_{up} take their heigher values in triply resonance condition, moreover E_{NL} is maximum when perfect phase matching condition is achieved.

2.8 Experimental setup

The part of the whole experimental scheme, devoted to the generation of the entangled cross polarized modes is depicted in fig 2.5. The laser source (whose main characteristics are reported in table 2.1) is a Continuous Wave (CW) Nd:YAG laser (Innolight-Diabolo dual wavelength) emitting a single mode TEM_{00} linearly polarized @1064 nm with a slightly elliptical spot. The laser also provides a second output @532 nm

λ	nm	1064
P_{max}	mW	400
$FWHM$	kHz	< 1
Coherence length	Km	> 1
Waist location	mm	50
Drift frequency	MHz/min	2

Table 2.1: Laser properties.

used as the OPO pump. Once have been produced, the green pump beam passes through an Electro Optic Modulator (EOM) and a Faraday Rotator (FR). The first one is employed to modulate the phase of the laser beam in order to adjust the OPO cavity length thanks to a Pound-Drever-Hall (PDH) [33] control system that ensures the resonance of the pump beam. The second acts as an insulator protecting the laser source from back scattered light. A HWP, together with a Polarizing Beam Splitter (PBS), allows to control the pump power to be sent to the OPO. Another HWP adjusts the polarization of the beam before entering the OPO cavity. Before entering the cavity the beam crosses a matching lens that improves the coupling of the pump beam to the TEM_{00} mode of the cavity.

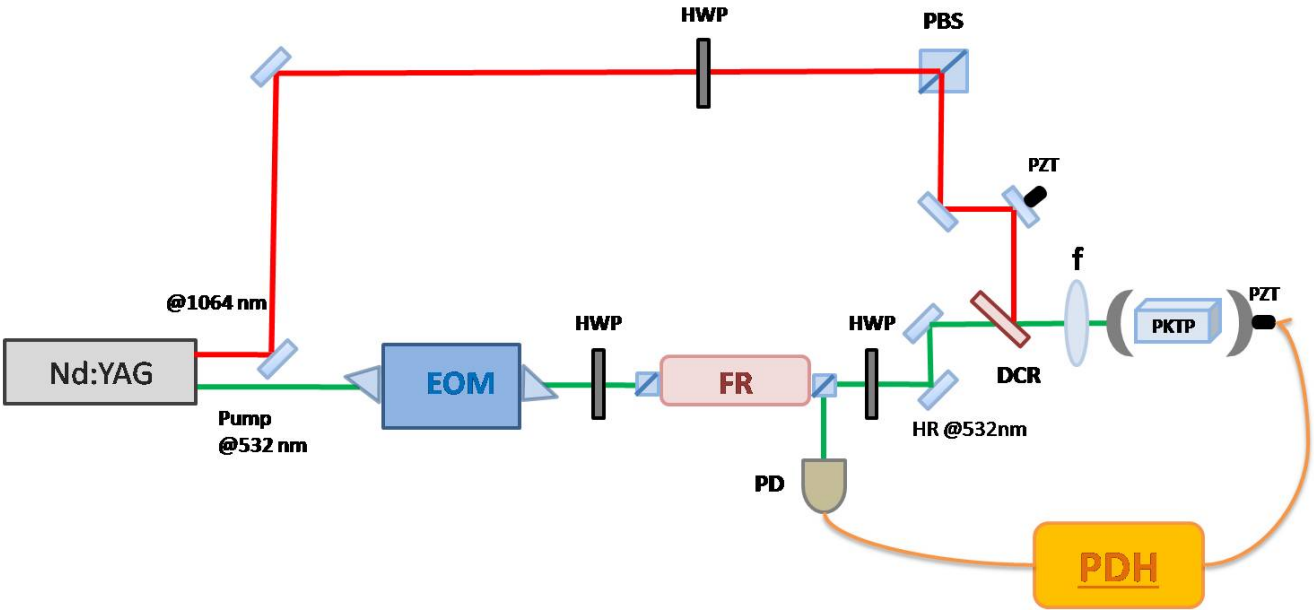

Figure 2.5: Experimental setup for the generation of the entangled cross polarized modes.

The non-linear crystal of the OPO is a $1 \times 1.5 \times 25$ mm^3 periodically poled (poling

period 448 μm) $\alpha-$cut KTP crystal (PKTP). It ensures a type-II phase matching for two collinear orthogonally polarized and frequency degenerate beams ($\lambda_s = \lambda_i = 2\lambda_p = 1064\ nm$) at $T = 326K$ (53°C). The crystal temperature is actively controlled with residual peak-to-peak fluctuations of $\lesssim 3\ mK$ over 20 min. The OPO cavity is composed by two mirrors having the same curvature radius $R = 51.68\ mm$. The cavity input mirror has a trasmittivity $T_{in}\,(1064\ nm) = 0.0075\%$ and $T_{in}\,(532\ nm) = 4.5\%$ while for output mirrors $T_{out}\,(1064\ nm) = 4.6\%$ and $T_{out}\,(532\ nm) = 0.1\%$. The cavity optical length at 1064 nm is approx 95 mm (between the confocal and the concentric configuration). The measured threshold power for the pump beam is $P_{th} \approx 70\ mW$. As previously said, in order to optimize the non-linear process inside the cavity, the system has to work in triply resonance conditions [32]. The resonance condition for the pump beam is insured by a PDH control system that allows to tailor the cavity length via a piezoelectric crystal mounted on the output cavity mirror. This system locks the cavity to the pump mode TEM_{00}. By finely controlling the temperature of the crystal it is possible to achieve the triply resonance condition while keeping the pump locking.

2.9 OAM imprinting of the SAM entangled modes

Once the two entangled modes have been produced by the OPO, the bipartite state is endowed by an additional d.o.f. represented by OAM. It constitutes a further way to distinguish between the two co-propagating modes and increases the information-carrying capacity of the state. The OAM-imprinting is realized thanks to the q-plate introduced in previous sections. The scheme for the OAM imprinting is shown in fig. 2.6.

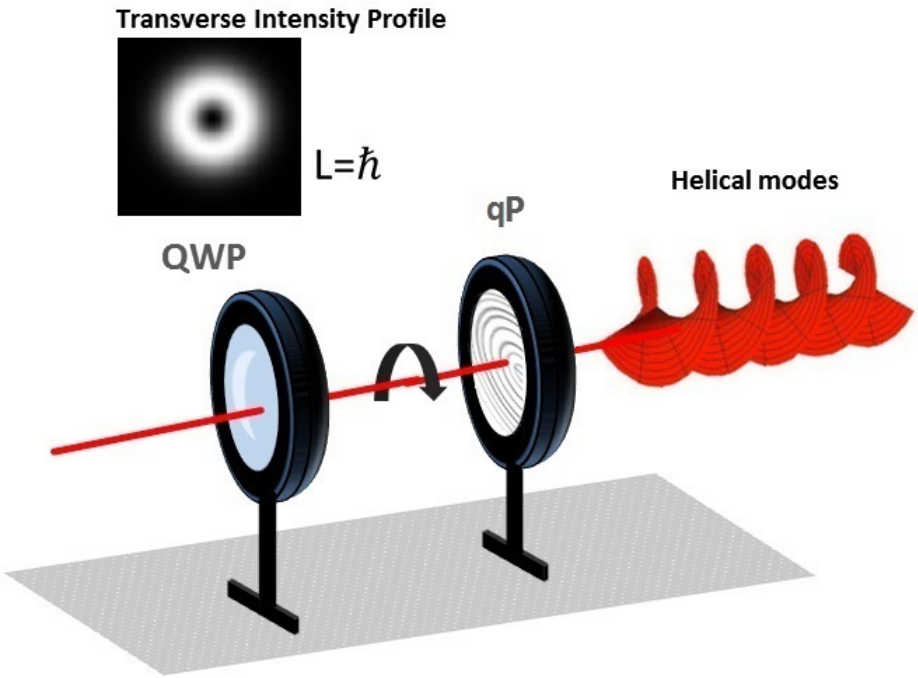

Figure 2.6: OAM-imprinting experimental scheme.

As discussed above the OPO source, working below threshold, generates a bipartite state in which the two modes have the same frequency but they are cross polarized. Let us indicate these modes as $\hat{a}_{H,0}$ and $\hat{b}_{V,0}$ where the labels H, V concern the SAM and stand respectively for the horizontal and vertical polarization. The second label, that is 0 for both the modes at the OPO output, indicates that none of the two modes carry OAM so being Gaussian TEM_{00} modes. The first QWP, placed at the OPO output, transforms the linear crossed polarizations of the two entangled beams into opposite circular ones.

The waveplate is placed in such a way that its fast axis forms 45° angle with the polarization of the ingoing beam. Let us recall the matrix representing the related transformation:

$$M_{QWP}\left(45°\right) = \frac{1}{\sqrt{2}} \begin{pmatrix} 1 & i \\ i & 1 \end{pmatrix} \tag{2.56}$$

This matrix acts on the two crossed polarizations as:

$$M_{QWP}\,|H\rangle = \frac{1}{\sqrt{2}}\begin{pmatrix} 1 & i \\ i & 1 \end{pmatrix}\begin{pmatrix} 1 \\ 0 \end{pmatrix} = \frac{1}{\sqrt{2}}\begin{pmatrix} 1 \\ i \end{pmatrix} = |L\rangle \tag{2.57}$$

$$M_{QWP}\,|V\rangle = \frac{1}{\sqrt{2}}\begin{pmatrix} 1 & i \\ i & 1 \end{pmatrix}\begin{pmatrix} 0 \\ 1 \end{pmatrix} = \frac{1}{\sqrt{2}}i\begin{pmatrix} 1 \\ -i \end{pmatrix} = i\,|R\rangle \tag{2.58}$$

Therefore the two modes outing from the OPO undergo the following transformation:

$$\hat{a}_{H,0} \longrightarrow \hat{a}_{L,0} \tag{2.59}$$

$$\hat{b}_{V,0} \longrightarrow i\hat{b}_{R,0} \tag{2.60}$$

These two circularly polarized modes then cross a q-plate having a topological charge $q = \frac{1}{2}$. As discussed in the section dedicated to this device, the QP, when crossed by a Gaussian circularly polarized mode, converts the TEM_{00} into a vortex beam by making it to acquire an OAM equal to $\pm 2q\hbar$ (depending on whether the initial polarization was left $(+)$ or right $(-)$) and inverts its polarization. Hence, in our specific case, the mode $\hat{a}_{L,0}$ acquires an OAM equal to $\hbar$ and its polarization becomes right. Conversely, the mode $\hat{b}_{R,0}$ acquires an opposite amount of OAM and its polarization becomes left. Therefore, schematically we have:

$$\hat{a}_{L,0} \longrightarrow \hat{a}_{R,1} \tag{2.61}$$

$$i\hat{b}_{R,0} \longrightarrow i\hat{b}_{L,-1} \tag{2.62}$$

Therefore the QP provides the two cross polarized modes with two opposite amounts of OAM in the propagation direction. The two modes, degenerate in frequency, that previously could be discerned by polarization, become now multi-distinguishable. Therefore our setup is capable of generating a bipartite entangled state carrying OAM. After being produced this state undergoes the characterization stage; its covariance matrix is measured via homodyne detection and entanglement between the two modes is assessed.

2.10 Helical squeezed single-modes generation

Our experimental setup is also capable of generating squeezed single modes carrying OAM. As previously discussed, the modes $\hat{c}, \hat{d}, \hat{e}$ and $\hat{f}$ are all squeezed single-modes obtained as combinations of the two entangled thermal modes $\hat{a}$ and $\hat{b}$ provided by the OPO.

In order to realize such modes and endow them with OAM, the following configuration of optical elements, shown in fig. 2.7, is implemented. As depicted in the figure, the beams encounter on their propagation a QWP that besides rotating (changing the direction of its fast axis with respect to the polarization of the crossing beam) can also be temporally removed from the setup. Then the beams outing from the OPO encounter a QP that provides them with OAM. Eventually the last two waveplates, free to rotate, act suitably on the polarization of the vortex modes, before sending the desired mode to the Homodyne Detector (HD).

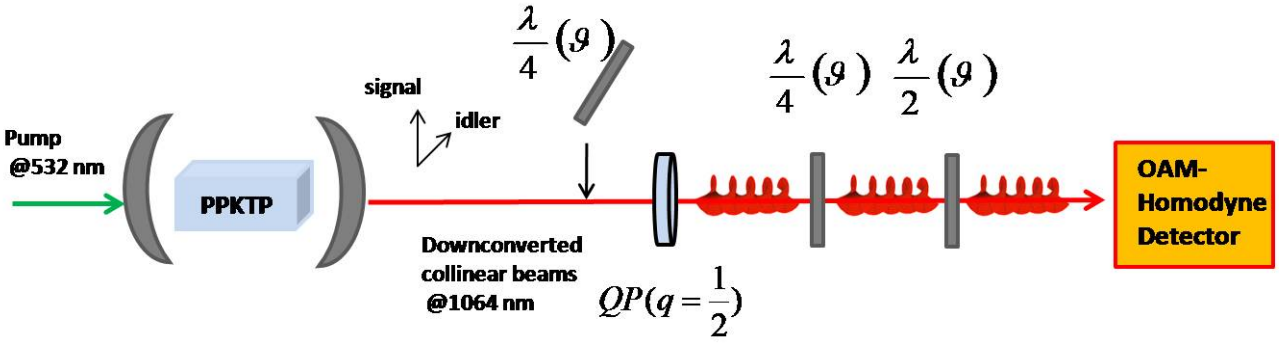

Figure 2.7: Experimental setup for the generation of the modes $\hat{a}, \hat{b}, \hat{c}, \hat{d}, \hat{e}$ and $\hat{f}$ provided with OAM.

2.10.0.1 Mode $\hat{c}$ and $\hat{d}$ generation

The configuration scheme for the generation of the modes $\hat{c}$ and $\hat{d}$ is depicted respectively in figs 2.8 and 2.9. This experimental configuration scheme aims to both achieve the wanted combination of the two initial modes and to endow these combinations with the intented amount of OAM. Once this goal is accomplished these modes are sent to HD to characterize the quantum state via the measure of the statistical distributions of their associated quadrature operators.

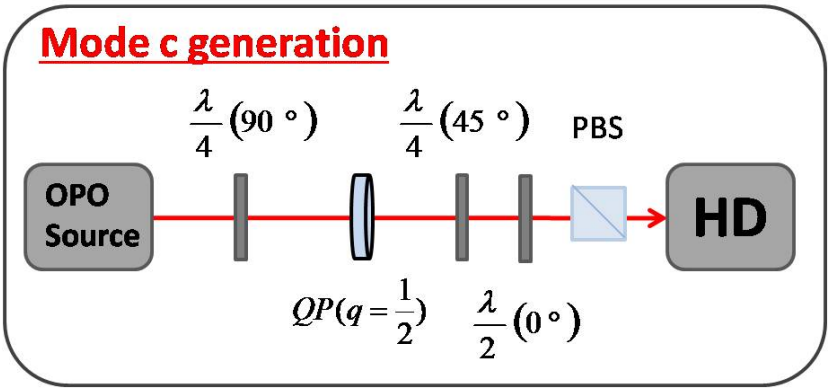

Figure 2.8: Experimental scheme for the generation of the mode $\hat{c}$.

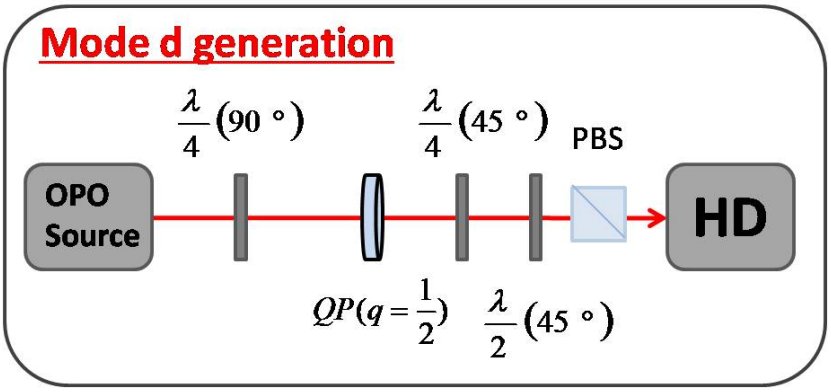

Figure 2.9: Experimental scheme for the generation of the mode $\hat{d}$.

By using the notation early adopted, the two modes outing from the OPO source are denoted by $\hat{a}_{H,0}$ and $\hat{b}_{V,0}$. It is convenient to rewrite such modes in the polarization circular basis $|R\rangle$ and $|L\rangle$ as:

$$\hat{a}_{H,0} = \frac{1}{\sqrt{2}}\left(\hat{a}_{L,0} + \hat{a}_{R,0}\right) \tag{2.63}$$

$$\hat{b}_{V,0} = \frac{1}{\sqrt{2}i}\left(\hat{b}_{L,0} - \hat{b}_{R,0}\right) \tag{2.64}$$

The first optical element they encounter is a QWP whose fast axis forms a 90° angle with the polarization of the beams. It is represented in the polarization space by the following Jones matrix:

$$M_{QWP}(90°) = e^{-i\frac{\pi}{4}} \begin{pmatrix} 1 & 0 \\ 0 & i \end{pmatrix} \tag{2.65}$$

in this way carrying out the following transormation on their polarizations:

$$\begin{cases} |H\rangle \rightarrow & e^{-i\frac{\pi}{4}} |H\rangle \\ |V\rangle \rightarrow & ie^{-i\frac{\pi}{4}} |V\rangle \end{cases} \tag{2.66}$$

Therefore, after passing through the quarter wave plate, the two modes undergo the following transformation:

$$\hat{a}_{H,0} \rightarrow \frac{e^{-i\frac{\pi}{4}}}{\sqrt{2}} (\hat{a}_{L,0} + \hat{a}_{R,0}) \tag{2.67}$$

$$\hat{b}_{V,0} \rightarrow \frac{e^{-i\frac{\pi}{4}}}{\sqrt{2}} \left(\hat{b}_{L,0} - \hat{b}_{R,0}\right) \tag{2.68}$$

Subsequently the two modes encounter the QP that endows each component in the circular basis with an OAM equal to $\pm\hbar$

$$\frac{e^{-i\frac{\pi}{4}}}{\sqrt{2}} (\hat{a}_{R,1} + \hat{a}_{L,-1}) \tag{2.69}$$

$$\frac{e^{-i\frac{\pi}{4}}}{\sqrt{2}} \left(\hat{b}_{R,1} - \hat{b}_{L,-1}\right) \tag{2.70}$$

Eventually the last QWP oriented at 45°realizes the following transformation:

$$\frac{e^{-i\frac{\pi}{4}}}{\sqrt{2}} (\hat{a}_{H,1} + i\hat{a}_{V,-1}) \tag{2.71}$$

$$\frac{e^{-i\frac{\pi}{4}}}{\sqrt{2}} \left(\hat{b}_{H,1} - i\hat{b}_{V,-1}\right) \tag{2.72}$$

At this stage if these two modes cross a HWP oriented at 0°, represented by the following Jones matrix:

$$M_{WP}(\pi, 0°) = i \begin{pmatrix} 1 & 0 \\ 0 & -1 \end{pmatrix} \tag{2.73}$$

up to a phase factor this transformation act essentaly as an identity so the two modes become:

$$\frac{e^{-i\frac{\pi}{4}}}{\sqrt{2}} (i\hat{a}_{H,1} + \hat{a}_{V,-1}) \tag{2.74}$$

$$\frac{e^{-i\frac{\pi}{4}}}{\sqrt{2}}\left(i\hat{b}_{H,1}-\hat{b}_{V,-1}\right) \tag{2.75}$$

To obtain the above relations we have used the fact that $M_{WP}(\pi,0°)$ carries out the following transformation on the vectors representing the horizontal and the vertical polarizations:

$$\begin{cases} |H\rangle \rightarrow & i\,|H\rangle \\ |V\rangle \rightarrow & -i\,|V\rangle \end{cases} \tag{2.76}$$

The PBS placed after the HWP will leave to pass only the horizontally polarized components. Therefore the mode that will reach the HD in such a case is the following combination:

$$\hat{c}=\frac{e^{-i\frac{\pi}{4}}}{\sqrt{2}}i\left(\hat{a}_{H,1}+\hat{b}_{H,1}\right) \tag{2.77}$$

corresponding to the mode $\hat{c}$.

If the last HWP is instead oriented at 45° , then it carries out the transformations reported in (2.57) and (2.58) so it inverts the polarizations giving:

$$\frac{e^{-i\frac{\pi}{4}}}{\sqrt{2}}\left(i\hat{a}_{V,1}-\hat{a}_{H,-1}\right) \tag{2.78}$$

$$\frac{e^{-i\frac{\pi}{4}}}{\sqrt{2}}\left(i\hat{b}_{V,1}+\hat{b}_{H,-1}\right) \tag{2.79}$$

This time the PBS will leave to pass the combination:

$$\hat{d}=-\frac{e^{-i\frac{\pi}{4}}}{\sqrt{2}}\left(\hat{a}_{H,-1}-\hat{b}_{H,-1}\right) \tag{2.80}$$

corresponding to mode $\hat{d}$.

2.10.0.2 Mode $\hat{e}$ and $\hat{f}$ generation

The scheme for the generation of the modes $\hat{e}$ and $\hat{f}$ is depicted respectively in figs 2.10 and 2.11.

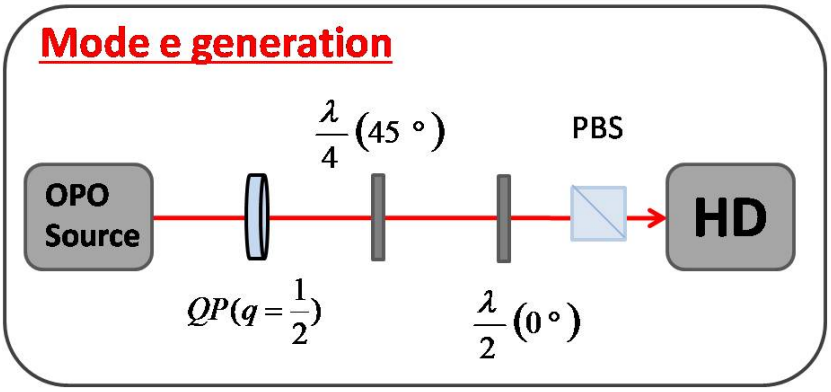

Figure 2.10: Experimental scheme for the generation of the mode $\hat{e}$.

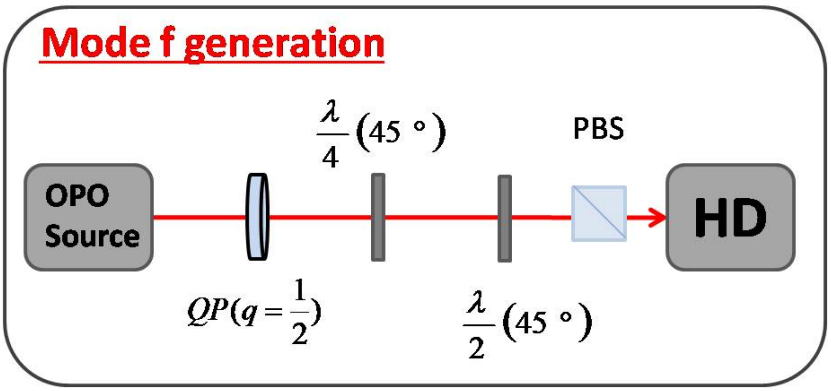

Figure 2.11: Experimental scheme for the generation of the mode $\hat{f}$.

In order to generate the combinations of the initial entangled modes corresponding to the fields $\hat{e}$ and $\hat{f}$ the first QWP is removed from the setup and the two modes directly ungergo the action of the QP. By remembering the relations between the linear and the circular basis (2.63),(2.64) we have:

$$\hat{a}_{H,0} \rightarrow \frac{1}{\sqrt{2}}\left(\hat{a}_{R,1} + \hat{a}_{L,-1}\right) \tag{2.81}$$

$$\hat{b}_{V,0} \rightarrow \frac{1}{\sqrt{2}i}\left(\hat{b}_{R,1} - \hat{b}_{L,-1}\right) \tag{2.82}$$

When crossing the QWP the two modes become:

$$\frac{1}{\sqrt{2}}\left(\hat{a}_{H,1} + i\hat{a}_{V,-1}\right) \tag{2.83}$$

$$\frac{1}{\sqrt{2}i}\left(\hat{b}_{H,1} - i\hat{b}_{V,-1}\right) \tag{2.84}$$

From now on the evolution of the two modes depends on the orientation of the HWP. In particular if it is oriented at 0° the polarizations remain the same up to an overall phase factor:

$$\frac{1}{\sqrt{2}}\left(i\hat{a}_{H,1} + \hat{a}_{V,-1}\right) \tag{2.85}$$

$$\frac{1}{\sqrt{2}}\left(\hat{b}_{H,1} + i\hat{b}_{V,-1}\right) \tag{2.86}$$

In such a case the PBS will leave to pass the following combination:

$$\hat{e} = \frac{1}{\sqrt{2}}i(\hat{a}_{H,1} - i\hat{b}_{H,1}) \tag{2.87}$$

corresponding to the $\hat{e}$ mode endowed with an OAM equal to $\hbar$. Differently, in the configuration shown in fig. 2.11, the two modes, after the HWP will be:

$$\frac{1}{\sqrt{2}}\left(i\hat{a}_{V,1} - \hat{a}_{H,-1}\right) \tag{2.88}$$

$$-\frac{1}{\sqrt{2}}i\left(i\hat{b}_{V,1} + \hat{b}_{H,-1}\right) \tag{2.89}$$

so the mode that will reach the HD is:

$$\hat{f} = -\frac{1}{\sqrt{2}}(\hat{a}_{H,-1} + i\hat{b}_{H,-1}) \tag{2.90}$$

corresponding to the mode $\hat{f}$ carrying $-\hbar$ of OAM.

Chapter 3

OAM-entangled states characterization

Optical balanced homodyne is a widely consolidated technique used to reconstruct, via tomographic measurements, the quantum state of the electromagnetic field since it yields phase-sensitive measurements allowing this way for the detection of squeezing. This kind of detector has been used up to now only for Gaussian modes and never for more complex spatial structured modes. In the present chapter besides recalling its basic concept we will present an extension of this technique to fields carrying OAM. In particular we report on the development of a homodyne detector suitably designed to be able to infer the quadrature statistics of a travelling optical field provided of OAM. Such a powerful scheme meets the need, in the quantum information context, of accessing the information carried by a single quantum EM mode by employing photonic degrees of freedom with a higher Hilbert space dimensionality. In this more complex case the problem of the mode matching between the signal and the Local Oscillator (LO) becomes more critical requiring a structured LO with the same characteristics of the signal mode under scrutiny.

3.1 Optical Balanced Homodyne

The basic scheme of four-port HD of the quadrature components of single-mode fields is depicted in fig 3.1

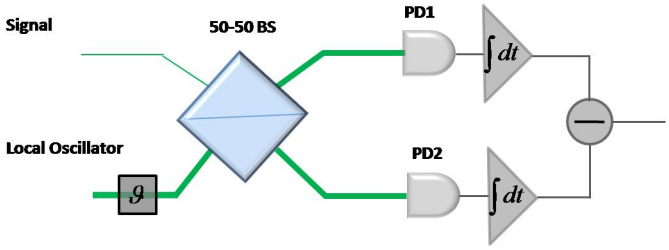

Figure 3.1: Basic scheme of four port homodyne detector.

It is based on the controlled inteference between a weak field and a strong coherent beam called LO. These two beams are coherently mixed on a 50% reflecting BS whose two output ports are recoiled by two linear high efficiency photodiodes (PD1 and PD2), temporally integrated and eventually electronically subtracted.

Let $\hat{a}_{LO}$ and $\hat{a}_S$ be the bosonic mode operators associated respectively to the LO reference beam and to the signal. These two fields are transformed by the BS, represented by the unitary matrix [6]:

$$M = \begin{pmatrix} \frac{1}{\sqrt{2}} & -\frac{1}{\sqrt{2}} \\ \frac{1}{\sqrt{2}} & \frac{1}{\sqrt{2}} \end{pmatrix} \tag{3.1}$$

into the modes $\hat{a}_1$ and $\hat{a}_2$ given by:

$$\begin{pmatrix} \hat{a}_1 \\ \hat{a}_2 \end{pmatrix} = M \begin{pmatrix} \hat{a}_S \\ \hat{a}_{LO} \end{pmatrix} \iff \begin{cases} \hat{a}_1 &= \frac{1}{\sqrt{2}}(\hat{a}_S - \hat{a}_{LO}) \\ \hat{a}_2 &= \frac{1}{\sqrt{2}}(\hat{a}_S + \hat{a}_{LO}) \end{cases} \tag{3.2}$$

Since the LO is an intense beam consituted by many photons we can treat it classically by setting $\hat{a}_{LO} \longrightarrow A_{LO} = |A_{LO}|\, e^{i\vartheta}$. Currents measured by the two photodiodes (PD1 and PD2) are both proportional to the number of photons impinging on their active area, so we have:

$$\hat{n}_1 = \hat{a}_1^\dagger \hat{a}_1 = \frac{1}{2}(\hat{a}_S^\dagger \hat{a}_S - \hat{a}_S^\dagger A_{LO} - A_{LO}^* \hat{a}_s + |A_{LO}|^2) \tag{3.3}$$

$$\hat{n}_2 = \hat{a}_2^\dagger \hat{a}_2 = \frac{1}{2}(\hat{a}_S^\dagger \hat{a}_S + \hat{a}_S^\dagger A_{LO} + A_{LO}^* \hat{a}_s + |A_{LO}|^2) \tag{3.4}$$

The difference between the two photocurrents will be:

$$\hat{n}_{12} = \hat{n}_2 - \hat{n}_1 = |A_{LO}| \left(\hat{a}_S e^{-i\vartheta} + \hat{a}_S^\dagger e^{i\vartheta}\right) = \sqrt{2}\,|A_{LO}|\,\hat{X}_S\left(\vartheta\right) \tag{3.5}$$

where $\hat{X}_S\left(\vartheta\right) = \frac{\hat{a}_s e^{-i\vartheta} + \hat{a}_s^\dagger e^{i\vartheta}}{\sqrt{2}}$ is the generalized quadrature. This interferometric scheme allows measurement of the input state quadrature as a function of the relative phase angle ϑ since the difference in the two measured photocurrents is proportional, through the LO amplitude, to the field quadrature selected by varying the LO phase. This phase shift can be introduced by changing the relative optical path lenghts. Similarly for the variance we have:

$$\triangle n_{12} \propto |A_{LO}|\,\triangle X\left(\vartheta\right) \tag{3.6}$$

We also can see that in such a way classical noise associated to laser amplitude fluctuations is rejected.

3.1.1 Mode Matching between the signal and the LO

HD efficiency is influenced by several factors, among which, one is taken into account by the *mode matching coefficient* [34]. This coefficient is related to the matching between the spatial-temporal mode of the signal to be detected and the LO one. Besides behaving as an amplifier for the quadrature under study, the LO selects the only part of the signal that interferes with the LO field. To give a quantitative measure of this concept, let us start from the following expression of the quantized electric field:

$$\begin{aligned} \hat{E}(\mathbf{x},t) &= \sum_k \mathcal{E}_k(\hat{a}_k v_k(\mathbf{x}) e^{-i\omega_k t} + \hat{a}_k^\dagger v_k^*(\mathbf{x}) e^{i\omega_k t}) \\ &= \hat{E}^{(+)}(\mathbf{x},t) + \hat{E}^{(-)}(\mathbf{x},t) \end{aligned} \tag{3.7}$$

where without loss of generality the field is linearly polarized. The functions $v_k(\mathbf{x})$ are the spatial modes of the field and are particular solutions of the Helmholtz equation depending on the specific problem. Due to the Hermiticity of the Laplace operator, they are orthogonal,

so they satisfy the following condition:

$$\int_{-\infty}^{\infty}\int_{-\infty}^{\infty}\int_{-\infty}^{\infty} d\mathbf{x}\ v_k^*(\mathbf{x})v_{k'}(\mathbf{x}) = \delta_{kk'} \tag{3.8}$$

moreover they fullfill the completeness relation:

$$\sum_k v_k^*(\mathbf{x})v_k(\mathbf{x}') = \delta^{(3)}(\mathbf{x}-\mathbf{x}') \tag{3.9}$$

Photodiodes measure the intensity of the field, related to the energy density that is proportional to $|E(\mathbf{x},t)|^2$. However, at optical frequency, the terms $\left(\hat{E}^{(+)}(\mathbf{x},t)\right)^2\left(\hat{E}^{(-)}(\mathbf{x},t)\right)^2$ oscillate too rapidly to be observed by real photodiodes that require a temporal integration. So, the quantity actually measured in photodetection is the flux of photons recoiled by the active area of the PD rather than the energy density of the field. For this purpose it is convenient to define the flux operator:

$$\hat{\phi}(\mathbf{x},t) = \sum_k \hat{a}_k v_k(\mathbf{x}) e^{-i\omega_k t} \tag{3.10}$$

that, once integrated over all the space, gives the total number of photons for unit time:

$$\int_{-\infty}^{\infty}\int_{-\infty}^{\infty}\int_{-\infty}^{\infty} dxdydz\ \hat{\phi}^\dagger(\mathbf{x},t)\hat{\phi}(\mathbf{x},t) = \sum_k \hat{a}_k^\dagger \hat{a}_k \tag{3.11}$$

We can assume that the photocurrent measured by the photodiodes is proportional to the flux of photons that reaches the detector surface D during the time interval $[0,T]$

$$\hat{n} = \int_0^T dt \iint_D dx_D dy_D\ \hat{\phi}^\dagger(\mathbf{x_D},t)\hat{\phi}(\mathbf{x_D},t) \tag{3.12}$$

Since for the whole field (including the spatial part) relations similar to (3.2) stand:

$$E_1^{(+)}(\mathbf{x},t) = \frac{1}{\sqrt{2}}(E_S^{(+)} - E_{LO}^{(+)}) \tag{3.13}$$

$$E_2^{(+)}(\mathbf{x},t) = \frac{1}{\sqrt{2}}(E_S^{(+)} + E_{LO}^{(+)}) \tag{3.14}$$

we can write also for the fluxes:

$$\hat{\phi}_1(\mathbf{x},t) = \frac{1}{\sqrt{2}}(\hat{\phi}_S - \hat{\phi}_{LO}) \tag{3.15}$$

$$\hat{\phi}_2(\mathbf{x},t) = \frac{1}{\sqrt{2}}(\hat{\phi}_S + \hat{\phi}_{LO}) \tag{3.16}$$

The photon number difference is:

$$\hat{n}_{12} = \int_0^T dt \iint_D dx_D dy_D \; [\hat{\phi}_{LO}^\dagger \hat{\phi}_S + \hat{\phi}_S^\dagger \hat{\phi}_{LO}] \tag{3.17}$$

Supposing $\phi_{LO} \propto \alpha_{LO} v_{LO}(\mathbf{x},t) + h.c.$ with $\alpha_{LO} = |\alpha_{LO}|\, e^{i\vartheta}$ and with $v_{LO}(\mathbf{x},t) = v_{LO}(\mathbf{x})e^{-i\omega t}$, let us define:

$$\hat{a} \equiv \int_0^T dt \iint_D dx_D dy_D \hat{\phi}_S(\mathbf{x}_D,t) v_{LO}^*(\mathbf{x}_D,t) \tag{3.18}$$

Let us now suppose that the flux $\hat{\phi}_S$ consists of two parts:

$$\hat{\phi}_S = \hat{a}_s v_S(\mathbf{x},t) + \hat{\phi}_0 \tag{3.19}$$

where the first addend is the signal one wishes to observe, while the other is a vacuum field that takes into account other potential modes in $\hat{\phi}_S$. Let us define the quantity:

$$\eta_M^{1/2} \equiv \int_0^T dt \iint_D dx_D dy_D v_S(\mathbf{x}_D,t) v_{LO}^*(\mathbf{x}_D,t) \tag{3.20}$$

such that $\eta_M^{1/2} \leq 1$, as to be the *mode matching coefficient* that takes into account the superposition between the spatio-temporal part of the signal under scrutiny and the LO. Let

us also define the quantity:

$$(1-\eta_M)\,\hat{a}_M = \int_0^T dt \iint_D dx_D dy_D \hat{\phi}_0(\mathbf{x}_D,t) v^*_{LO}(\mathbf{x}_D,t) \tag{3.21}$$

then:

$$\begin{aligned} \hat{a} &\equiv \int_0^T dt \iint_D dx_D dy_D \left[\hat{a}_s v_S(\mathbf{x},t)\, v^*_{LO}(\mathbf{x}_D,t) + \hat{\phi}_0(\mathbf{x}_D,t) v^*_{LO}(\mathbf{x}_D,t)\right] \\ &= \eta_M^{1/2}\hat{a}_s + (1-\eta_M)\,\hat{a}_M \end{aligned} \tag{3.22}$$

So

$$\begin{aligned} \hat{n}_{12} &= |\alpha_{LO}|\sqrt{\eta_M}\left(e^{-i\vartheta}\hat{a}_S + e^{i\vartheta}\hat{a}_S^\dagger\right) \\ &\quad + |\alpha_{LO}|\sqrt{1-\eta_M}\left(e^{-i\vartheta}a_M + e^{i\vartheta}\hat{a}_M^\dagger\right) \end{aligned} \tag{3.23}$$

In conclusion the mode mismatch can be described by a simple model in which the mode matching coefficient can be regarded as the trasmission coefficient of a fictitious beam splitter; the transmitted part is detected while the reflected one is lost. As we can observe, if the perfect mode macthing conditions are achieved ($\eta_M = 1$) then homodyne detects exactly the signal mode and:

$$\hat{n}_{12} = \sqrt{2}\,|\alpha_{LO}|\,\hat{X}_S(\vartheta) \tag{3.24}$$

$$\triangle\hat{n}_{12} = |\alpha_{LO}|^2\,\triangle\hat{X}_S(\vartheta) \tag{3.25}$$

3.1.2 Homodyne efficiency

Homodyne efficiency depends not only on the mode matching between the signal and the reference LO beam. Indeed, so far we have assumed the photodiodes to possess a perfect quantum efficiency $\eta_{PD} = 1$ such that all impinging photons are detected. However this whished situation is far from being real and losses due to the real $\eta_{PD} < 1$ have to be taken

into account [34].

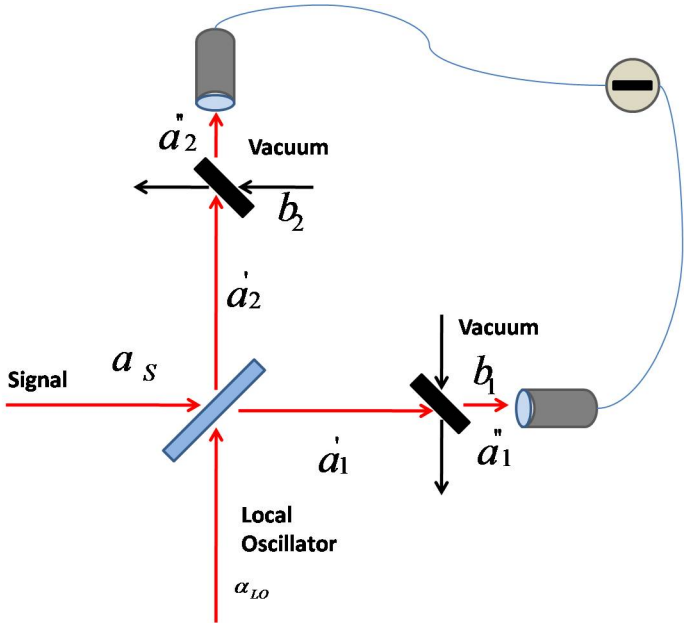

Figure 3.2: Schematic representation in which the finite efficiency η_{PD} of the HD photodiodes is modeled with a BS of transmittivity equal to η_{PD} positioned before each of the two photodiodes.

Let us suppose that the quantum efficiencies of the two HD photodiodes coincide and let us model this loss effect by figuring the presence of two BSs, preceding the photodiodes, and possessing a trasmission coefficient equal to the quantum efficiency of the photodiodes η_{PD} (see fig 3.2). If $\hat{a}_1'$ and $\hat{a}_2'$ are the modes outing from the two ports of the 50-50 homodyne detector BS:

$$\hat{a}_1'' = \sqrt{\eta_{PD}}\hat{a}_1' + \sqrt{1-\eta_{PD}}\hat{b}_1 \tag{3.26}$$

$$\hat{a}_2'' = \sqrt{\eta_{PD}}\hat{a}_2' + \sqrt{1-\eta_{PD}}\hat{b}_2 \tag{3.27}$$

where $\hat{b}_1$ and $\hat{b}_2$ are the annihilation operators of vacuum that fill the two unused ports of

the two BSs. It can be shown that:

$$\begin{aligned}\hat{n}_{21} &= \hat{a}_2''^{\dagger}\hat{a}_2'' - \hat{a}_1''^{\dagger}\hat{a}_1'' && (3.28)\\ &= \eta_{PD}\left(\hat{a}_2'^{\dagger}\hat{a}_2' - \hat{a}_1'^{\dagger}\hat{a}_1'\right) \\ &\quad + \sqrt{\eta_{PD}\left(1-\eta_{PD}\right)}\left(\hat{a}_2'^{\dagger}\hat{b}_2 + \hat{b}_2^{\dagger}\hat{a}_2' - \hat{a}_1'^{\dagger}\hat{b}_1 - \hat{b}_1^{\dagger}\hat{a}_1'\right) \\ &\quad + \left(1-\eta_{PD}\right)\left(\hat{b}_2^{\dagger}\hat{b}_2 - \hat{b}_1^{\dagger}\hat{b}_1\right) && (3.29)\end{aligned}$$

By supposing the LO to be very intense, we eventually get:

$$\hat{n}_{21} = \sqrt{\eta_{PD}}\alpha_{LO}^{*}\left(\sqrt{\eta_{PD}}\hat{a}_S + \sqrt{1-\eta_{PD}}\hat{b}\right) + h.c. \quad (3.30)$$

where $\hat{b} = \frac{1}{2}\left(\hat{b}_2 - \hat{b}_1\right)$. So in conclusion losses due to the not perfect mode matching and to quantum efficiency of photodiodes can by combined by immagining a BS before the HD with transitttivity equal to $\eta = \eta_{PD}\eta_M$ that corresponds to the overall HD efficiency.

3.1.3 Homodyne detector visibility

As seen before a crucial role in homodyne detection is played by the "mode matching" between the signal and the reference coherent beam. HD is essentially an interferometeric device so it is characterized by a visibility and a related contrast. These two quantities are a measure of the degree of superposition between the two beams and consequently of the HD efficiency.

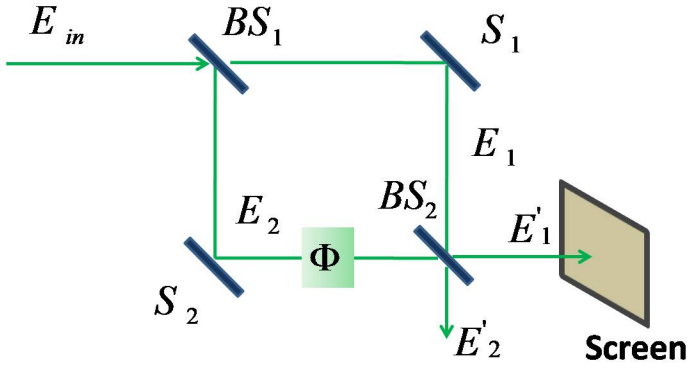

Figure 3.3: Schematic representation of an interferometric device.

By looking fig. 3.3, if r_1 is the reflectivity of BS_1 we have:

$$E_1 = \sqrt{1 - r_1^2} E_{in} \qquad E_2 = r_1 E_{in} \tag{3.31}$$

After passing through the phase shifter, if r_2 is the reflectivity of BS_2 we get:

$$E_1^{'} = -r_2 E_1 + \sqrt{1 - r_2^2} E_2 e^{i\Phi} \tag{3.32}$$

$$E_2^{'} = \sqrt{1 - r_2^2} E_1 + r_2 E_2 e^{i\Phi} \tag{3.33}$$

By setting:

$$A = r_2\sqrt{1 - r_1^2} \qquad B = r_1\sqrt{1 - r_2^2}$$
$$C = \sqrt{(1 - r_1^2)(1 - r_2^2)} \qquad D = r_1 r_2$$

It is easy to show that:

$$E_1^{'} = \left(-A + Be^{i\Phi}\right) E_{in} \tag{3.34}$$

$$E_2^{'} = \left(C + De^{i\Phi}\right) E_{in} \tag{3.35}$$

So the two intensities are proportional to:

$$I_1^{'}(\Phi) = \left|E_1^{'}\right|^2 = \left(A^2 + B^2 + 2AB\cos\Phi\right) I_{in} \tag{3.36}$$

$$I_2^{'}(\Phi) = \left|E_2^{'}\right|^2 = \left(C^2 + D^2 + 2CD\cos\Phi\right) I_{in} \tag{3.37}$$

Visibility is defined as:

$$VIS = \frac{CNT}{VIS_{perf}} = \frac{I_1 + I_2}{2\sqrt{I_1 I_2}} VIS_{perf} \tag{3.38}$$

being:

$$CNT = \frac{I_{max}^{'} - I_{min}^{'}}{I_{max}^{'} + I_{min}^{'}} = \frac{AB}{A^2 + B^2} \tag{3.39}$$

the contrast, while:

$$VIS_{perf} = \frac{2\sqrt{I_1 I_2}}{I_1 + I_2} \tag{3.40}$$

the perfect visibility. In case of perfect balancing of the interferometer branches $VIS_{perf} = 1$ and consequently $VIS = CNT$.

3.1.3.1 Interference between Gaussian beams

Let us recall that the expression describing a Gaussian beam is given by:

$$E(x,y,z) = E_{00}\frac{w_0}{w(z)} e^{-\frac{x^2+y^2}{w^2(z)}} e^{-i\left(\frac{kr^2}{2R(z)}+kz+\xi\right)} \tag{3.41}$$

We want to calculate the contrast, just defined, between two Gaussian beams having the following expressions:

$$\begin{aligned} E_1(x,y,z) &= \sqrt{\frac{2}{\pi}} \exp\left[-(x-x_0)^2 - y^2\right. & (3.42)\\ &\quad \left. -ikz - i\frac{(x^2+y^2)}{2R} + i\xi + i\eta\right] & (3.43)\\ E_2(x,y,z) &= \sqrt{\frac{2}{\pi}} \exp\left[-x^2 - y^2\right. & (3.44)\\ &\quad \left. -ikz - i\frac{(x^2+y^2)}{2R} + i\xi\right] & (3.45) \end{aligned}$$

where η is an external phase shift and the expressions are renormalized with respect $w(z)$. Here we are supposing the beams to have the same linear polarization and to propagate along the z axis. By recalling that the waist of the beam is given by:

$$w_0 = \sqrt{\frac{\lambda z_0}{\pi}} \tag{3.46}$$

if we suppose that the two beams have the same confocal parameter $b = 2z_0$ then they have the same waist. The two wave vectors are parallel but not collinear since the centers of the two Gaussian envelopes do not coincide (they are shifted by x_0). Moreover since the waist is located for both the beams in $z = 0$, the two beams have the same curvature radius. The

situation is pictorially depicted in fig 3.4.

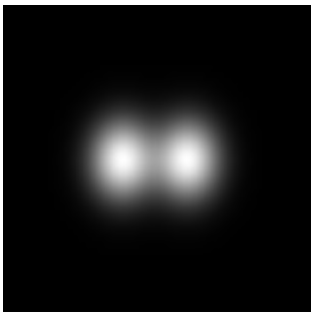

Figure 3.4: Pictorial representation of two non-concetric Gaussian baeams impinginig on a screen.

The contrast is given by:

$$CNT = \frac{\int\int dx\ dy\ \Omega\left(x,y\right)}{2} \tag{3.47}$$

where $\Omega\left(x,y\right)$ is the interference term in $I = I_1 + I_2 + \Omega$:

$$\Omega\left(x,y\right) = E_1^* E_2 + c.c \tag{3.48}$$

and we have supposed:

$$\iint dx\ dy\ I_1 = \iint dx\ dy\ I_2 = 1 \tag{3.49}$$

Integration is carried out over all the space since the dimensions of the beam are supposed to be smaller than the active area of photodiodes and so integrating over this area or over all the space leads to the same result. By doing the explicit calculation we get:

$$CNT\left(x_0\right) = e^{-\frac{x_0^2}{2}} \cos\left[\eta\right] \tag{3.50}$$

By setting $\eta = 0$ the behaviour of the contrast with varying the distance between the centers of the two Gaussian envelopes is shown in the following fig. 3.5.

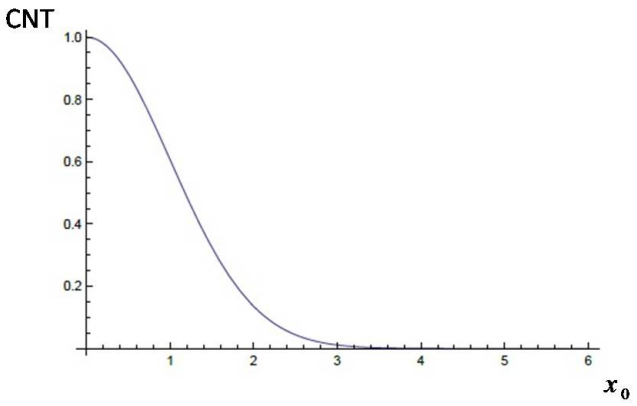

Figure 3.5: CNT for two Gaussian beams vs the separation between the Gaussian centers x_0.

As it is evident from the plot, the maximum CNT is achieved when the two beams are concentric.

3.1.4 Homodyne for structured beams

Up to now we have considered the case of Gaussian beams. However the entangled beams we produce carry OAM and their spatial structure is more complex than the Gaussian ones. In ordinary HD, in which the signal is not spatially structured, the factors playing a leading role in enhancing interference are essentially those related to the optical path, to the polarization and to the the geometrical properties of the two beams. When introducing OAM d.o.f., a further effort is required in order to improve the mode matching and, in such a way, to enhance the overall homodyne detector efficiency.

In particular, it is important that, when impinging the homodyne beam splitter, both the beams have the same spatial structure. Since these modes have a peculiar spatial structure, related to the OAM amount they carry, it is important in order to ensure interference that the two beams possess the same OAM value. However, as will be more clear in the following, this request alone is not enough, since a central role is played by the OAM component along the propagation axis.

3.1.4.1 Interference between Laguerre-Gauss beams

Let us now perform the calculation of the contrast in the case of two Laguerre-Gauss modes as an example of beams carrying OAM and having a peculiar spatial structure. We recall that the expression describing the LG modes is the following:

$$\begin{aligned} E(r,\theta,z) &= E_{mp}\frac{w_0}{w(z)}\left(\frac{\sqrt{2}r}{w(z)}\right)^{|m|} L_p^{|m|}\left(\frac{2r^2}{w^2(z)}\right) e^{-\frac{r^2}{w^2(z)}} \\ & \quad e^{-i\left(k\frac{r^2}{2R(z)}+kz+m\theta-(2p+1+|m|)\xi\right)} \end{aligned} \tag{3.51}$$

In particular we want to calculate the interference term, and consequently the contrast, between two beams carrying the same amount of OAM $\hbar$ and having the same component along the propagation direction:

$$\begin{aligned} E_1(x,y,z,\theta) &= \sqrt{\frac{2}{\pi}}\left(\sqrt{2}\sqrt{(x-x_0)^2+y^2}\right) \\ & \quad \exp\left[-(x-x_0)^2-y^2-ikz-i\frac{x^2+y^2}{2R}-i\theta+2i\xi+i\delta\right] \\ E_2(x,y,z,\theta) &= \sqrt{\frac{2}{\pi}}\left(\sqrt{2}\sqrt{x^2+y^2}\right) \\ & \quad \exp\left[-x^2-y^2-ikz-i\frac{x^2+y^2}{2R}-i\theta+2i\xi\right] \end{aligned} \tag{3.52}$$

where δ is an external phase shift and the beams are supposed to propagate along the z direction with the same linear polarization. As in the previous case the confocal parameters of the two beams coincide, the wave vectors are parallel and the waist is located in the same position $z = 0$. The centers of the two Gaussian envelopes are separated by a distance x_0 and the two expressions are renormalized with respect to $w(z)$. For both the beams $m = 1$ and $p = 0$ $\left(L_0^{|m|}(x) = 1\right)$. This situation is pictorially depicted in fig 3.6

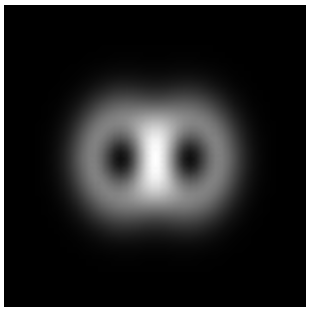

Figure 3.6: Pictorial representation of two non-concentric LG beams impinging on a screen.

In this case the interference term turns to be:

$$\begin{aligned} \Omega(x,y) &= 4\left(\frac{2}{\pi}\right)\exp\left[-2x^{2+2xx_0-x_0^2-2y^2}\right] \\ &\quad \sqrt{x^2+y^2}\sqrt{(x-x_0)^2+y^2}\cos[\delta] \end{aligned} \tag{3.53}$$

By setting $\delta = 0$ we get the following behaviour shown in figure 3.7

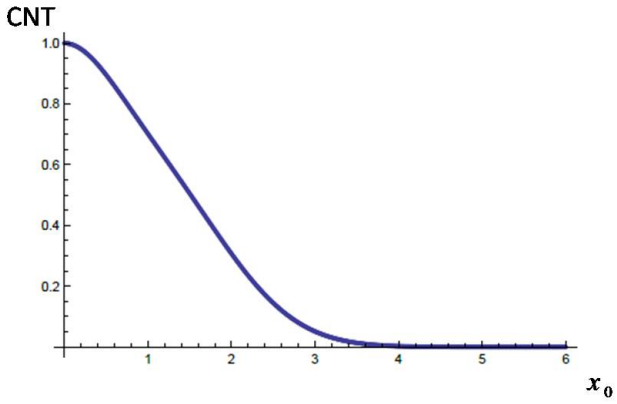

Figure 3.7: CNT for two LG beams vs the separation between the Gaussian centers x_0.

As in the case of Gaussian beams the maximum contrast is reached when the centers of the two Gaussian envelopes coincide. In fig 3.8 is displaced a plot in which the contrasts for Gaussian and LG beams are compared.

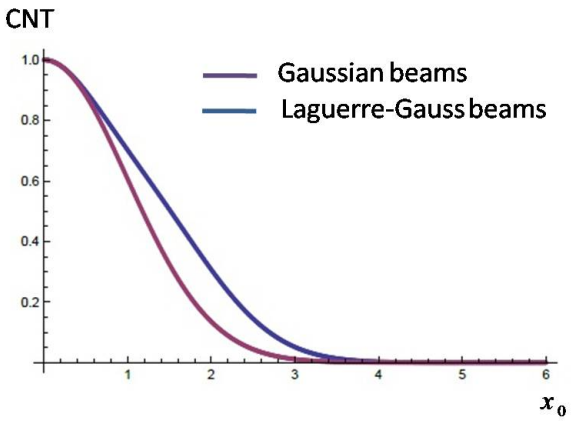

Figure 3.8: Comparison of the behaviours of CNT at varying the separation between the center of the two beams for Gaussian and LG beams.

As it is possible to infer from the plot Gaussian beams are more sensitive to concentricity with respect to vortex beams. It is also possible to show that when the two beams have opposite (or more in general different) amounts of OAM along the propagation direction they do not interfere.

3.2 The Homodyne detector

The experimental scheme of the homodyne detector is depicted in fig 3.9.

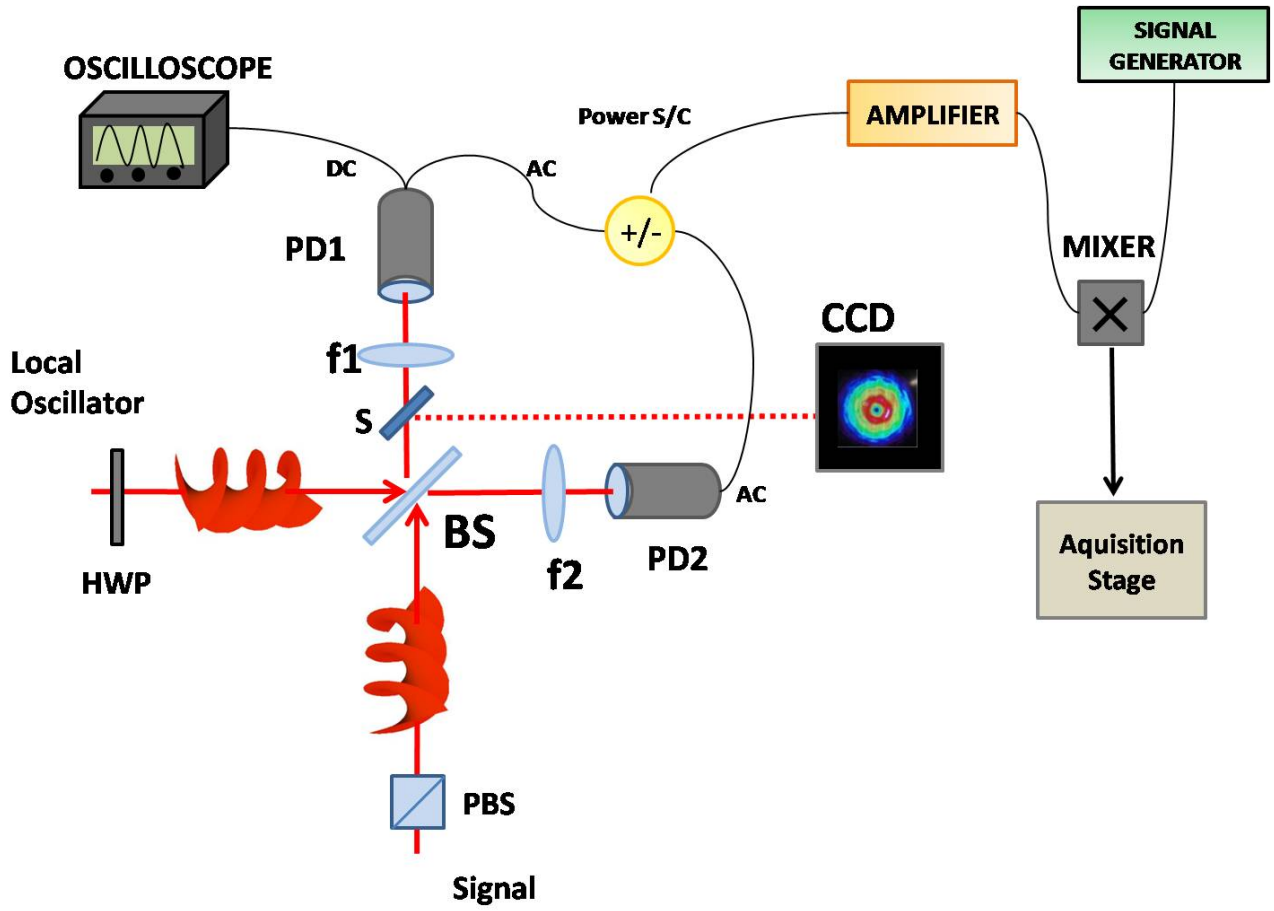

Figure 3.9: Homodyne detector experimental scheme

It consists of a 50% reflecting BS (optimized to work in p polarization) to whom are sent both the OPO output and the LO after being endowed with OAM. The polarization of the ingoing beams are adjusted thanks to a PBS placed on the signal branch and a HWP on the LO branch that permits polarization rotations. The BS is positioned on a support provided of a rotatory stage with micrometric screws that allow to tailor the system alignement. BS outputs are sent to a pair of high quantum efficiency photodiodes (Epitaxx ETX300) PD1 and PD2 $\eta_{PD} \simeq 0.97$

Dark currents	$1.0 - 5.0\ nA$
Responsivity (@1300nm)	$0.80 - 0.90\ A/W$
Parasite capacity	$5.0 - 8.0\ pF$
Active area	$300\ \mu m$
Bandwidth	$0.4\ GHz$
Saturation power	$6\ mW$

Table 3.1: Photodiodes characteristics

Due to their small active area, two focusing lenses f1 and f2 ($f = 50\ mm$) are placed in front of each photodiode. Before the photodiode PD1 a movable mirror allows to divert the beam to a CCD in order to monitorate its shape and to facilitate the measurement of both HD visibility and contrast. The two photodiodes are internally amplified and possess two outputs. The AC outputs are connected to an hybrid power splitter/combiner (power s/c) returning both the sum and the difference of the incoming signals. The difference between the two photocurrents is amplified by a low noise high gain amplifier (Miteq AU1442 $G = 34\ dB$, noise) and is sent to a mixer connected to a signal generator that realizes the product between the two signals. Lastly after being filtered the mixer output is sent to the acquisition stage.

The two DC outputs of the photodiodes are used to check homodyne balancing.

3.3 Mode matching between the signal and the LO

As previously discussed, the achievement of a good mode matching is essential to enhance the efficiency in detection. A testbed for the goodness of mode matching is given by the visibility of our interferometric setup. In order to experimentally determine the visibility, the OPO cavity is locked to the TEM_{00} mode of an IR beam that travels all the way down to the HD to interfere with the LO. Both the LO and the signal are endowed with the same amount of OAM in the propagation direction for the reasons discussed above.

In particular the mode that is used in this procedure is the mode $\hat{a}$ outing from the OPO. As discussed before this mode is produced by the OPO with a linear polarization and, thanks to the setup described in section 2.1.8 it acquires along its propagation an amount of OAM equal to $\hbar$. The IR laser output (@1064 nm) is tailored in order to interfere with the beam

coming from the OPO. Their intensities are kept to be equal during this procedure (only when HD is ready to use LO amplitude is increased). The matching between the confocal parameters is achieved by making the LO beam to pass through a passive cavity (Mode Cleaner, (MC)), with the same properties of the OPO one. This cavity is resonant with the Gaussian TEM_{00} mode thanks to a PDH active control system identical to the OPO one. The equality of the optical paths followed by the two beams after outing the cavities is ensured by adjusting the optical path of the LO by means of an optical delay line, positioned at the MC output. The relative phase of the LO with respect to the OPO is changed thanks to a PZT, driven by a linear ramp, that changes the length of the optical delay line so changing the phase in an interval of $[0, 2\pi]$. After outing from the MC cavity the beam is made to acquire the same amount of OAM, along the propagation direction, thanks to the experimetal scheme shown in figure 3.10

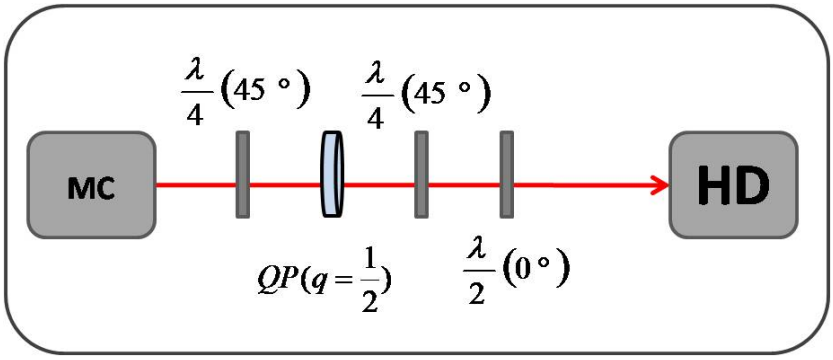

Figure 3.10: Setup to endow LO beam with OAM equal to $\hbar$ in the propagation direction

The first QWP at 45° transforms the horizontal polarization of the LO into left circular one, then the beam crosses the QP by aquiring OAM equal to $\hbar$ in the propagation direction and flips its polarization that turns to be right. The following QWP, with the same orientation, makes the beam linearly polarized again in the horizontal direction, eventually the HWP oriented at 0° adds nothing but that an overall phase factor. As seen in previous calculation the superposition between the two LG beams is maximum when they are coaxial (when their singularities are made to coincide). This condition is achieved thanks to a beam steering (HR @1064) that aligns the LO direction, monitored during the procedure thanks

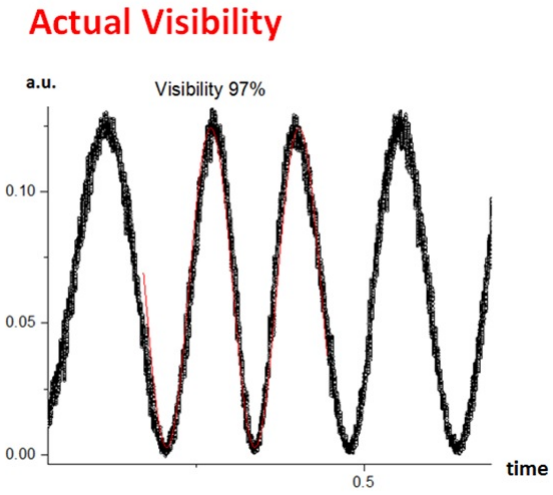

Figure 3.11: Signal measured by an oscilloscope connected to the DC output of one of HD photodiodes. The oscillatory behaviour is due to the interference between the seeded OPO and the LO, both provided with OAM, achieved by varying their relative phase in time.

to a CCD (TM 745 Spiricon). A further HWP after the beam steering corrects potential rotation due to the presence of the mirrors.

The phase shift between the LO and the OPO beams makes each of the beams outing from the two HD beam splitter outputs to show an oscillatory behaviour. One of these two beams is recoiled by one of the two HD photodiodes whose DC output is sent to an oscilloscopy. A quantitative measurement of the contrast:

$$CNT = \frac{I_{max} - I_{min}}{I_{max} + I_{min}} \tag{3.54}$$

is carried out so that mode matching quality is monitored by measuring deviations from the value 1 of the contrast. Typical visibility:

$$VIS = \frac{2\sqrt{I_s I_{LO}}}{I_S + I_{LO}} CNT \tag{3.55}$$

obtained are $VIS = 0.97 \pm 0.02$.

Chapter 4

Data acquisition and processing

In this last chapter we report the main experimental results of this dissertation together with the procedure for the acquisition of the data and their subsequent processing. The goal of the experiment, whose building blocks have been illustrated in previous chapters, consists in characterizing the quantum bipartite state we produce in order to establish whether entanglement between the two subparts persists. Witnessing the presence of entanglement is of huge importance to establish if the state can be exploited as a support for quantum protocols. Indeed as previously pointed out, entanglement is a pure quantum feature and, as such, it can easly be corrupted by decoherence due to the interaction with the external environment. In order to assess the presence of quantum correlations, the knowledge of the covariance matrix is essential, since in it, the whole information on the state is stored. Its elements are measured via homodyne detection technique, by elaboration of the acquired data. Since the generation stage produces a helical bipartite Gaussian state, its CM is a 4×4 matrix whose elements are the second moments of quadrature operators. As will be clarified in the following section, it would be needed in principle a double HD scheme in order to fully evaluate the CM. However a trick to avoid the second HD will be presented and its experimental realization will be depicted.

In the first part of this chapter the technique to characterize bipartite states using a single HD will be explained, then it will be presented the aquisition stage.

Eventually a typical CM is presented and the information on the properties of this state will be discussed.

4.1 Full characterization of a bipartite state using a single HD

GSs have the priviledge of being fully characterized by the knowledge of their CM. The elements of this matrix assume, the form of equation (1.152) so the whole CM for a bipartite state is:

$$\sigma = \begin{pmatrix} \triangle\hat{X}_a^2 & \triangle\hat{X}_a\hat{Y}_a & \triangle\hat{X}_a\hat{X}_b & \triangle\hat{X}_a\hat{Y}_b \\ \triangle\hat{Y}_a\hat{X}_a & \triangle\hat{Y}_a^2 & \triangle\hat{Y}_a\hat{X}_b & \triangle\hat{Y}_a\hat{Y}_b \\ \triangle\hat{X}_b X_a & \triangle\hat{X}_b\hat{Y}_a & \triangle\hat{X}_b^2 & \triangle\hat{X}_b Y_b \\ \triangle\hat{Y}_b\hat{X}_a & \triangle\hat{Y}_b\hat{Y}_a & \triangle\hat{Y}_b\hat{X}_b & \triangle\hat{Y}_b^2 \end{pmatrix} \tag{4.1}$$

where the labels a and b indicates the two subsystems of the state. Let us consider for instance the term σ_{13}, whose expression is the following:

$$\triangle\hat{X}_a\hat{X}_b = \frac{1}{2}\left\langle\left\{\hat{X}_a, \hat{X}_b\right\}\right\rangle - \left\langle\hat{X}_a\right\rangle\left\langle\hat{X}_b\right\rangle$$

In this element of the covariance matrix, belonging to one of the two blocks concerning with correlations between the two modes, the expectation value of the product of the two modes appears. This means that during the acquisition stage an experimental scheme consisting of two HDs simultaneously working would be needed. However it has been proposed a powerful scheme [35], involving repeated measurements of single-mode quadratures that is capable of circumvent this issue.

It is possible to introduce four additional modes, combination of the modes $\hat{a}$ and $\hat{b}$, in such a way to rewrite the matrix (4.1) in a more convenient way for pratical experimental

uses. These four modes are the following combination of $\hat{a}$ and $\hat{b}$:

$$\hat{c} = \frac{\hat{a} + \hat{b}}{\sqrt{2}} \qquad \hat{d} = \frac{\hat{a} + \hat{b}}{\sqrt{2}}$$
$$\hat{e} = \frac{\hat{a} - i\hat{b}}{\sqrt{2}} \qquad \hat{f} = \frac{\hat{a} + i\hat{b}}{\sqrt{2}}$$

It is possible to show, with some algebra, that the matrix (4.1) can be rewritten as a summation of two matrices:

$$\sigma = V - M \tag{4.2}$$

being,

$$V = \frac{1}{2}\begin{pmatrix} 2\left\langle \hat{X}_a^2 \right\rangle & \left\langle \hat{Z}_a^2 \right\rangle - \left\langle \hat{T}_a^2 \right\rangle & \left\langle \hat{X}_c^2 \right\rangle - \left\langle \hat{X}_d^2 \right\rangle & \left\langle \hat{Y}_e^2 \right\rangle - \left\langle \hat{Y}_f^2 \right\rangle \\ \left\langle \hat{Z}_a^2 \right\rangle - \left\langle \hat{T}_a^2 \right\rangle & 2\left\langle \hat{Y}_a^2 \right\rangle & \left\langle \hat{X}_f^2 \right\rangle - \left\langle \hat{X}_e^2 \right\rangle & \left\langle \hat{Y}_c^2 \right\rangle - \left\langle \hat{Y}_d^2 \right\rangle \\ \left\langle \hat{X}_c^2 \right\rangle - \left\langle \hat{X}_d^2 \right\rangle & \left\langle \hat{X}_f^2 \right\rangle - \left\langle \hat{X}_e^2 \right\rangle & 2\left\langle \hat{X}_b^2 \right\rangle & \left\langle \hat{Z}_b^2 \right\rangle - \left\langle \hat{T}_b^2 \right\rangle \\ \left\langle \hat{Y}_e^2 \right\rangle - \left\langle \hat{Y}_f^2 \right\rangle & \left\langle \hat{Y}_c^2 \right\rangle - \left\langle \hat{Y}_d^2 \right\rangle & \left\langle \hat{Z}_b^2 \right\rangle - \left\langle \hat{T}_b^2 \right\rangle & 2\left\langle \hat{Y}_b^2 \right\rangle \end{pmatrix} \tag{4.3}$$

and,

$$M = \begin{pmatrix} \left\langle \hat{X}_a \right\rangle^2 & \left\langle \hat{X}_a \right\rangle \left\langle \hat{Y}_a \right\rangle & \left\langle \hat{X}_a \right\rangle \left\langle \hat{X}_b \right\rangle & \left\langle \hat{X}_a \right\rangle \left\langle \hat{Y}_b \right\rangle \\ \left\langle \hat{Y}_a \right\rangle \left\langle \hat{X}_a \right\rangle & \left\langle \hat{Y}_a \right\rangle^2 & \left\langle \hat{Y}_a \right\rangle \left\langle \hat{X}_b \right\rangle & \left\langle \hat{Y}_a \right\rangle \left\langle \hat{Y}_b \right\rangle \\ \left\langle \hat{X}_a \right\rangle \left\langle \hat{X}_b \right\rangle & \left\langle \hat{X}_a \right\rangle \left\langle \hat{X}_b \right\rangle & \left\langle \hat{X}_b \right\rangle^2 & \left\langle \hat{X}_b \right\rangle \left\langle \hat{Y}_b \right\rangle \\ \left\langle \hat{Y}_b \right\rangle \left\langle \hat{X}_a \right\rangle & \left\langle \hat{Y}_b \right\rangle \left\langle \hat{Y}_a \right\rangle & \left\langle \hat{Y}_b \right\rangle \left\langle \hat{X}_b \right\rangle & \left\langle \hat{Y}_b \right\rangle^2 \end{pmatrix} \tag{4.4}$$

Where, recalling the definition of generalized quadrature:

$$\hat{X}_k(\vartheta) = \frac{\hat{a}_k e^{i\vartheta} + \hat{a}_k^\dagger e^{-i\vartheta}}{\sqrt{2}} \tag{4.5}$$

the following notations have been employed:

$$\hat{X}_k \equiv \hat{X}_k(0) \qquad \hat{Y}_k \equiv \hat{X}_k\left(\frac{\pi}{2}\right)$$
$$\hat{Z}_k \equiv \hat{X}_k\left(\frac{\pi}{4}\right) \qquad \hat{Z}_k \equiv \hat{X}_k\left(\frac{\pi}{4}\right)$$

For simmetry reasons, this method involves the measurement of 14 different quadratures pertaining to six single-mode fields in order to reconstruct the full CM and to extract from it the needed information. However, it is possible to show that one of the modes is not necessary so that five modes are sufficient to reconstruct the CM.

4.2 Experimental implementation and data acquisition

We now describe the procedure carried out to measure the CM of the bipartitie state applying of the above proposed conceptual scheme.

Let us recall the main features of our experimental setup, by looking to fig 4.1.

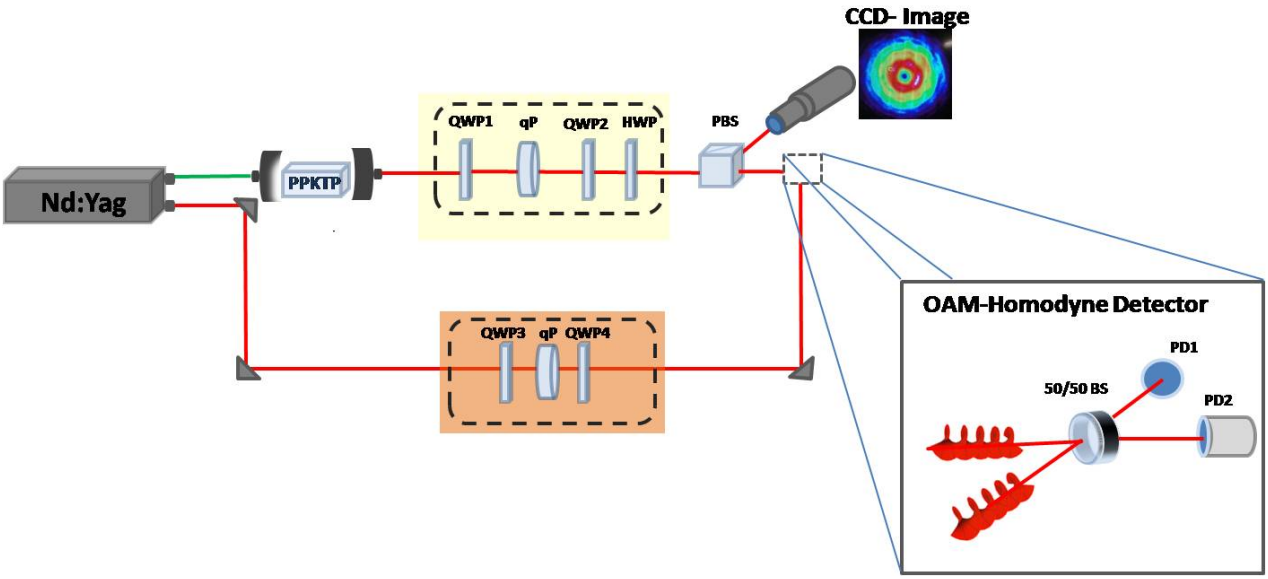

Figure 4.1: Schematic representation of the overall experimental setup employed both for the generation and the characterization, via HD of the bipartite OAM-entangled state.

As explained in previous sections, the laser provides two outputs @1064 nm and @532 nm, the green beam is used as a pump for the OPO. After adjusting the alignment of the interferometer in order to achieve a good visibility the threshold power for the pump is evaluated (minimum value for which the SPDC occurs). Typical threshold values are about 70 mW and, in order to make the OPO to work below threshold, its power has been sat at about the 70% of the measured threshold. Then the triply resonance condition for the OPO cavity

is achieved by suitably tailoring the crystal temperature and the laser frequency [32]. Eventually the OPO cavity is locked on the Gaussian TEM_{00} mode thanks to the PDH control system. The other IR laser output is used as LO. Its power is augmented in order to a have a strong coherent beam. A fraction of the LO is used as OPO seed and it is injected into the OPO cavity with a diagonal polarization in order to stimulate the production of parametric down converted beams with orthogonal polarizations. The seed is then obscured during the actual acquisition stage. After passing through the MC cavity, whose function as been already discussed, the LO encounters on its propagation direction the optical elements depicted in fig 4.1. When the optimal working conditions have been accomplished, the OPO cavity provides two collinear and orthogonally polarized modes that then undergo the sequence of optical elements shown in figure 4.1.

In order to evaluate the covariance matrix, aiming at applying the single HD scheme described in previous section, modes $\hat{a}, \hat{b}, \hat{c}, \hat{d}$ and $\hat{f}$ are obtained by suitably choosing the relative orientations of the waveplates on the OPO branch. This experimental configuration permits both to select the wanted mode to be sent to the detection stage and to endow these modes with the desired amount of OAM. The way to select each of the modes and transform it into an helical beam has been exaustively explained in sections 2.1.8 and 2.1.9. Here we recall the configuration corresponding to each mode schematically in table 4.1

OPO branch	**QWP1**	**QP**	**QWP2**	**HWP**
$\hat{a}$ **mode**	45°	Y	45°	0°
$\hat{b}$ **mode**	45°	Y	45°	45°
$\hat{c}$ **mode**	90°	Y	45°	0°
$\hat{d}$ **mode**	90°	Y	45°	45°
$\hat{e}$ **mode**	N	Y	45°	0°
$\hat{f}$ **mode**	N	Y	45°	45°

Table 4.1: Recap of the configuration scheme to obtain the combination of the modes outing from the OPO with OAM.

$\hat{a}$, $\hat{c}$ and $\hat{e}$ are provided with OAM equal to $\hbar$ while $\hat{b}$, $\hat{d}$ and $\hat{f}$ show OAM equal to $-\hbar$. Then, these modes are sent one at a time to the HD by suitably changing the configuration of optical elements thanks to a remote LabView control routine.

In order to detect the modes via HD, as previously discussed, it is essential in order to have interference, that the two modes, LO and signal, carry the same amount of OAM along the propagation direction.

In order to achieve this condition LO is tailored thanks to the sequence of waveplates on its branch so to aquire the right amount of OAM depending on the mode that has been sent to HD. In particular the wave plates on the LO branch switch between the configurations $|H\rangle|1\rangle$ and $|H\rangle|-1\rangle$, shown in table 4.2, corresponding to the two different components of OAM in the propagation direction involved in the experiment.

LO branch	**QWP3**	**QP**	**QWP4**
$\hat{a},\ \hat{c},\ \hat{e}$ **modes**	45°	Y	45°
$\hat{a},\ \hat{d},\ \hat{e}$ **modes**	−45°	Y	−45°

Table 4.2: Recap of the configurations of the vaweplates on the LO branch corresponding to OAM $\pm\hbar$.

During the acquisition stage the LO phase is spanned over the interval $[0, 2\pi]$. Homodyne traces, obscuring both the LO and the OPO branch, are collected in order to take into account of the background noise. Subsequently a trace of the vacuum state obtained obscuring only the OPO branch is acquired in order to fix the shot noise level. Subsequently instantaneous measures of the quadrature corresponding to the mode sent to HD are acquired thanks to a data acquisition board. For each mode the corresponding LO configuration is chosen . In fig 4.2 picture a typical homodyne trace corresponding to the the single-mode field $\hat{c}$ exhibiting squeezing is shown.

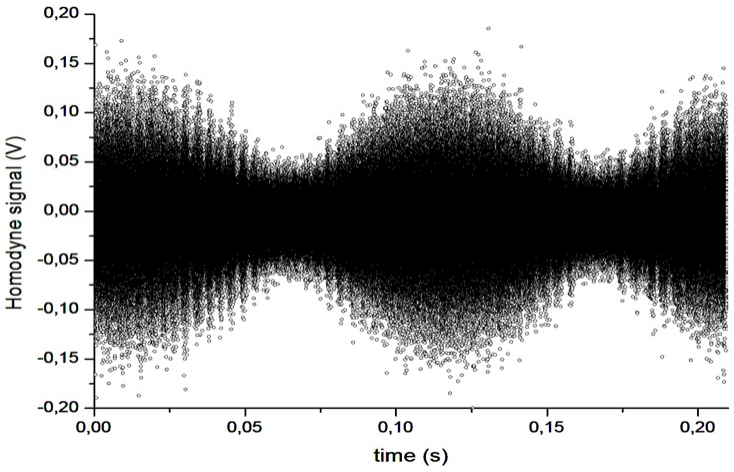

Figure 4.2: Homodyne trace of the mode $\hat{c}$ exhibiting squeezing.

4.3 Data processing

After collecting the values of the quadratures for the six modes discussed above thanks to a *Mathematica* © routine data are processed in order to extract from them the quadratures needed to reconstruct the CM according to the procedure discussed in section 4.1. A typical CM experimentally obtained is the following:

$$\sigma = \begin{pmatrix} 0.61 \pm 0.02 & -0.00(3) \pm 0.02 & 0.29 \pm 0.02 & -0.00(08) \pm 0.02 \\ -0.00(3) \pm 0.06 & 0.61 \pm 0.02 & -0.00(5) \pm 0.02 & -0.23 \pm 0.02 \\ 0.29 \pm 0.02 & -0.00(5) \pm 0.02 & 0.60 \pm 0.02 & -0.00(1) \pm 0.02 \\ -0.00(08) \pm 0.02 & -0.23 \pm 0.05 & -0.00(1) \pm 0.06 & 0.60 \pm 0.02 \end{pmatrix} \tag{4.6}$$

where the elements confident with 0 are reported with the highest significant digit in parenthesis. In order to establish whether entanglement subsists the PHS and the Duan criteria have been applied to the matrix. Let us recall that, according to the PHS (PPT) criterion a bipartite state represented by a CM of the form (1.170) is separable if:

$$a^2 + b^2 + 2\,|c_1 c_2| - 4(ab - c_1^2)(ab - c_2^2) \leq \frac{1}{4} \tag{4.7}$$

since this inequality is violated by our state (the lhs results to be 0.51) the helical modes a and b generated by the setup described above are OAM-entangled beams. The state results

to be non-separable also according to the Duan criterion for which a state is entangled if:.

$$\sqrt{(2n-1)(1m-1)} - c_1 c_2 < 0 \tag{4.8}$$

indeed the lhs for the CM (4.6) is -0.31.

From experimental single-mode data, corresponding to the squeezed modes $\hat{c}$, $\hat{d}$, $\hat{e}$, $\hat{f}$, have been extracted, thanks to the equation (1.191), the values of the trasmission coefficients. This coefficent is a marker of the losses due to the efficiency of the whole setup. By averaging the values of these four modes we have obtained the value 0.53 corresponding to losses of the 47%. This value is compatible with losses evaluated by considering the effects due to the various building blocks of the experimental setup. One of these factors is associated to the transmittivity of the cavity output mirror T_{out} that is chosen in order to ensure, toghether with the crystal losses (κ), and other losses mechanisms (T_{in}), an output coupling parameter $\eta_{out} = T_{out}/(T_{in} + \kappa)$ that @1064 nm results to be ~ 0.73. Another factor that has to be taken into account are the losses due to the QP that possess a transmission of about 0.85% ; eventually, as previoulsy said, PDs efficiency is (~ 0.9) while the HD visibility (> 0.95) . All these factors lead to an overall efficiency of detection equal to 0.53, in agreement with the experimental value.

4.4 Joint probability distribution

Given the CM of the state it is also possible to retrive the joint photon number distribution $p(n,m)$. This distribution is given by [9] the following expression:

$$p(n,m) = \int_{C_2} \frac{d^2\lambda_1 d^2\lambda_2}{\pi^2} \chi(\lambda_1,\lambda_2)\, \chi_n(-\lambda_1)\, \chi_m(-\lambda_2) \tag{4.9}$$

with $\chi(\lambda_1,\lambda_2)$ being the characteristic function of the bipartite state defined as:

$$\chi(\lambda_1,\lambda_2) = e^{-\frac{1}{2}\left(\Lambda^T \sigma \Lambda\right)} \tag{4.10}$$

where σ is the covariance matrix of the bipartite state while,

$$\Lambda = \begin{pmatrix} a \\ b \\ c \\ d \end{pmatrix} \tag{4.11}$$

and $\lambda_1 = a + ib$, $\lambda_2 = c + id$ are complex numbers. $\chi_n(\lambda_1)$ has the following expression:

$$\chi_n(\lambda_1) = e^{-\frac{1}{2}|\lambda|^2} Ln\left(|\lambda|^2\right) \tag{4.12}$$

with $Ln\left(|\lambda|^2\right)$ being the Laguerre polynomials. In the picture 4.3 is shown the joint photon number distribution for the experimental state represented by the CM (4.6)

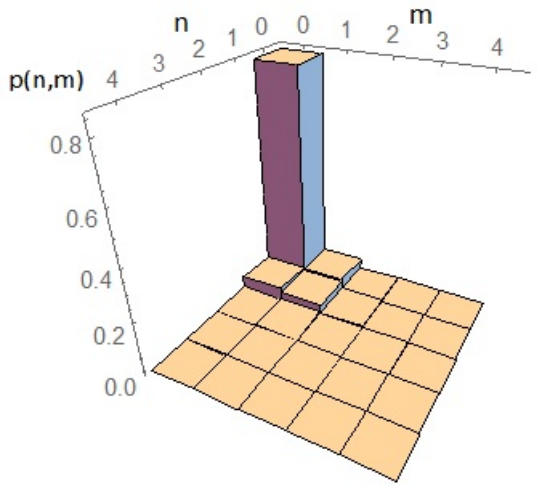

Figure 4.3: Joint photon number probability distribution $p(n,m)$ of the experimental entangled state of modes a and b outing from the OPO and then provided with OAM.

In fig.4.4 are instead shown the single-mode distributions $p(n)$ for the modes b and d .

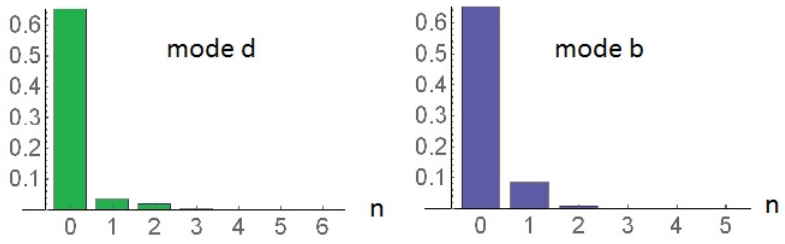

Figure 4.4: Single-mode distributions $p(n)$ for the modes b and d.

The CM (4.6) is not the one corresponding to the state generated into the OPO crystal. Indeed this state is not a pure state since it has interacted with the environment. The pure state generated inside the crystal has the following covariance matrix:

$$\sigma_p = \begin{pmatrix} 0.79 & 0 & 0.61 & 0 \\ 0 & 0.79 & 0 & -0.61 \\ 0.61 & 0 & 0.79 & 0 \\ 0 & -0.61 & 0 & 0.79 \end{pmatrix} \tag{4.13}$$

This matrix can be retrived thanks to equation (1.191) and by calculating the purity it is easy to see that it is a pure state, indeed:

$$\mu = \frac{1}{4(\det \sigma_p)} = 1 \tag{4.14}$$

When taking into account of losses the distributions shown above turn to be the ones depicted in fig. 4.5.

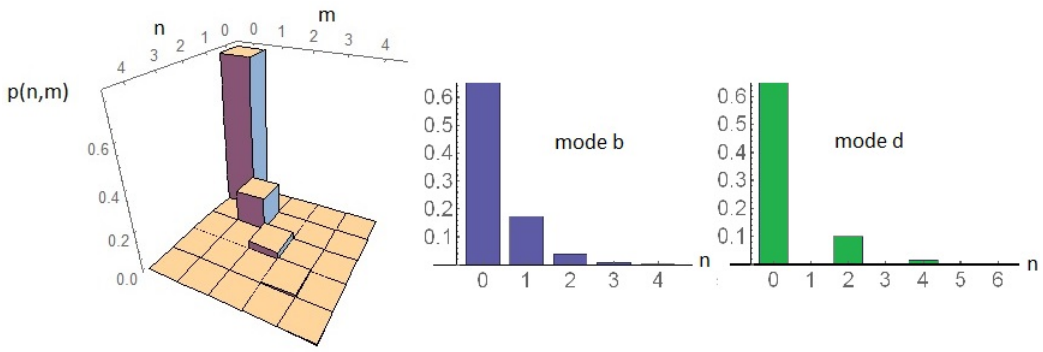

Figure 4.5: Joint photon number probability distribution $p\,(n,m)$ of the pure entangled state of modes a and b.

The distribution of the mode $\hat{b}$ is typical of a thermal state, while for the mode $\hat{d}$ the probability of having a two-photon state is greater than the single-photon state as expected. For what concerns the joint probability it is possible to see that there are only states in which the numbers of photons n and m are equal. The pure state that is the one generated inside the crystal before any transmission takes place, is a twin beam entangled state. The population of levels with two different numbers of photons shown in the plot of fig 4.3 is probably due to the interaction with the environment.

In order to obtain these plots the CM corresponding to the pure state at the OPO output has been retrived from the experimental one (4.6) by means of equation (1.191).

4.5 The Fidelity Criterion

A further evidence of the presence of entanglement between the modes $\hat{a}$ and $\hat{b}$ can be provided by applying the fidelity criterion introduced in subsection 1.4.6. Let us recall that according to this criterion when mixing two squeezed not-correlated states through a bilinear exchange Hamiltonian, the resultant state will be entangled if and only if the fidelity between the two input states is less than the threshold value of equation (1.188). In our case the modes $\hat{c}$ and $\hat{d}$ fullfill the criterion hypotesis since they are uncorrelated modes exhibiting fluctuations on the quadratures under the shot noise level. From data corresponding to single modes, CMs

relative to these two squeezed modes have been reconstructed,

$$\sigma_c = \begin{pmatrix} 0.89 & 0 \\ 0 & 0.38 \end{pmatrix} \qquad \sigma_d = \begin{pmatrix} 0.32 & 0 \\ 0 & 0.83 \end{pmatrix}$$

By following expression (1.187) evaluation of fidelity leads to the value $Fid_{cd} = 0.87$. The corresponding threshold value for $\tau = 0.5$ in expression (1.188) leads to the value$Fid_{cd(Th)} = 0.97$. So the bipartite state that is obtained by mixing the modes $\hat{c}$ and $\hat{d}$ in a 50-50 BS (typical example of a process described by a bilinear exchange Hamiltonian) is, according to the theorem, an entangled state. By remembering the definition of these two modes in terms of the modes provided by OPO source it is easy to convince themselves that the state provided by this bilinear exchange Hamiltonian is nothing but that the bipartite state constituted by the two modes $\hat{a}$ and $\hat{b}$ (see fig. 4.6). Indeed we have:

$$\hat{a} = \frac{\hat{c} + \hat{d}}{\sqrt{2}} \qquad \hat{b} = \frac{\hat{c} - \hat{d}}{\sqrt{2}}$$

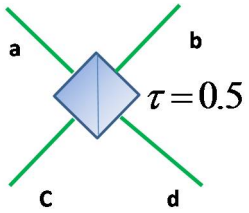

Figure 4.6: Mixing the modes $\hat{c}$ and $\hat{d}$ into a 50-50 BS gives back the modes $\hat{a}$ and $\hat{b}$

Therefore this is a further criterion according to which the OAM- entangled state provided by our setup shows non-classical correlations.

Conclusions

This dissertation concernes the designing and the experimental realization of a setup capable of generating entanglement between CV states of the radiation field carrying orbital angular momentum. The setup has been drawn up with the dual purpose to provide the entangled state, produced by the parametric down conversion source, with OAM but also to make possible its detection via the single homodyne detection scheme, directly acting in OAM space.

The characterization stage allows to assess the presence of entanglement between the two modes. A homodyne detector directly working in OAM space has been conceived by extending the ordinary homodyne detection technique to structured beams. A homodyne detector capable of inferring the quadrature statistics of vortex traveling modes must be able to reconfigure the local oscillator spatial-temporal structure in order to maximize its projection onto the state under detection. In other words the local oscillator has to span part of OAM Hilbert space in which the states to be detected live.

The setup has been described by stressing the strategies adopted to optimize the detection. The matrix measured and reported in the thesis is a typical CM we have. Both the entanglement criteria employed have confirmed that the state we produce is entangled so being a potential resource for achieving quantum communication and information tasks. An estimation of losses have turn to be compatible with the expected value. The quantumness of the state is not corrupted by the propagation and the interaction with the environment whose only effect is that of modifying the photon distribution probabilities both in the bipartite entangled state and in the single mode squeezed state. In the reported joint probability

distribution it is possible to notice the population of levels such as $|0,1\rangle$ and $|1,0\rangle$. The population ot these levels is probably due to the interaction of the state with the environment that causes a coupling of the state with the background photons.

Eventually the fidelity criterion has been used in order to obtain a further evidence of the presence of entanglement between the modes $\hat{a}$ and $\hat{b}$. Non classical correlations have been deduced by comparing the values of the experimental fidelities between modes $\hat{c}$ and $\hat{d}$ and the threshold value that fixes an upper limit in order to assess the arising of correlations between the modes resulting from a bilinear interaction between them.

The scheme that has been proposed not only makes possible to extend homodyne technique to structured beams but also sets the stage for arbitrary dimension multipartite entanglement. It is possibile in principle to modify this setup in order to provide multipartite entanglement among helilcal modes also opening the possibility to extend the dimensionality of the OAM Hilbert space. Definitely the experiment that has been carried on can be beneficial for the whole field of continuous variable quantum information that uses OAM degree of freedom to encode information both for what concernes the generation and the detection of OAM carrying states.

Bibliography

[1] K.Kreis, P.V. Loock "Classifying, quantifying, and witnessing qudit-qumode hybrid entanglement" Phys.Rev. A, 85, (2012)

[2] Z.Y. Zhou, Y. Li, D. S. Ding, W. Zhang, S. Shi, and B.S. Shi, "Classical to quantum optical network link for orbital angular momentum-carrying light," Opt. Express 23, 18435-18444 (2015)

[3] M. Erhard, R. Fickler, M. Krenn and A. Zeilinger "Twisted photons: new quantum perspectives in high dimensions" Light: Science & Applications accepted article preview 17 October 2017; doi: 10.1038/lsa.2017.146

[4] M. Lassen, G.Leuchs and U. L. Andersen ,"Continuous Variable Entanglement and Squeezing of Orbital Angular Momentum States", Phys. Rev. Lett,102, (2009).

[5] Jackson J D 1999 "Classical Electrodynamics" 3rd edn (New York: Wiley).

[6] Marlan O. Scully, M. Suhail Zubairy 1997 "Quantum Optics" (Cambridge University Press).

[7] Y. Yamamoto and H. A. Haus, "Preparation Measurement and information capacity of optical quantum states", Rev. Mod. Phys. 58, 1001 (1986).

[8] C.M. Caves, "Quantum mechanical noise in an interferometer", Phys. Rev. D 23, 1693 (1981).

[9] A.Ferraro, S.Olivares, M.G.A. Paris, "Gaussian States in quantum information" (Bibliopolis, Napoli, 2005).

[10] S. J. Van Enk and G. Nienhuis, "Commutation rules and eigenvalues of spin and orbital angular momentum of radiation fields" J. Mod. Opt., 41,963 – 977 (1994).

[11] S. J. Van Enk and G.Nienhuis "Eigenfunction description of laser beams and orbital angular momentum of light", Opt. Commun. 94 (1992).

[12] B.Piccirillo, S. Slussarenko, L.Marrucci, E.Santamato,"The orbital angular momentum of light: Genesis and evolution of the concept and of the associated photonic technology", Rivista del nuovo Cimento36 (11).

[13] A. M. Yao, and M. J Padgett, "Orbital angular momentum: origins, behavior and applications" Adv. Opt. Photon. 3, 161–204 (2011).

[14] H. He, M. E. J. Friese, N. R. Heckenberg, and H. Rubinsztein-Dunlop, "Direct Observation of Transfer of Angular Momentum to Absorptive Particles from a Laser Beam with a Phase Singularity", Phys. Rev. Lett., 75 (1995).

[15] R. A. Beth ,"Mechanical Detection and Measurement of the Angular Momentum of Light", Phys. Rev., 50 (1936).

[16] S. M. Barnett, "Optical angular-momentum flux", Journal of Optics B: Quantum and Semiclassical Optics 4 (2001).

[17] M. A. Bandres and J. C. Gutierrez-Vega. "Ince Gaussian beams", Optics Letters, 29 (2004).

[18] F. Gori, G. Guattari, and C. Padovani, "Bessel-Gauss beams" Optics Communication, 64,491-495 (1987).

[19] V. V. Kotlyar, R. V. Skidanov, S. N. Khonina, and V. A. Soifer. "Hypergeometric modes" Optics Letters, 32,742–744 (2007).

[20] E. Karimi, B. Piccirillo, L. Marrucci, and E. Santamato "Hypergeometric-Gaussian modes" Optics Letters, 32 3053–3055, (2007).

[21] B.Piccirillo, V. D'Ambrosio, S. Slussarenko, L. Marrucci and E. Santamato, "Photon spin-to-orbital angular momentum conversion via an electrically tunable q-plate" Applied Physics Letters 97 (2010).

[22] E. Karimi, B. Piccirillo, E. Nagali, L. Marrucci and E. Santamato, "Efficient generation and sorting of orbital angular momentum eigenmodes of light by thermally tuned q-plates" Applied Physics Letters 94, (2009).

[23] A.Peres,"Separability Criterion for Density Matrices", Phys. Rev. Lett. **77**, (1996).

[24] P.Horodecki,"Separability criterion and inseparable mixed states with positive partial transposition" , Phys. Lett. A 232 (1997).

[25] S.Olivares, "Quantum optics in the phase space" , Eur. Phys J.Special Topics 203,(2012).

[26] J.Williamson,"On the Algebraic Problem Concerning the Normal Forms of Linear Dynamical Systems", Am. J. of Math.58, (1936).

[27] R.Simon, "Peres-Horodecki Separability Criterion for Continuous Variable Systems", Phys. Rev. Lett. 84, (2000).

[28] L.M. Duan, G. Giedke, J.I. Cirac and P.Zoller, "Entanglement purification of Gaussian continuous variable quantum states", Phys. Rev. Lett 84, (2000).

[29] S.Olivares, M.G.A. Paris, "Fidelity matters: the birth of entanglement in the mixing of Gaussian states ", Phys. Rev. Lett. 107, (2011).

[30] H.-P. Breur and F. Petruccione, The Theory of Open Quantum Systems (Oxford University Press, Oxford, 2002).

[31] R.W. Boyd, "Nonlinear Optics" 1992 , (Academic Press).

[32] V. D'Auria, "Dynamics and Behaviour of Triply Resonant OPOs below the thereshold", Tesi di dottorato, UniversitÃ di Napoli "Federico II", (2005).

[33] Eric D. Black, "An introduction to Pound-Drever-Hall laser frequency stabilization", American Association of Physics Teachers 69, (2001).

[34] U. Leonhard,1997 "Measuring the Quantum State of Light", (Cambridge Univ. Press)

[35] V. D' Auria, A.Porzio, S.Solimeno, S.Olivares, M.G.A. Paris, "Characterization of bipartite states using a single homodyne detector", Journal of Optics B: Quantum and Semiclassical Optics7 (2005).